INVESTIGATING PHASE BEHAVIOUR AND NANO-DOMAIN CHARACTERISTICS OF SPHINGOMYELIN/CHOLESTEROL MEMBRANE, USING ^{2}H NMR

by

Amirmohamad Keyvanloo
M.Sc., Brock University 2005

THESIS SUBMITTED IN PARTIAL FULFILLMENT OF
THE REQUIREMENTS FOR THE DEGREE OF

DOCTOR OF PHILOSOPHY

In the
Department of Physics

SIMON FRASER UNIVERSITY

Summer 2010

APPROVAL

Name: **Amirmohamad Keyvanloo**

Degree: **DOCTOR OF PHILOSOPHY**

Title of Thesis: **Investigating Phase Behaviour and Nano-Domain Characteristics of Sphingomyelin/Cholesterol Membrane, Using ^{2}H NMR**

Examining Committee:

Chair: **Dr. John Bechhoefer**
Professor

_____

Dr. Jenifer Thewalt
Senior Supervisor
Professor Physics/MBB

_____

Dr. Martin Zuckermann
Supervisor
Professor Physics

_____

Dr. Barbara Frisken
Supervisor
Professor Physics

_____

Dr. David Broun
Internal Examiner
Associate Professor Physics

_____

Dr. James H. Davis
External Examiner
Professor
University of Guelph

_____

Date Defended/Approved: Aug 09, 2010

Declaration of
Partial Copyright Licence

Abstract

Sphingomyelin (SM) and cholesterol are major components of the mammalian cell plasma membrane. It is suggested that assemblies of sphingolipids and cholesterol lead to the formation of domains known as “rafts”. In the SM/Cholesterol binary system cholesterol induces formation of a “liquid-ordered” (**lo**) phase that can coexist with either the “liquid-disordered” (**ld**) phase or the “solid-ordered” (**so**) phase. Similar **lo**-phase domain formation is observed in DPPC/Cholesterol and DPPC/ergosterol systems. Furthermore, cholesterol interacts more strongly with sphingomyelin than DPPC. Deuterium nuclear magnetic resonance spectroscopy (NMR) is used to study the dependence of the phase and nanodomain structure of sphingomyelin/cholesterol membranes on sterol content and temperature. NMR spectra of N-palmitoyl (D31)-D-erythro-sphingosylphosphorylcholine (PSM) were taken for temperatures from 25 to 70^{o}C and cholesterol concentrations 0 - 40%. Analogous experiments were done using 1-palmitoyl,2-palmitoyl(D31)-*sn*-glycero-3-phosphocholine (DPPC)/cholesterol membranes in order to carefully compare the data obtained using palmitoyl chains which have similar “kinked” conformations. The constructed phase diagrams exhibit both **so** + **lo** and **ld** + **lo** phase coexistence regions, however macroscopic (micron-sized) coexistence of **ld + lo** does not occur. Instead, we observed line-broadening in the **ld** + **lo** region which was characterized by examining the cholesterol dependence of the quadrupolar splittings and linewidths of the peaks in the depaked spectra, at a given temperature. These results were analyzed by assuming fast exchange of lipids between **ld** and **lo** nanodomains which were found to be generally less than 10 nm across. By analyzing the depaked spectrum, information from all orientations of the lipid long axis relative to the magnetic field is pooled. This may obscure the results used to characterize domain size. Selectively deuterated sphingomyelin, labeled at C9 of

the N-linked palmitoyl chain, was used to measure the orientation dependence of T_2 relaxation time and to more directly calculate domain size. A phenomenological theory based on the hypothesis that fluctuations in local curvature and bilayer thickness are responsible for the orientation dependence of T_2 provides an excellent fit to the data. The **ld** + **lo** domain sizes calculated using the C9 data agree well with those calculated from the depaked spectrum of PSM.

Keywords: sphingomyelin; cholesterol; DPPC; phase diagram; deuterium NMR; lipid membranes

TO Mom and Dad

With love

Acknowledgements

I thank my supervisor, Professor Jenifer Thewalt, and my co-supervisor, Professor Martin Zuckermann, for their mentorship and support over the course of my Ph.D. studies. I learned a great deal of lipid science and ^{2}H NMR from them and without their constant encouragement and patience, this work would have not made possible. I would also like to thank Professor Barbara Frisken for providing valuable advice and guidance as a member of supervisory committee. I greatly appreciate my lab-mate Sherry Leung for helping me quickly switch from theory to experiment by teaching me how to prepare samples, run experiments, and analyze data.

Financial support from the National Science and Engineering Research Council is gratefully acknowledged. Funding has been partially provided by Simon Fraser University Graduate Fellowships.

I would like to thank my family for the support and encouragement they have given me throughout the years. I dedicate this thesis to my wife Shiva Haghighat and my daughter Hasti.

Table of Contents

List of Figures

List of Tables

Chapter 1: Introduction

Lipid-lipid interactions are important determinants of membrane organization and function in living systems and have been thoroughly researched for a great variety of membranes. Despite the ongoing effort, however, many elements of even simple lipid mixtures used to model cell membranes are still poorly understood. The work presented in this thesis contributes to the body of knowledge pertinent to the interactions between two major mammalian cell lipids, sphingomyelin and cholesterol.

1.1 Cell Plasma Membrane

The lipid bilayer of cell membranes is a fundamental molecular assembly in Biology due primarily to its role in the maintenance of the functional integrity of the cell or organelle (unit of cellular machinery) it encloses. Eukaryotic cells have several distinct membranes, the plasma membrane surrounding the cell and membranes around organelles such as mitochondria. The description of the lipid structure in membranes as a bilayer was originally proposed by Gorter and Grendel [1] and was further detailed by Danielli and Davson [2]. The plasma membrane is an assembly of lipid and protein molecules held together by non-covalent bonds. Lipids are amphiphilic molecules; they have hydrophilic headgroup and hydrophobic hydrocarbon chains and, thus, self-assemble into a bilayer structure in aqueous environment. The hydrophobic regions of proteins

are sequestered away from the hydrophilic extracellular and intracellular spaces forming an energetically favourable structure (corresponding to the minimum free energy).

The structures of both the chain and headgroup components, along with cholesterol and protein, contribute to membrane function.The lipids are arranged as a continuous double layer 4 to 5 nm thick (Figure 1-1) and serves as a relatively impermeable barrier to the flow of most water-soluble molecules. The selective permeability of the plasma membrane to large and small molecules, which largely maintains their intracellular and extracellular concentrations, is one of the major membrane functions. The diversity in membrane lipid composition can help to achieve this function of selective permeability while satisfying packing requirements around integral membrane proteins. Membranes are asymmetrical structures; the lipid and protein composition differs between the inner and outer layer of the bilayer since different functions are performed at each surface. The plasma membrane of a biological cell is a dynamic, pseudo two dimensional fluid structure and most lipids and proteins are able to move about rapidly in the plane of the membrane. This is essentially the fluid mosaic model of Singer and Nicolson [4] where the membrane is a fluid-like lipid bilayer within which various lipids and proteins undergo lateral diffusion. In recent years more and more effort has been directed towards understanding the nature of compositionally-distinct regions or domains within cell membranes (see Section 1.3: Lipid Rafts below).

The cell membrane is an extremely complex system and the arrangement of its components can have important consequences for cell functioning. Lipid

molecules constitute about 50 % of the mass of mammalian cell membranes, with the remaining part being mostly proteins. In eukaryotic cell membrane there are three major types of lipids: *phospholipids* (the most abundant), *cholesterol*, and *glycolipids*. The membrane of many mammalian cells contains four major phospholipids: *phosphatidylcholine*, *sphingomyelin*, *phosphatidylserine* and *phosphatidylethanolamine*. The *β*–OH cholesterol is the most common sterol found in the plasma membrane of eukaryotic cells and constitutes nearly 25 % of its lipid mass. It is believed that the high cholesterol composition in the cell membrane plays an important role as a stabilizer against mechanical stress, increasing durability of the plasma membrane compared to the internal membranes [7].

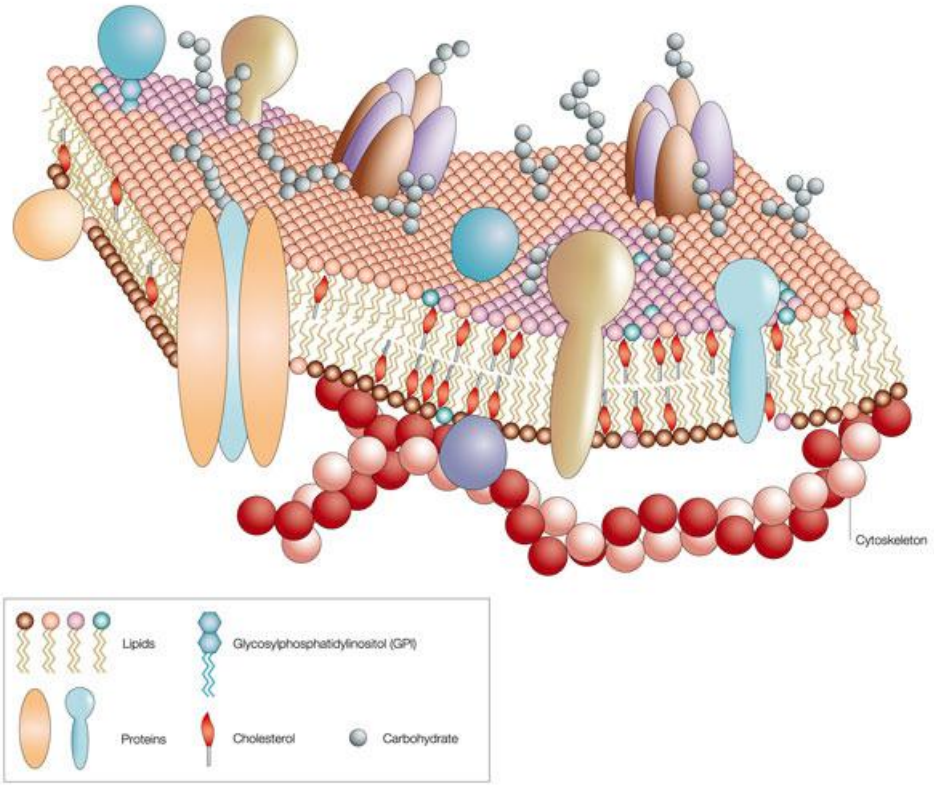

Figure 1-1: The fluid-mosaic-model of the cell membrane.

Like a mosaic, the cell membrane is a complex structure made up of many different parts, such as proteins, phospholipids and cholesterol. The relative amounts of these components vary from membrane to membrane, and the types of lipids in membranes can also vary (courtesy of [3]).

1.2 Phase Behavior of Lipids

Lipids can exist in various phases depending on temperature and compositions of other components in the system. The phase behaviour of a multi-component system satisfies the Gibbs phase rule:

$$F = C - P + 2 \tag{1.1}$$

where F is the number of intrinsic thermodynamic variables that can vary freely (*e.g.* temperature, composition), C is the number of components and P is the number of phases in the system. In a two component system ($C = 2$) the maximum number of phases that can coexist is two ($P = 2$) if both temperature and composition can be varied independently ($F = 2$). If one of these variables is fixed, such as at an isotherm where temperature is fixed, then three phases can coexist.

The cell membrane is a very complicated entity and in order to study lipid-lipid interactions via spectroscopic techniques one needs to make model membranes, usually consisting of two or three components. The interesting two-component model membrane is a binary mixture of lipid and cholesterol in excess water. Full hydration is essential to make sure that the phase behaviour of the membrane is not sensitive to the amount of water present and therefore the model membrane is a two-component system. A binary lipid/cholesterol membrane can exist in two well-known phases: Gel and liquid crystalline. The gel phase is also known as solid ordered (**so**) or L_β phase, and the liquid crystalline phase is also referred to as liquid disordered (**ld**) or L_α phase. In dipalmitoylphosphatidylcholine **(**DPPC), the **so** phase is referred to as L_β, where

the prime designates chain tilt. In addition, the **so** phase of DPPC includes the ripple phase ($P_{\beta'}$). “Solid” versus “liquid” refers to the degree of lateral motion and freedom of the lipids within the bilayer (2D lattice). “Ordered” versus “disordered” refers to the degree of rigidity of the hydrocarbon chains.

When the bilayer is completely ordered the chains are in the all-*trans* configuration, resulting in the lipids forming a closely packed structure. The gel phase is a more ordered, less energetic state and is hence found at lower temperatures. The main motions present in the **so** phase are a type of axial diffusion of the lipid molecules. When the bilayer is disordered the lipid tails are free to undergo fast rotational motion about the director axis (bilayer normal) and conformational trans-gauche isomerisation (fluctuations about individual carbon-carbon segments). Hence, in the liquid-disordered phase, the lipids can undergo fast translational motion and the tails are free to rotate. Kinks can be found where hydrocarbon chains are in the gauche-configuration. As a result, the lipids pack more loosely than in the gel phase. Cell plasma membranes are typically considered liquid crystalline bilayers.

In the absence of cholesterol the lipid membrane undergoes a solid ordered to liquid disordered phase transition at a sharp melting point. The temperature where this occurs (T_m) varies depending on the length of the hydrocarbon chains and the degree of unsaturation: it is lower if the hydrocarbon chains are short or have double bonds. Introducing cholesterol to the lipid bilayer increases the average lipid chain order in the fluid phase and interferes with the membrane’s ability to form the **so** phase below T_m. Once cholesterol is

introduced, depending on temperature, the lipid bilayer can still be found in the **so** or **ld** phase. However, above a certain concentration of cholesterol the bilayer adopts a third type of phase: liquid-ordered (**lo**) phase [5]. In this state the lipid acyl chains are highly conformationally "ordered" yet the lipid molecules retain fluid-like motions (lateral freedom) and thus the "liquid" state of the membrane is maintained [6]. Thus, cholesterol functions as an "alloying" agent in the membrane, straightening out (orientationally ordering) the acyl chains, reducing the average lipid cross- sectional area and thickening the bilayer [7]. It has been postulated that the *β* hydroxyl group of cholesterol forms hydrogen bonding with the lipid phosphate group which positions the lipid in the bilayer environment [8]. An important biological function of cholesterol is the reduction in the passive bilayer permeability (10 fold for water through membranes containing 30 mole% cholesterol [9]) while maintaining the fluidity of the bilayer.

Once different phases of a lipid/cholesterol membrane are identified a phase diagram can be established, where the effects of changing temperature and concentration on chain structure and dynamics are measured. Then one can map regions of phase equilibria (two and three phase coexistence) using various spectroscopic techniques. The first experimentally determined phase diagram was that of DPPC/cholesterol, using DSC and ^{2}H NMR [10]. The results indicated that cholesterol disorders the gel phase and orders the fluid phase of a membrane. The phase diagram showed regions where the two phases coexist: **so**/**lo** and **ld**/**lo** coexist, with a clear three-phase line separating them. However micron-sized phase separation in the **ld**+**lo** region was not observed. Hsueh *et*

al. [11] also mapped the phase diagram of DPPC/ergosterol and observed a similar region of **ld**/**lo** domain heterogeneity, again separated from the **so**/**lo** two-phase region by a three-phase line.

The theoretical investigations of the phase diagram started from the pioneer work of Ipsen *et al.* [5] where the idea of an "**lo**" phase was first introduced. In this work a thermodynamic model was proposed to describe the liquid phases of the bilayer, followed by a microscopic model for PC/cholesterol system which was solved in the mean-field approximation. In a second study, numerical studies of Ising Models defined on a random lattice was applied to the phase behavior of lipid bilayer systems [12]. Calculations based on a mean-field theory of the model predicted a phase diagram of DPPC/cholesterol bilayers that agreed qualitatively with the experimental phase diagram.

1.3 Lipid Rafts

Sphingomyelin and cholesterol are two of the three most abundant lipids in the plasma membrane outer leaflet of a typical mammalian cell [13]. Ever since plasma membrane domain heterogeneity began to be actively researched, these two have been found to be preferentially associated. Initial investigations were into the composition of detergent resistant membranes [14], followed by the introduction of the "rafts" hypothesis [15]. Rafts, enriched in sterols and sphingolipids, were thought to be small dynamic domains implicated in many important cell functions. It was also thought that rafts have a different 'phase' from the rest of the membrane: *liquid ordered* (**lo**). Raft membranes were then modelled as a three-component system by mixing a low-melting PC, DPPC, and

cholesterol. Giant unilamellar vesicles (GUVs), i.e. vesicles tens of microns in diameter, were cooled from 60^{o}C and at some point the 'miscibility threshold' was encountered, and macroscopic **lo**/**ld** phase coexistence was observed [16, 17]. Further experiments were performed to investigate the possibility of large **ld**+**lo** regions in cell membranes [18]. Plasma membrane 'blebs' were created in living cells and then separated from the cell. These 'giant plasma membrane vesicles' retain much of the natural membrane's characteristics with respect to protein and lipid content and distribution, however the membranes are no longer in contact with the cytoskeleton and the lipid-regulatory cell machinery. Macroscopic **ld** + **lo** phase coexistence is observed at temperatures slightly below physiological *T*. Advanced optical techniques delineate nano-scale variations in mobility: a recent study has succeeded in the direct observation of small domains in the membranes of living cells [19]. In this study, single fluorescently labeled PE or SM is trapped in the membrane. "Trapping" event is measured and is thought to be "cholesterol-assisted". It was found that SM is trapped approximately 4 times longer, on average, than PE, with the size of traps being less than 20 nm. Thus, from the earliest to the most recent studies of membrane domain organization, SM and cholesterol have been found to interact preferentially.

There are several outstanding questions about the role of cholesterol and other sterols in forming the tightly-packed liquid ordered (**lo**) phase. Most research into model membrane systems has employed lipid mixtures containing phosphatidylcholine (PC) to understand **ld**/**lo** phase coexistence. PC shares several important physical characteristics with sphingomyelin and since the latter

was not commercially available in pure form, PC has been used instead. A particularly important controversy concerns the phase behaviour of binary PC/sterol membranes: in dipalmitoylPC (DPPC)/sterol systems liquid disordered (**ld**) and **lo** phases have been found to coexist [10, 11, 20] but the two phases have not been observed to coarsen, remaining sub-microscopic in size. Since their small size renders these dynamic domains invisible by most imaging techniques, and since an explanation for the lack of coarsening remains elusive, a number of researchers have postulated that there is no **ld/lo** phase coexistence in DPPC/cholesterol. An alternative explanation for **ld/lo** membrane heterogeneity invokes lipid composition fluctuations due to proximity to a critical point [21]. Theoretical descriptions of phospholipid/sterol interactions are numerous [22, 23, 24] and the area continues to be very active as simulation strategies improve and accurate experimental input parameters become available [25]. Recently a modification to the original PC/sterol “condensed complex” model [26] predicted phase coexistence in DPPC/cholesterol above the main transition temperature [27].

1.4 Thesis Summary and Motivation

The lipid composition of the outer leaflet of the plasma membrane is mainly sphingomyelin, cholesterol and unsaturated PC. Many investigations into membrane phase behavior have attempted to reproduce the important elements of the outer leaflet by combining a “low melting” lipid, often dioleoylPC (DOPC), and a high melting lipid, often DPPC, with cholesterol. Such membranes are not “natural”, as neither DOPC nor DPPC is found in most biological membranes, but

their study has provided tremendous insights into fundamental lipid physical chemistry, and particularly into the **lo+ld** phase coexistence region of the ternary phase diagram. Furthermore, DPPC has been postulated to be a reasonable analogue for sphingomyelin (SM) in such studies, since palmitoyl sphingomyelin (PSM) and DPPC have very similar chain-melting transition temperatures, chain lengths and identical phosphocholine head groups Figure 1-2. Sphingomyelin-containing lipid membranes have been studied in some detail (for a review see [28]). The combination of POPC, PSM and cholesterol is particularly attractive since all three lipids are found in nature and together they make an excellent plasma membrane outer leaflet model. Large-scale **lo**+**ld** phase coexistence was observed for some regions of the phase diagram [16, 17] and at sufficiently high cholesterol concentration an **lo** phase membrane exists [29]. Despite this ongoing progress with the three-component system, there is still much to learn about the simpler sphingolipid/sterol membrane. Several groups have published results indicating that **ld**+**lo** phase coexistence occurs in SM/cholesterol [17, 30], providing insight into and partial determinations of the binary phase diagram.

Comparing different groups' explorations into the SM/cholesterol membrane is complicated by the fact that SM from different sources differs in the chemical mixture of its constituent chains. To assess the nature of the interaction between sphingomyelin and cholesterol directly, we have thus performed a detailed phase diagram determination using deuterium nuclear magnetic resonance (^{2}H NMR). Earlier studies [31, 32] used chicken egg sphingomyelin, which is composed of lipids with varying chain lengths. In this thesis, synthetic

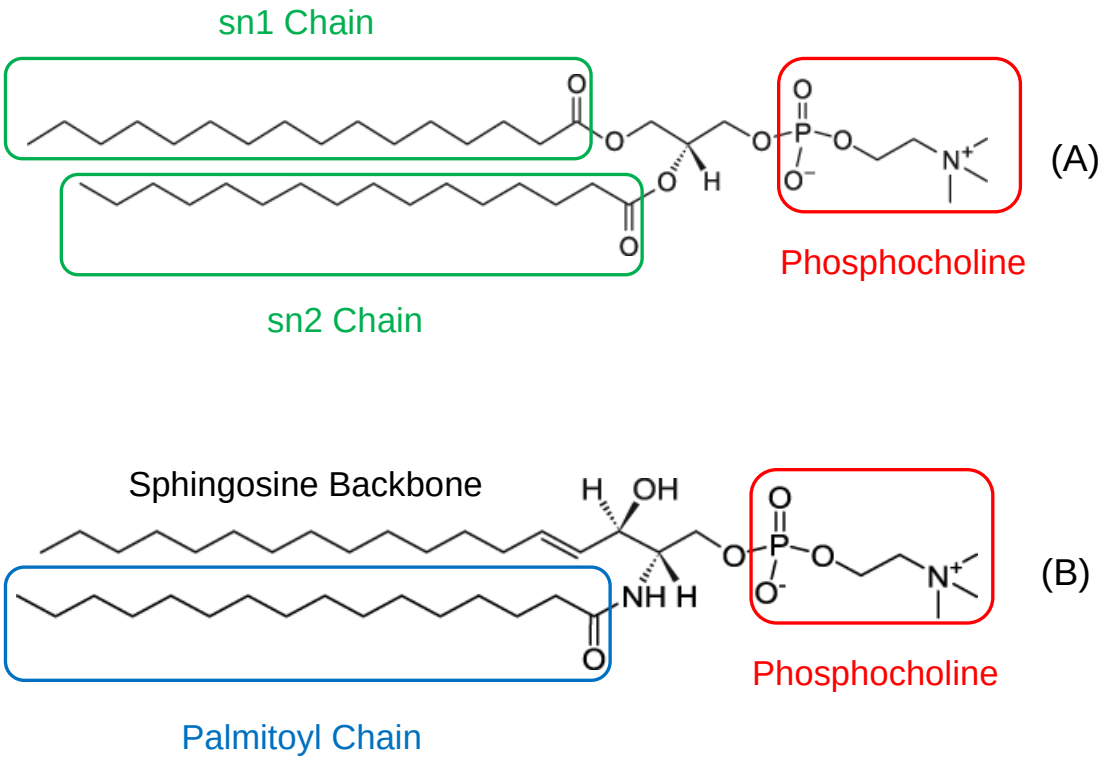

Figure 1-2: Structure of (A) DPPC, (B) palmitoyl sphingomyelin.

perdeuterated sphingomyelin having an amide-linked palmitoyl chain (PSM-d31) is used to eliminate chain length effects, Figure 1-3 A. Since the N-linked palmitoyl chain of PSM is structurally analogous to the *sn*-2 chain of DPPC, we chose to re-determine the DPPC/cholesterol phase diagram using *sn*-2 chain perdeuterated DPPC (DPPC-d31), Figure 1-3 B. Thus, we can directly compare and contrast cholesterol's effects on these two lipids' phase behaviour and chain order. Mapping phase diagrams requires collecting a significant amount of data; therefore, we performed ^{2}H NMR experiments for series of cholesterol compositions over a wide range of temperature. We estimated the length-scale characterizing the **ld**/**lo** domains by mapping (dePakeing) the spectra of

perdeuterated lipids into a single orientation of the bilayer normal. By analyzing the depaked spectra, information from all orientations of the lipid long axis relative to the magnetic field is pooled, and we were concerned that this might obscure the results used to characterize domain size. Therefore we used selectively deuterated sphingomyelin to measure the orientation dependence of the transverse relaxation time and to calculate domain size more directly. The results from selectively labelled PSM allowed us to gain unexpected insight into the membrane dynamics characteristic of the **ld** and **lo** phases.

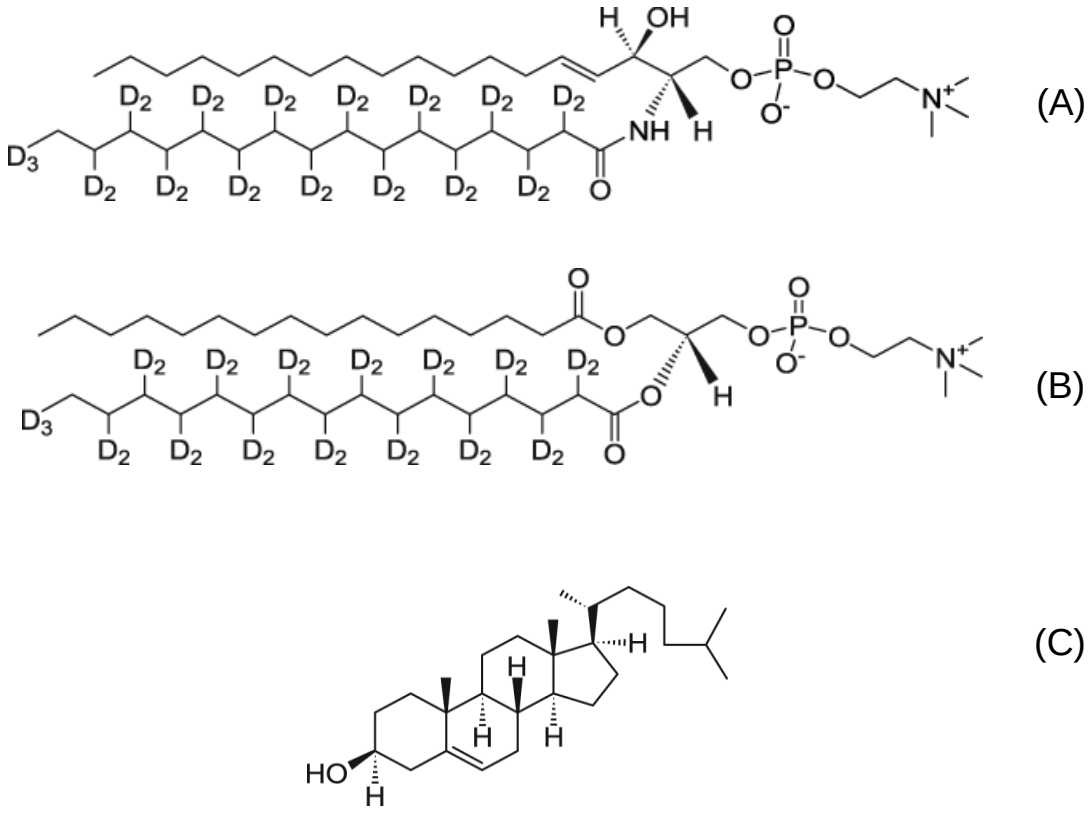

Figure 1-3: Structure of (A) chain-perdeuterated (sn2) DPPC, (B) chain-perdeuterated palmitoyl sphingomyelin, and (C) cholesterol.

Chapter 2: NMR theory and background

Different phases observed in DPPC/cholesterol and PSM/cholesterol membranes have distinct characteristics and exhibit distinct ^{2}H NMR spectral shapes. The ^{2}H NMR data can accurately report on the phase behaviour of the systems and therefore is a powerful spectroscopic technique to study thermodynamic properties such as phase equilibria. Furthermore, the ^{2}H NMR quadrupolar splitting is proportional to the order parameter of the acyl chain and, thus, can report on the chain packing properties of the lipids. In contrast to commonly used techniques such as fluorescence NMR does not require bulky chemical probes which can distort the system.

In this chapter a brief introduction to deuterium NMR is given. The reader is referred to [33, 34, 35] for more detailed descriptions pertaining to lipid membranes. Here, the Hamiltonian for the system is discussed and the resulting quadrupolar splittings in the absence and presence of motions, fast on the NMR timescale, are presented. The rest of the chapter is devoted to the relaxation mechanisms in lipid membranes and, in particular, orientation dependence of the transverse relaxation time.

2.1 Introduction

Nuclear magnetic resonance is a spectroscopic technique that reports on the structural and dynamical properties of the lipid membranes. The large nuclear

concentrations and the small distances that exist between nuclear spins in bulk matter cause relatively strong spin interactions. These interactions, influenced by molecular motions, often lead to a broadening of spectral resonances since each spin now experiences, besides the applied field, a small local field due to its neighbours. This local field provides different local environments for different spins in the sample, leading to a spread in the observed resonance frequencies. It is useful to define the concept of spectroscopic time scale based on the observed line-broadening ($\tau_s \sim \frac{1}{\Delta\omega}$). The spectroscopic time-scale for ^{2}H NMR, of the order of $\tau_s \approx 10^{-6}$s, is long enough that some of the interactions are averaged out by fast molecular motions, leading to significant reduction of the line broadening in the spectrum. Thus, NMR occupies a unique place among spectroscopic techniques.

It is important to realize that there is a wide range of molecular motions that have been examined in model membranes. These range from molecular vibrations occurring in about 10^{-14} s to transbilayer flip-flop of lipids which can take many days to occur. There is a variety of techniques for investigating these motions and each technique has a specific range of frequency sensitivity. These techniques include Infrared spectroscopy (IR), X-ray diffraction, atomic force microscopy (AFM), fluorescence microscopy, fluorescence spectroscopy, single particle tracking and electron spin resonance spectroscopy (ESR). The frequency range for some of these techniques used to investigate lipid bilayers is illustrated in Figure 2-1 along with the correlation times of the motions of lipid molecules in membranes. This figure points out that some techniques report on the static

picture of the membrane since the molecular motions are slow relative to the measurement timescale, whereas other techniques only see a time-averaged picture of molecules that sample different environments very rapidly relative to the spectroscopic timescale. The sensitivity of NMR relaxation to a wide range of correlation times, in particular, stands out.

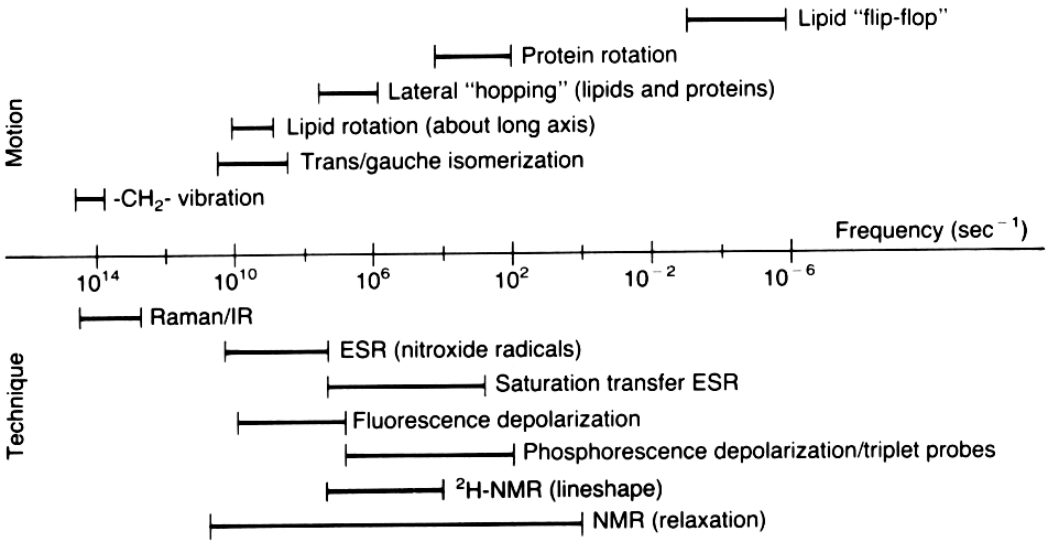

Figure 2-1: Timescales of lipid bilayer dynamics and measurement techniques for their investigation [Gennis 1989, page 167].

Motions can be conveniently divided into two classes. The slow motions which have correlation times, τ_c, satisfying $\tau_c \gg \tau_s$, have negligible influence on the spectrum. The fast motions, where $\tau_c \ll \tau_s$, give rise to motional averaging in which some of the molecular interactions are averaged out, resulting in narrower spectral lines. Local structural information is obtained by analyzing the ^{2}H NMR spectrum, whereas information on thermally driven molecular motions is provided by relaxation time measurements. A further distinction between ranges of correlation times is useful in the study of T_1 and T_2 relaxation processes. Motions with correlation times satisfying $\tau_c \gg \tau_s$ include the "slow" and a subset of the "fast" motions, in the context of the definition of "adiabatic" (pages 427ff. of Abragam [36]). Motions with correlation times $\tau_c \ll \tau_s$ are "non-adiabatic" and will be labeled "very fast". With these definitions the timescales can be divided into three categories: slow adiabatic, fast adiabatic, and very fast non-adiabatic, as shown in Figure 2-2. The NMR parameters affected by motions in the three ranges are also shown, as well as representative motions present in fluid bilayers.

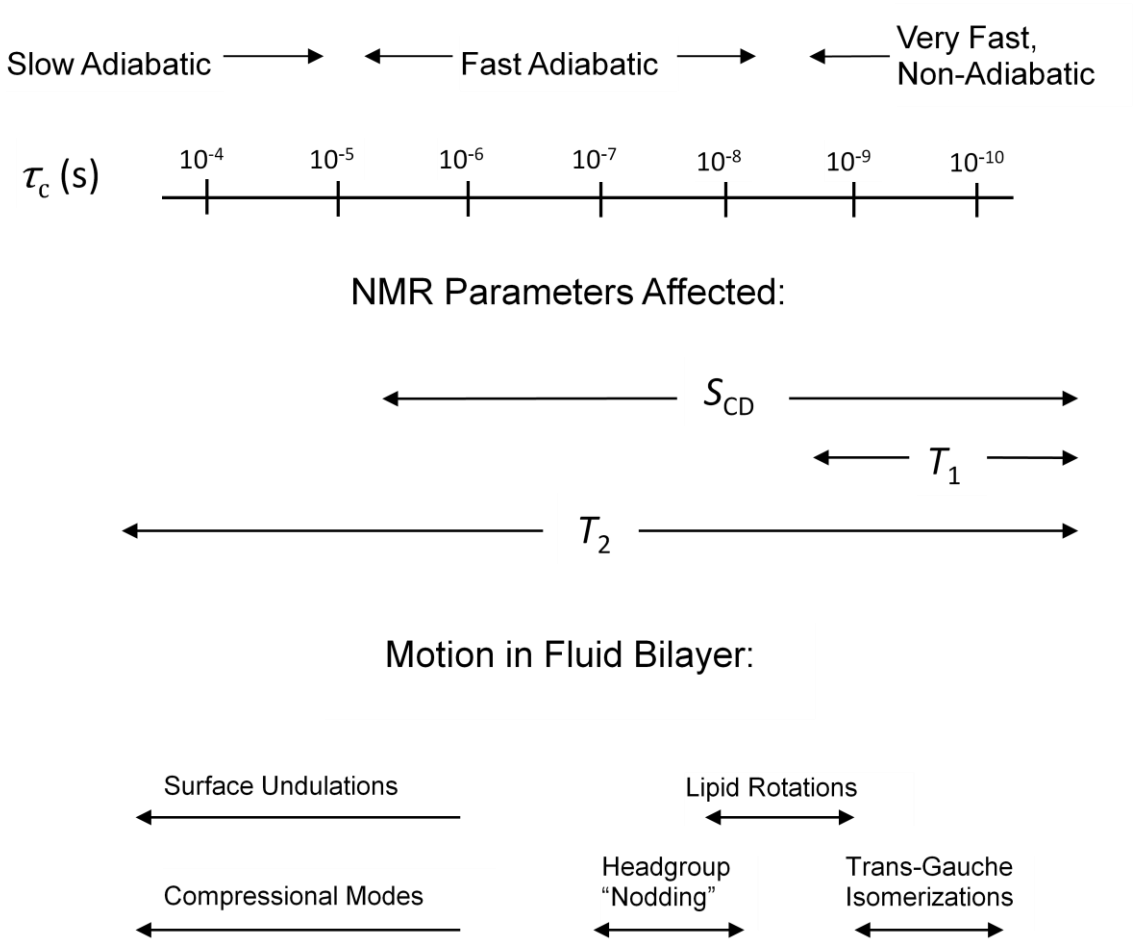

Figure 2-2: Summary of important timescales in NMR experiments, showing the three categories of motions.

Note that the precise boundaries will be determined by the field strength (influencing $1/\omega_0$ and thus the limit of "adiabatic" times) and the spectroscopic time-scale (τ_s), reproduced from [37].

2.2 Principles of NMR

The NMR sample consists of a large number of identical molecules. In a liquid, the interaction between the spins in different molecules is negligible due to the rapid isotropic motions. Furthermore, some of the interactions between the spins within the same molecule are averaged out by the motion of the liquid and, typically, the scalar coupling is the dominating interaction. The set of interacting spins in a molecule forms the “spin system” whose nuclei are distinguished by their chemical shifts, and the sample is an ensemble of identical spin systems.

The members of the ensemble, i.e. the spin systems, have the same set of quantized energy levels. Taking the sample as a whole it is possible to talk about the population of a particular energy level. At equilibrium, the population of energy level *i* with energy E_i is governed by Boltzmann distribution:

$$n_i = \frac{g_i N}{Z} e^{-E_i/kT}, \tag{2.1}$$

where g_i is the degeneracy of the energy level, *N* is the number of spin systems in the ensemble, *k* is Boltzmann’s constant and *T* is temperature. *Z* is the partition function and is defined as

$$Z = \sum_j g_j e^{-E_j/kT}, \tag{2.2}$$

where the sum is over all energy levels of the spin system. There are two consequences associated with the Boltzmann distribution: higher energy levels are less populated, and only levels with energies of the order of *kT* or less are significantly populated.

For a spin *I* nucleus at equilibrium there are (2*I* + 1) degenerate energy levels $|I,m\rangle$, where $m = -I, -I+1, \ldots, I-1, I$ is the quantum number for the *z*-component of the spin angular momentum I_z. In an external magnetic field $\vec{B}_0 = B_0\hat{z}$ the energy of a spin in state $|I,m\rangle$ is

$$E_m = -\hbar\omega_0 m, \tag{2.3}$$

where γ is the gyromagnetic ratio of the nucleus, $\hbar$ is Planck's constant divided by 2π, and $\omega_0 = \gamma B_0$ is known as the Larmor frequency.

In typical NMR frequencies, $\hbar\omega_0 \ll kT$ so the approximation $e^{-E_j/kT} = 1 - E_j/kT$ can be used:

$$Z \approx \sum_j \left(1 - \frac{E_j}{kT}\right). \tag{2.4}$$

The population of spins in state E_i is therefore

$$n_i \approx \frac{N}{\sum_j \left(1 - \frac{E_j}{kT}\right)}\left(1 - \frac{E_i}{kT}\right). \tag{2.5}$$

The population difference between energy level E_α and E_β, using the above equation, becomes

$$n_\alpha - n_\beta \approx \frac{N}{\sum_j \left(1 - \frac{E_j}{kT}\right)}\left(\frac{E_\beta}{kT} - \frac{E_\alpha}{kT}\right). \tag{2.6}$$

Using equation (2.3), this difference can be written as

$$n_\alpha - n_\beta \approx \frac{N}{\sum_j \left(1 - \frac{\hbar\omega_0}{kT} m_j\right)} \frac{\hbar\omega_0}{kT} \left(m_\alpha - m_\beta\right). \quad (2.7)$$

It follows from $m = -I, -I+1, \ldots, I-1, I$ that $\sum_j m_j = 0$ and (2.7) reduces to

$$n_\alpha - n_\beta \approx \frac{N}{(2I+1)} \frac{\hbar\omega_0}{kT} \left(m_\alpha - m_\beta\right). \quad (2.8)$$

This population difference leads to the equilibrium (longitudinal) magnetization:

$$M_z \propto \left(n_\alpha - n_\beta\right). \quad (2.9)$$

If a radiofrequency pulse is applied to the spin system at the Larmor frequency the spins will undergo a transition between the energy levels, and the spin population of the states changes. This results in a non-zero magnetization in the transverse plane orthogonal to the external magnetic field. When the radiofrequency pulse is switched off, the spins undergo relaxation processes and the magnetization returns to equilibrium. The time-dependent transverse magnetization can be detected in the NMR coil by means of Faraday's law: the time-varying magnetic flux induces a current (NMR signal) in the coil.

2.3 ^{2}H NMR Theory

^{1}H and ^{13}C NMR techniques can provide valuable information on the structure and dynamic behaviour of lipid bilayer and other biological membranes. However, their spectra are generally dominated by strong proton-proton and proton-carbon dipolar interactions, resulting in overlapping resonances which makes them difficult to analyze.

In deuterium NMR, some of the hydrogen atoms on the lipid acyl chains are replaced by deuterium. Nuclei with spin $I > 1/2$ have nonspherical charge distribution at the nucleus and, in the case of deuterium nucleus, possess an electric field quadrupolar moment, Q. The interaction of Q with the electric field gradient (efg) at the position of the nucleus gives rise to the quadrupolar interaction. ^{2}H NMR has several advantages over conventional proton and carbon NMR: (1) the spectrum of a deuterated lipid molecule consists of well-resolved peaks, which can be assigned to their respective carbons on the lipid chain. The overlapping between the resonances can be completely eliminated by selectively labeling the chains. (2) The magnetic moment of the deuteron is much smaller than that of the proton (the gyromagnetic ratios $\gamma_{\mathrm{D}}/\gamma_{\mathrm{H}} = 1/6.5$). Therefore in ^{2}H NMR the line broadening effect due to dipolar couplings is much weaker compared to proton NMR. (3) Deuterium NMR is sensitive to the molecular motions and orientations. For fast isotropic motions the observed spectrum is a single line, while for anisotropic motions each deuteron contributes a doublet due to the quadrupolar moment of the deuterium nucleus. The quadrupolar splitting, $\Delta\nu_{\mathrm{Q}}$, depends on several important molecular parameters: degree of anisotropy, average orientation of the carbon-deuteron bond with respect to the axis of symmetry of molecular motions (director axis), and the angle between the magnetic field and the director axis.

In studying lipid membranes one is generally interested in extracting information about the *structure* and *dynamical properties* of the bilayer. Deuterium NMR offers distinct advantages in this regard. The structural

information, mainly the average orientation of the hydrocarbon chains and the polar head-groups and the amplitudes of fluctuation of the lipid segments, can be measured through the quadrupolar splittings (and thus the order parameters). T_1 and T_2 relaxation times contain information about dynamics of the lipid bilayer; e.g. the rate of lateral diffusion of the lipid molecules can be obtained by means of Pulsed-Field-Gradient (pfg) NMR and measuring the T_1 and T_2 relaxation times. In ^{2}H NMR the dominant relaxation mechanism is due to the quadrupolar interaction and thus the interpretation of T_1 and T_2 in deuterium NMR is less ambiguous than in proton or carbon NMR.

An advantage of ^{2}H NMR over other techniques is that substituting deuterium for hydrogen has a minimal effect on the membrane, changing the transition temperature only slightly, thus it is a non-invasive technique. In electron paramagnetic resonance (EPR), for instance, one can easily measure the order parameter from the anisotropy of the hyperfine splitting. Also, the correlation times can be determined from the linewidth. However, the attachment of the bulky nitroxide spin label group, which perturbs the lipid system, is necessary in EPR [1]. Furthermore, other techniques require the use of external probe. For example, fluorescence microscopy requires the use of fluorescent probes that disturb phase boundaries [38].

It should be noted that ^{2}H NMR has its own drawbacks. The abundance of deuterium is very low in natural biological membranes therefore lipids must be deuterated synthetically, which is a non-trivial chemical process. The fact that

hydrocarbon chains can be labelled entirely or at a specific carbon position can be used to obtain precise information. Because of low sensitivity associated with

deuterium NMR considerable amount of deuterated lipid is required to gain an acceptable signal-to-noise ratio. Most deuterated lipids are commercially available but many at high cost (for example, chain-perdeuterated sphingomyelin only became commercially available after 2004 and currently is available from one company at a cost of ~ $4000 for 50 mg). Furthermore, when deuterated lipid molecules sample a heterogeneous membrane individual peaks in deuterium NMR spectrum broaden. In perdeuterated lipids, the line broadening imposes ambiguities in the interpretation of some results pertaining the structure and dynamics of the membrane. Selectively deuterated lipids, e.g. palmitoyl sphingomyelin labeled at C9 used in this thesis, can help resolve ambiguities but they are even more expensive to obtain and significantly increase data acquisition time.

2.3.1 ^{2}H NMR in the Absence of Motion

The Hamiltonian of a deuterium nucleus (spin $I = 1$) in a magnetic field $\vec{B}_0$ consists of Zeeman interaction, $\mathcal{H}_M$, and quadrupolar interaction, $\mathcal{H}_Q$. The total Hamiltonian can be written as

$$\mathcal{H} = \mathcal{H}_M + \mathcal{H}_Q. \tag{2.10}$$

The magnetic energy term, $\mathcal{H}_M$, describes the interaction between the nuclear magnetic dipole moment $\vec{\mu} = \gamma\hbar\vec{I}$ and the external magnetic field,

$$\mathcal{H}_M = -\vec{\mu} \cdot \vec{B}_0 = -\gamma \hbar I_z B_0. \tag{2.11}$$

This Hamiltonian gives rise to the energy described by (2.3) and the deuterium nucleus will have $m = +1, 0, -1$ energy levels. Given a pure Zeeman interaction at the nucleus, two transitions are observable as shown in Figure 2-3.

Nuclei with spin $I > 1/2$ have nonspherical charge distribution at the nucleus and, in the case of deuterium nucleus, possess an electric quadrupole moment, Q. The interaction of Q with the electric field gradient (efg), $\nabla \vec{E} = V$, at the position of the nucleus gives rise to the quadrupolar Hamiltonian $\mathcal{H}_Q$ with energy E_Q. Note that Q and V are second rank tensors and

$$Q_{\alpha\beta} = \int \left(3x'_\alpha x'_\beta - \delta_{\alpha\beta} r'^2\right) \rho(\vec{x}') d\tau', \tag{2.12}$$

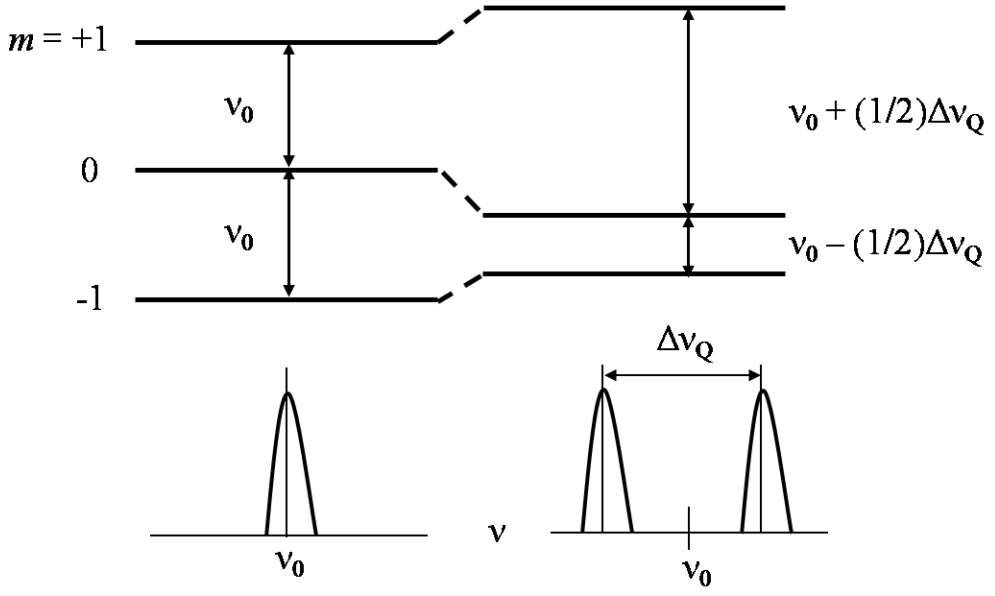

Figure 2-3: The energy level diagram for a spin-1 nucleus perturbed by the quadrupolar interaction at the nucleus.

where $\alpha, \beta = x, y, z$, $\rho(\vec{x}')$ is the charge density and τ' is the volume of the nucleus. The quadrupolar moment Q is equal to Q_{zz} and for deuterons $Q = 2.875 \times 10^{-27}\mathrm{cm}^2$. The quadrupolar Hamiltonian in its full form is

$$\mathcal{H}_Q = \frac{eQ}{4I(2I-1)}\left[V_0(3I_z^2 - I^2) + V_{\pm 1}(I_\mp I_z + I_z I_\mp) + V_{\pm 2}{I_\mp}^2\right], \qquad (2.13)$$

where e is the elementary charge, $I_\pm = I_x \pm iI_y$ are the usual raising and lowering operators, and the following abbreviations are used:

$$\begin{aligned} V_0 &= V_{zz}, \\ V_{\pm 1} &= V_{xz} \pm iV_{yz}, \\ V_{\pm 2} &= \frac{1}{2}\left(V_{xx} - V_{yy} + 2iV_{xy}\right). \end{aligned} \qquad (2.14)$$

The double subscripts indicate second derivative of the electrostatic potential V with respect to the molecular *x*, *y*, *z* axes.

The electrostatic field gradient is a symmetric and traceless tensor and can be transformed into the principal axis coordinate system in which $V_{xx} + V_{yy} + V_{zz} = 0$ and all off-diagonal terms are zero. Choosing *x*, *y*, *z* such that $|V_{zz}| \geq |V_{xx}| \geq |V_{yy}|$, the largest field gradient and the asymmetry parameter are defined as

$$\begin{aligned} eq &= V_{zz}, \\ \eta &= \frac{V_{xx} - V_{yy}}{V_{zz}}. \end{aligned} \qquad (2.15)$$

respectively, and it follows that $0 \leq \eta \leq 1$. In Eqn. (2.15) the parameter q is the second derivative of the electric potential at the nucleus. In the principal axis coordinate system of the efg the quadrupolar Hamiltonian reduces to

$$\mathcal{H}_Q = \frac{eQ}{4I(2I-1)} V_{zz} \left[(3I_z^2 - I^2) + \frac{1}{2}\eta (I_+^2 + I_-^2) \right]. \tag{2.16}$$

The Zeeman interaction at high fields (46.8 MHz in our case) dominates the quadrupolar interaction (≈ 200 kHz). Therefore the quadrupolar interaction can be treated as a small perturbation to $\mathcal{H}_M$. Also, quite often the efg asymmetry parameter is small ($\eta \leq 0.05$ for CD bonds) and can be neglected [33]. In this case, the electric field is approximately axially symmetric and V_{zz} is parallel to the CD bond axis. Employing first order perturbation theory, the energy levels of the total Hamiltonian becomes

$$E = -\gamma \hbar m B_0 + \frac{eQ}{4I(2I-1)} V_{zz} [3m^2 - I(I+1)]. \tag{2.17}$$

In the case of deuterium, $I = 1$, the three shifted energy levels for $m = +1, 0, -1$ are expressed as

$$E_{+1} = -\gamma \hbar B_0 + \frac{1}{4} eQV_{zz},$$

$$E_0 = -\frac{1}{2} eQV_{zz},$$

$$E_{-1} = \gamma \hbar B_0 + \frac{1}{4} eQV_{zz}. \tag{2.18}$$

These energies dictate the spin population of each state and the net macroscopic magnetization. The selection rule, $\Delta m = \pm 1$, restricts the allowed transitions to

$$h\nu_+ = E_{-1} - E_0 = \gamma\hbar B_0 + \frac{3}{4}eQV_{zz},$$

$$h\nu_- = E_0 - E_{+1} = \gamma\hbar B_0 - \frac{3}{4}eQV_{zz}, \qquad (2.19)$$

where $\nu_\pm$ are the frequencies of the lines arising from the quadrupolar interaction in a ^{2}H NMR spectrum. The spectrum is usually plotted such that it is centered on the Larmor frequency, $\omega_0 = \gamma B_0$. The two lines resulting from the two transitions thus appear symmetric on either side of zero with a frequency separation (quadrupolar splitting) of

$$\Delta\nu_Q = \nu_+ - \nu_- = \frac{3}{2}\frac{eQ}{h}V_{zz} = \frac{3}{2}\frac{e^2qQ}{h}. \qquad (2.20)$$

The term e^2qQ/h is known as the static quadrupolar coupling constant and is equal to 168 kHz for C-D bonds. The efg tensor is defined in terms of the molecular axes but the spin operators I_x, I_y, and I_z are quantized along the laboratory frame. Therefore it is necessary to rotate V_{ik} from the molecular based reference frame to the laboratory coordinate system. This is done by making successive rotations through Euler angles φ, θ, ξ [39]. A natural choice of basis is the spherical basis where the efg tensor can be expressed in terms of its irreducible components $V_m^{(2)}$, $(m = 0, \pm1, \pm2)$. In the principal axis coordinate system,

$$V_P^{(2,0)} = V_{zz},$$

$$V_P^{(2,\pm1)} = 0,$$

$$V_P^{(2,\pm 2)} = \sqrt{\frac{1}{6}}\left(V_{xx} - V_{yy}\right), \tag{2.21}$$

where subscript *P* in $V_P^{(2,m)}$ indicates that the efg is represented in the molecular reference frame. The transformation from one frame to another simply involves the Wigner rotation matrices $D^{(2)}_{m\,m'}(\varphi,\theta,\xi)$ [39],

$$V^{(2,m')} = \sum_{m=-2}^{2} D^{(2)}_{m\,m'}(\varphi,\theta,\xi)\, V_P^{(2,m)}. \tag{2.22}$$

In the case of the axial symmetry (the asymmetry parameter $\eta = 0$) transforming $V_P^{(2,0)}$ from the molecular frame to the lab frame yields

$$\begin{aligned} V^{(2,0)} &= \sum_{m=-2}^{2} D^{(2)}_{m\,0}(\varphi,\theta,0)\, V_P^{(2,m)} \\ &= V_{zz}\left[\frac{1}{2}\left(3\cos^2\theta\ -1\right)\right]. \end{aligned} \tag{2.23}$$

Substituting (2.23) into (2.20) shows that the quadrupolar splitting varies with θ as follows:

$$\Delta\nu_Q(\theta) = \frac{3}{2}\frac{e^2qQ}{h}\frac{1}{2}\left(3\cos^2\theta\ -1\right). \tag{2.24}$$

And, when the asymmetry parameter is not neglected appropriate elements of Wigner rotation matrices produce the general form of the quadrupolar splitting in the lab frame:

$$\Delta\nu_Q(\varphi,\theta) = \frac{3}{2}\frac{e^2qQ}{h}\left[\frac{1}{2}\left(3\cos^2\theta\ -1\right) + \frac{1}{2}\eta\sin^2\theta\cos 2\varphi\right], \tag{2.25}$$

where θ is the polar angle and φ is the azimuthal angle, that the molecular based frame makes with the static magnetic field. More explicitly, θ is the angle between the external magnetic field and the C−D bond for an oriented sample composed of C−D bonds in a single direction (Figure 2-4).

In multilamellar vesicles, there are random distributions of deuterium nuclear spin orientations. Assuming a uniform distribution of *N* nuclei over the surface of a sphere of radius *r*, the surface area density of nuclei is $N/4\pi r^2$. The number of nuclei oriented between θ and $\theta + d\,\theta$ with respect to $\vec{B}_0$ is

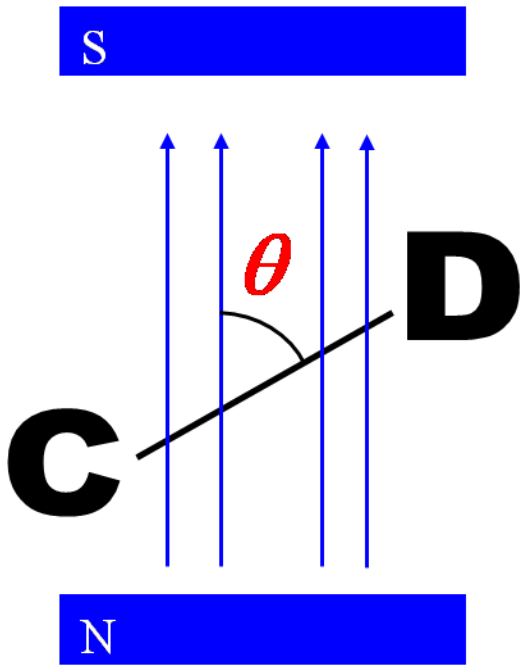

Figure 2-4: Orientation dependence: the angle between the external magnetic field and the C−D bond in the absence of motion.

$$dN = \frac{N}{4\pi r^2} 2\pi r^2 \sin\theta \, d\theta = \frac{N}{2} sin\,\theta \, d\theta. \quad (2.26)$$

The probability density is thus

$$p(\theta) = \frac{sin\,\theta}{2}. \quad (2.27)$$

It follows that $\theta = 90°$ is the most probable and $\theta = 0$ is the least probable orientation. The ^{2}H NMR spectrum which arises from a superposition of doublets separated by $\Delta\nu_Q(\varphi, \theta)$ and weighted by $p(\theta)$ is referred to as a Pake doublet as shown in Figure 2-5.

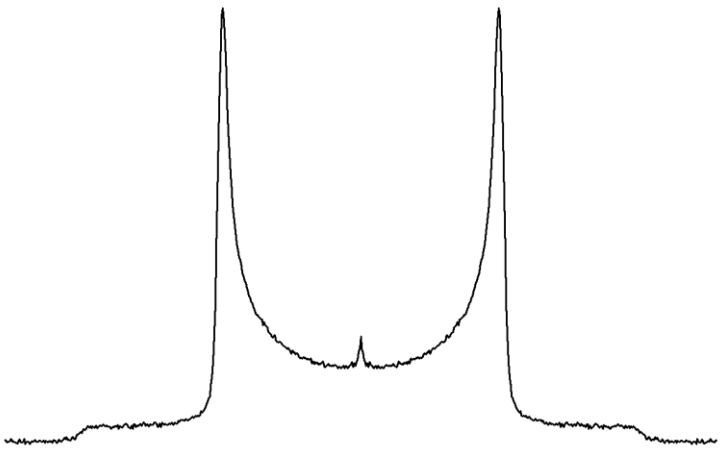

Figure 2-5: A Pake doublet.

^{2}H NMR spectrum of a sample showing all orientations of C−D bond in the magnetic field ($\eta = 0$). The most intense peaks correspond to 90^o orientation. (The *x*-axis shows the frequency)

2.3.2 ^{2}H NMR in the Presence of Motion

In general molecules are dynamic and, depending on the timescale of the motion, the dynamics may affect the quadrupolar splitting. In fact, deuterium NMR is a powerful tool for investigating anisotropic motion. The deuterium NMR spectrum for rapid isotropic motion consists of a single line, while for anisotropic motion each deuteron contributes a doublet due to the quadrupolar moment of the nucleus [33]. The doublet spacing $\Delta\nu_Q$ depends on the degree of anisotropy. In the liquid crystalline phase the chains can undergo angular excursions from the the molecular long axis. This is referred to as disordering and usually occurs by fluctuations in the carbon-carbon bonds, such as trans-gauche isomerisation. For molecular motions fast on the NMR timescale, 10^{-6}s, such as rotations about the director axis of lipids (axis of symmetry of the reorientational motion) with a period of about 10^{-9}s, only an average orientation of the C−D bond can be detected. A convenient measure of the degree of the fluctuations is the so-called order parameter S_{CD}:

$$S_{\mathrm{CD}} = \frac{\langle 3\cos^2\theta_{\mathrm{CD}} - 1\rangle}{2}, \tag{2.28}$$

where θ_{CD} is the angle between the C−D bond at a carbon position and the acyl chain axis of symmetry of the motions, and the angular brackets denote the time average. The motionally averaged powder spectra will be similar to the static ones, but the powder splitting is narrowed by a factor of S_{CD}. Rotation of an all-trans chain will narrow the spectrum by a factor of 2. The quadrupolar splitting in the presence of motion can be written as

$$\Delta\nu_Q(\varphi,\theta_n) = \frac{3}{2}\frac{e^2qQ}{h}|S_{CD}|\left[\frac{1}{2}(3\cos^2\theta_n - 1)\right], \qquad (2.29)$$

where θ_n and φ are the polar and azimuthal angles, respectively, of the magnetic field direction in terms of the principal axis coordinate system (PACS) of the time-averaged efg experienced by the nuclear spins. In other words, θ_n is the angle between the external magnetic field and the axis of symmetry of fast motions (the lipid long axis). Note that it is crucial to distinguish between the two angles, θ_{CD} and θ_n, as are depicted in Figure 2-6.

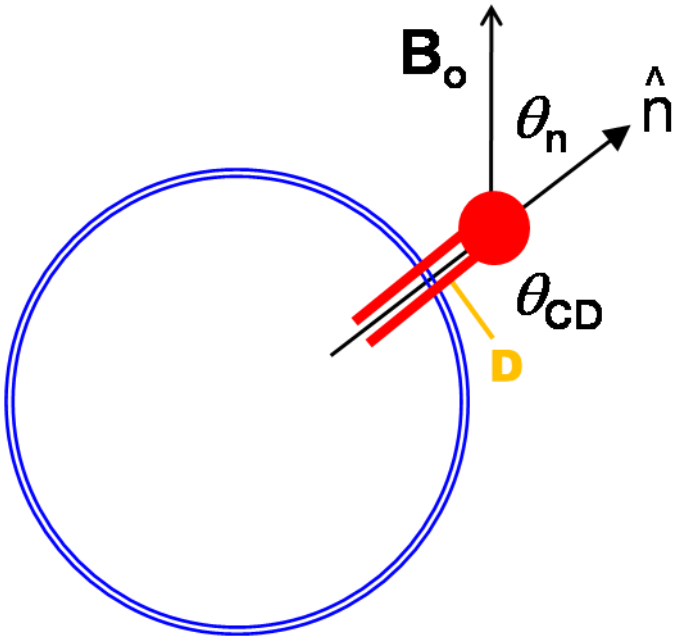

Figure 2-6: Orientational dependence, in the presence of axially symmetric motion.

θ_n represents the angle between the external magnetic field and the axis of symmetry of motion (the director axis of the lipid) while θ_{CD} is the angle between the C−D bond and the director axis.

The magnitude of the order parameter $|S_{\mathrm{CD}}|$ is determined by measuring the quadrupolar splitting at $\theta_{\mathrm{n}} = 90°$. The asymmetry parameter can be measured from the spectrum at $\theta_{\mathrm{n}} = 0°$ and $\varphi = 0°$ and $90°$. For systems where $\eta = 0$ the splitting collapses to 0 at the magic angle $\theta_{\mathrm{n}} = 54.74°$.

2.4 Relaxation Studies in ^{2}H NMR

2.4.1 Introduction to T_1 and T_2 Relaxation Times

"Spin-lattice" (T_1) and "spin-spin" (also called transverse) (T_2) relaxation times are very useful tools for investigating the dynamical properties of spin systems, in particular lipid membranes. NMR relaxation in membranes has been studied in detail [34, 40, 41, 42, 43, 44, 45]. Experiments described in this thesis deal exclusively with T_{2e}, the transverse relaxation time of a spin 1 system as measured by a two-pulse quadrupolar echo sequence. A general description of the two relaxation times T_1 and T_2 will be presented here and the rest of this section will be devoted to the orientation dependence of T_2 relaxation time as it pertains to the study of domains structure in multilamellar membranes.

Relaxation is the process by which the spins in a system evolve towards statistical equilibrium with the surroundings. The inter-molecular interactions in the spin system are time dependent and random since they are modulated by molecular motion. What drives the spins towards equilibrium is the random nature of these interactions. Equilibrium is the state in which the populations of the energy levels obey the Boltzmann distribution and there are only small coherences present in the system. This definition refers to an ensemble, a

system in which there are many spins present. Coherence arises when there is a particular relation between the phases of the wave functions of the spins in the sample. An example of such coherence is a detectable transverse magnetization in a spin system prepared along the *z*-direction at equilibrium.

In nuclear magnetic resonance it is essential to discriminate between the spin system and the lattice. The spin system is the ensemble consisting of all nuclear spins, which are characterized by the spin operators. When a transition between energy levels occurs in the spin system, there is an energy flow between the spin system and the surrounding. The source of this energy, associated with the molecular rotations and translations, is called the lattice. The spin-lattice relaxation is a mechanism whereby the nuclear spins come into equilibrium with the lattice, as if they were “informed” of its temperature. The amount of energy involved in an NMR transition is very small and the lattice is a large source, thus the temperature of the lattice is not affected significantly by the exchange of energy with the spin system and it can be considered to be an “infinite” bath.

When a static magnetic field is applied along the *z* axis, all the spins align with the field and the longitudinal magnetization M_z builds up. This equilibrium magnetization arises from the unequal population of the energy levels, which are split due to Zeeman interaction, and is proportional to the population difference. When the magnetization is moved off the equilibrium (e.g. tilted along the *x*-axis) by an additional field, M_z decreases. After the extra field is switched off, the system starts moving back towards the equilibrium and M_z builds up again. This

process involves an exchange of energy with the lattice and has a time constant or relaxation time T_1 associated with it. Based on the phenomenological theory of Felix Bloch (1946) the evolution of M_z towards equilibrium is exponential. A second relaxation mechanism occurs in the system where the spins start losing their phase coherence, while the magnetization is still on the transverse plane. The coupling between the nuclear spins allows rapid energy transfer from one spin to another, leading to the establishment of a thermal equilibrium inside the spin system itself in a time much shorter than T_1, and at a temperature that can be completely different from that of the lattice. This time is referred to as the spin-spin relaxation time T_2.

In deuterium NMR the dominant spin-lattice interaction that leads to T_1 relaxation is the coupling of the electric field gradient with the quadrupolar moment of the nucleus. T_2 relaxation in this case is due to thermally driven fluctuations in the quadrupolar splitting, causing the loss of phase coherence in transverse nuclear magnetization. The general theory of spin relaxation [36] describes how these processes arise from fluctuations in spin-dependent interactions due to various motions present in the system. The relaxation rates can be conveniently expressed in terms of the *reduced spectral densities,* $j(\omega)$*,* of the correlation functions. The *correlation functions* are characterized in turn by a spectrum of correlation times τ_c [34, 36]. For fluctuations with $\tau_c \ll \tau_s$ the following expressions are obtained:

$$\frac{1}{T_1} = C_1[a_1\, j_1(\omega_0) + a_2\, j_2(2\omega_0)],$$

$$\frac{1}{T_2} = C_2[b_0\, j_0(0) + b_1\, j_1(\omega_0) + b_2\, j_2(2\omega_0)], \tag{2.30}$$

where C_1 and C_2 are coupling constants for the interaction in question, a_i and b_i are proportional to the mean-squared amplitude of the fluctuations at the appropriate frequencies, and ω_0 is the Larmor frequency. It is evident from the above equations that T_1 relaxation processes are sensitive to fluctuations at $\omega = \omega_0$ and $\omega = 2\omega_0$, while T_2 relaxation rate has contributions from spectral densities evaluated at zero frequency, in addition to those evaluated at ω_0 and $2\omega_0$.

2.4.2 Orientation Dependence of T_2

The following is a summary of the "phenomenological theory" of the dependence of deuterium T_2 relaxation rates on θ_n, the angle between the membrane surface normal and the external magnetic field. The theory was first developed by Myer Bloom [46, 47].

The ^{2}H NMR spectra of bilayer membranes in the fluid phase exhibit axial symmetry with respect to the bilayer normal so that the averaging of the quadrupolar interaction by fast molecular motions, on the "NMR time scale", gives rise to a quadrupolar splitting 2ω which depends only on the angle θ between $\vec{B}_0$ and bilayer normal. More precisely, approximating the electric field gradient (efg) as an axially symmetric tensor about the C–D bond, one can express the quadrupolar splitting in the following form

$$\omega = \omega_{\mathrm{Q}} P_2(\cos\theta_n) S_{\mathrm{CD}}, \tag{2.31}$$

where $\omega_{\mathrm{Q}} \approx 2\pi \times 1.26 \times 10^5 s^{-1}$, $P_2(x) = (3x^2 - 1)/2$ is a Legendre polynomial, and the orientational order parameter $S_{\mathrm{CD}} = \langle P_2(\cos\theta_{\mathrm{CD}})\rangle_{\mathrm{fast\ motions}}$ is a measure of the averaging of the quadrupolar interaction due to modulation of the angle β between the C–D bond vector and bilayer normal by fast molecular motions.

The motions that give rise to this motional averaging are also responsible for spin-lattice and spin-spin relaxation. T_1 gives information on relatively fast dynamical molecular processes having correlation times in the vicinity of approximately 10^{-9} s. Fast motions that contribute to T_1 also contribute to T_2 so $T_2 \leq T_1$ is always satisfied. Slow motions which satisfy the condition described in Abragam [4] as "adiabatic motions", i.e. $(\omega_0\tau_c)^2 \gg 1$, contribute appreciably to T_2, but not to T_1. Therefore, in the presence of adiabatic motions the condition $T_2 \ll T_1$ holds.

A study of the dependence of ${T_1}^{-1}$ on ω_0 in DMPC extending to very low magnetic fields [48] shows that the correlation times fall into two classes, those associated with relatively fast motions having values $\tau_c \leq {\tau_c}^f \approx 10^{-8} s$ that contribute to the field dependence of ${T_1}^{-1}$ only at high fields ($\omega_0 \geq 2\pi \times 10^7 s^{-1}$) and those associated with relatively slow motions having values of $\tau_c \geq {\tau_c}^s \approx 10^{-6} s$ that contribute appreciably to ${T_1}^{-1}$ only at very low magnetic fields. Based on this clumping of the correlation times into long and short categories the transverse relaxation can be written in terms of two distinct relaxation rates:

$$\frac{1}{T_2} = R_2^f + R_2^s, \tag{2.32}$$

where R_2^f is assumed to have its origin in motions satisfying $\tau_c \leq {\tau_c}^f$ and so evaluated from T_1 measurements, especially from the dependence of T_1 on ω_0. The second relaxation rate, R_2^s, can be characterized as the *adiabatic* contribution of the relatively slow motions to the transverse relaxation rate.

A general theory for the orientation dependence of longitudinal and transverse relaxation rates for spin = 1 systems, valid within the Redfield approximation, has already been established in [43]. For axially symmetric motions, the following form is obtained:

$$\frac{1}{T_i} = A_{0i} + A_{2i}P_2(\cos\theta_n) + A_{4i}P_4(\cos\theta_n), \qquad (2.33)$$

where the coefficients $A_{0i}, A_{2i}, \text{and } A_{4i}$ depend on ω_0, the correlation times, the orientational order parameters and the thermodynamic variables required to characterize the system.

It is assumed that the *fast molecular motions* discussed above lead to a quadrupolar splitting 2ω given by equation (2.31) in terms of S_{CD} and θ_n. The slower motions modulate ω adiabatically. It is also assumed that the adiabatic motions are divided into two classes, those that modulate θ_n and S_{CD} independently, with *effective correlation times* $\tau_{c\theta_n}$ and τ_{cA}, respectively. These motions are associated with:

i. Fluctuations in local curvature that give rise to changes in θ_n without any significant changes in bilayer thickness, and, consequently, without changes in S_{CD}. Motions capable of such fluctuations are *diffusion* on

smooth-curved membrane surfaces [42], thermally induced *surface undulations* [49], and *order director fluctuations*.

ii. Fluctuations in bilayer thickness x, or equivalently the membrane area A, that give rise to fluctuations in S_{CD} without any significant changes in θ_n.

It should be noted that the assumption of independence of the two types of fluctuations has not been justified on theoretical grounds. It is possible that the actual modes responsible for the adiabatic motions involve a coupling between membrane curvature and thickness fluctuations. A more rigorous theory of adiabatic motion might be established based on the assumption of codependence as a first approximation.

In several studies, explicit connections between x, A, and S_{CD} have been established for acyl chains (e.g. [6]). Using thermodynamic considerations one can relate the mean squared fluctuations $\langle(\delta\theta_n)^2\rangle$ and $\langle(\delta A)^2\rangle$ to measurable properties of membranes. These two types of fluctuations are governed, under some conditions, by the curvature energy κ_c [49] and the isothermal area compressibility $(1/K_a)$ [7, 50], respectively:

$$\langle(\delta\theta_n)^2\rangle = \langle{\theta_n}^2\rangle - \langle\theta_n\rangle^2 = \frac{k_B T}{4\pi\kappa_c}\ln\frac{\lambda_M}{\lambda_m}, \tag{2.34}$$

$$\langle(\delta A)^2\rangle = \langle A^2\rangle - \langle A\rangle^2 = \frac{k_B T}{K_a}, \tag{2.35}$$

where λ_M and λ_m in (2.34) are the maximum and minimum wavelengths for curvature fluctuation modes, respectively, and K_a is defined in terms of the fractional variation of area with surface tension σ as $1/K_a = (1/A)(\partial A/\partial\sigma)_T$.

Expressions analogous to equation (2.35) are obtained for volume fluctuations in three dimensional systems.

The thermal fluctuations in θ_n and A, given by equations (2.34) and (2.35) respectively, give rise to small renormalization of the quadrupolar splitting, which may be ignored for present purposes. For example curvature fluctuations lead to a reduction in S_{CD} by $\langle P_2(\cos\theta_{\mathrm{CD}})\rangle \approx 1-(3/2)\langle(\delta\theta)^2\rangle$. From the values used in [49] of $\kappa_c \approx 5\times10^{-13}\mathrm{ergs}$ and $\lambda_M/\lambda_m \approx 20$, equation (2.34) gives $\langle(\delta\theta_n)^2\rangle \approx 1.8\times10^{-2}$ at room temperature. Similarly, the typical value of $K_a \approx 200\ \mathrm{dynes/cm}$ for fluid membranes [51], gives $k_BT/K_a \approx 2\mathring{A}^2 \ll \langle A\rangle^2$, also leading to small changes in the quadrupolar splittings for practical cases.

If these motions give rise to uncorrelated fluctuations in the quadrupolar splitting they will result in adiabatic relaxation given by the classical formula [36]. The transverse relaxation rate arising from a fluctuating interaction can be characterized by a second moment ΔM_{2i} and correlation time τ_{ci} where the condition $\Delta M_{2i}\tau_{ci}^2 \ll 1$ is satisfied,

$$
\begin{aligned}
R_2^S &= \sum_i R_{2i}^S = \sum_i \Delta M_{2i}\tau_{ci} \\
&= (\delta\omega/\delta\theta_n)_A^2\,\langle(\delta\theta_n)^2\rangle\,\tau_{c\theta_n} + (\delta\omega/\delta A)_{\theta_n}^2\,\langle(\delta A)^2\rangle\,\tau_{cA} \\
&= \omega_{\mathrm{Q}}^2\left\{9S_{\mathrm{CD}}^2\sin^2\theta_n\cos^2\theta_n\langle(\delta\theta_n)^2\rangle\,\tau_{c\theta_n} + [P_2(\cos\theta_n)]^2\left[(\delta S_{\mathrm{CD}}/\delta A)_{\theta_n}\right]^2\langle(\delta A)^2\rangle\,\tau_{cA}\right\} \\
&= B\sin^2\theta_n\cos^2\theta_n + C[P_2(cos\,\theta_n)]^2. \qquad (2.36)
\end{aligned}
$$

Using equations (2.34) and (2.35), coefficients *B* and *C* can be written as

$$B = 9\left(\omega_{\mathrm{Q}} S_{\mathrm{CD}}\right)^2 \frac{k_B T}{4\pi\kappa_c} \ln\left(\frac{\lambda_M}{\lambda_m}\right) \tau_{c\theta_n}, \tag{2.37}$$

$$C = \left[\left(\partial S_{\mathrm{CD}}/\partial A\right)_{\theta_n}\right]^2 \left(\frac{k_B T}{K_a}\right) \tau_{cA}. \tag{2.38}$$

Expressing $\sin^2\theta_n \cos^2\theta_n$ and $[P_2(\cos\theta_n)]^2$ in equation (2.36) in terms of Legendre polynomials, we can return to equation (2.33). If in the underlying system there exist fast, nearly-isotropic motions, that also contribute to T_1 processes, a constant term can be added to the orientation dependence of T_2:

$$\frac{1}{T_2} = A + B\sin^2\theta_n \cos^2\theta_n + C[P_2(\cos\theta_n)]^2. \tag{2.39}$$

Chapter 3: Materials and Methods

3.1 Materials

Synthetic deuterated lipids used in this work were purchased from Avanti Polar Lipids (Alabaster, AL). These were chain-perdeuterated lipids, including N-palmitoyl (D31)-D-erythro-sphingosylphosphorylcholine (PSM-d31) and 1-palmitoyl,2-palmitoyl (D31)-*sn*-glycero-3-phosphocholine (DPPC-d31 (sn-2 chain perdeuterated)), and selectively deuterated sphingomyelin, labelled at C9 of the N-linked palmitoyl chain. Cholesterol and deuterium-depleted water (DDW) were obtained from Sigma-Aldrich Canada (Oakville, ON). Deuterium-depleted water (DDW) was from Sigma-Aldrich Canada.

The solvents used for chromatography were chloroform ($CHCl_3$), methanol (MeOH), and distilled water (H_2O). Fresh deuterated chloroform ($CDCl_3$) and methanol (CD_3OD) in ampoules were used for proton (^1H) NMR. Benzene and methanol were used for lyophilization. All solvents were “spectro” grade and were obtained from “Science Stores” at Simon Fraser University.

3.2 Multilamellar Vesicle Preparation

Lipid/cholesterol multilamellar dispersions (MLDs) were prepared by adding cholesterol concentrations of 0, 2.6, 5, 8, 10.1, 12, 16, 18, 20.5, 25, 29.9, 40, 45 mole% to DPPC-d31 and 0, 2.5, 5.4, 8.5, 11, 14.5, 17.5, 20, 22.5, 25, 28, 31.5, 35, 40 mole% to PSM-d31. Multilamellar vesicles (MLV) have an onion-like

structure in which each lipid bilayer is separated by a water layer. MLVs are made following standard techniques. Due to difficulties in weighing out small masses stock solutions were used to add appropriate amount of cholesterol to the lipids. Since enough amount of DPPC-d31 was available each DPPC-d31/cholesterol MLD was made separately, using a fresh batch of the lipid. Different procedure was used to make PSM-d31/cholesterol and PSM-d2/cholesterol samples, due to the high cost of these lipids: each PSM-d31/ or PSM-d2/cholesterol MLD was made by adding an appropriate amount of cholesterol to the previous sample (recovered from NMR tube), starting from pure lipids.

The protocol for making DPPC-d31/cholesterol samples is as follows:

i. Appropriate amount of cholesterol is added to DPPC-d31, using stock solution. Large quantity of cholesterol is dissolved in benzene:methanol 80:20 (v/v) and the required amount is separated by volume and is added to the lipid. The lipid mass was approximately 50 mg for each sample.

ii. The mixture in solvent is lyophilized until dry. Benzene:MeOH 80:20 is used to thoroughly mix the lipid and cholesterol. The mixture is then freeze-dried (lyophilized) to remove the solvent by sublimation, preventing the demixing that can occur during evaporation.

iii. Sample is hydrated in deuterium depleted water so that lipid molecules self-assemble into the bilayer structure, with cholesterol molecules in place. The hydration is done in excess water so that the behavior of the system is independent of the amount of solvent. This is important since

hydration effects have been observed in palmitoyl sphingomyelin [31]. 550 μL of DDW is used to ensure enough hydration while just filling up the space in the NMR tube that is directly covered by the coil.

iv. The sample undergoes a freeze-thaw-vortex process five times between -196^{o}C and ~ 60^{o}C. The thaw temperature must be sufficiently above the main phase transition temperature of the lipid, and below the boiling point of DDW so that all lipids in the sample become hydrated in the fluid phase. In practice, this is achieved by dipping the sample in liquid nitrogen followed by leaving it in the water bath for ~10-15 minutes, and then mixing it thoroughly with a vortex mixer for ~1 minute.

The protocol for making PSM-d31/cholesterol and PSM-d2/cholesterol samples is as follows:

i. Add appropriate amount of cholesterol, using stock solution, to pure lipids to make the first samples. There were approximately 50 mg of PSM-d31 and 25 mg of PSM-d2 to begin with.

ii. After finishing the experiments, transfer this “old” sample from the NMR tube into the scintillation vial in which the sample was made, using distilled water.

iii. Lyophilize the sample in the scintillation vial.

iv. Dissolve the sample in solvent by adding benzene:MeOH 80:20 to the scintillation vial, and then lyophilize the sample again. This step is added

to make sure that the residual water molecules, bound to the lipid head-groups, are removed from the sample.

v. Weigh the scintillation vial. Determine the amounts of lipid and cholesterol in the vial and calculate appropriate amount of cholesterol to add to make a new sample.

vi. Add appropriate amount of cholesterol using stock solution.

vii. Lyophilize, hydrate and freeze-thaw-vortex as explained above.

3.3 ^{1}H NMR to Check Sample Composition

^{1}H solution NMR (at 300 K) in methanol-d_4 was used to test concentrations of cholesterol by integrating non-composite peaks arising from the two components. Specifically, the peaks used were: the methyl peak at 0.74 ppm and the H-6 peak at 5.36 ppm for cholesterol; the glycerol-c2 peak at 5.26 ppm and the γ-(CH3)3 peak at 3.24 ppm for DPPC; the sphingosine C2 proton resonance at 5.47 ppm and the γ-(CH3)3 peak at 3.24 ppm for sphingomyelin. All chemical shifts were measured with respect to the methanol-d_4 methyl peak at 3.32 ppm. Assignments of cholesterol and DPPC peaks are from Muhr *et al.* [52] and Peng *et al.* [53] respectively. The actual concentrations of the prepared samples deviate only slightly from the nominal values, e.g. the nominal concentration of 5 mole% in PSM-d31/cholesterol MLD turned out to be 5.4 ± 0.5 mole%.

3.4 Thin Layer Chromatography

Thin layer chromatography (TLC) is used to check for any sign of degradation in the samples. A Lipid/cholesterol sample is loaded onto silica TLC plates and the solvent runs up the plate via capillary action. Depending on the solvent, different components move up the plate at different rates. For example, in PSM/cholesterol and DPPC/cholesterol systems cholesterol moves up faster than the lipid. The TLC plate is then developed using iodine vapors to visualize the presence of lipid and cholesterol as Iodine reacts with double bonds in the lipids and turns the lipid to a yellow or brown color. If there is any degradation in a lipid/cholesterol binary system, there will be more than two spots on the TLC plate. Several samples were checked for degradation after completion of the NMR experiments by TLC, eluting with $HCCl_3$/MeOH/H_2O 65:25:4 v/v. These include every other sample, in the case of PSM-d31/cholesterol, and every third sample, in the case of DPPC-d31/cholesterol. The ^2H NMR experiments took nearly 3-4 days per DPPC-d31/cholesterol samples, 4-10 days for PSM-d31/cholesterol samples, and 2-4 weeks for PSM-d2/cholesterol samples, but no degradation of any of the samples could be detected by TLC. Also, no sign of degradation was evident in the ^1H NMR spectra.

3.5 ^2H NMR

^2H NMR experiments were performed immediately after a sample was hydrated (fresh). The sample was heated from 25 to 70^oC and at each temperature was allowed to equilibrate for at least 20 minutes before data acquisition. The data was collected from low to high temperatures. At the end of data acquisition

(highest temperature), the reproducibility of the data was checked by repeating the experiment at the starting temperature (25^{o}C). Hysteresis was not observed in lipid/cholesterol samples studied in the work presented in this thesis, indicating that the results are independent of the thermal history of the sample. Hysteresis has been observed in the study of other lipid mixtures [54].

^{2}H NMR experiments were performed using a 300 MHz (7.0 T) Oxford Magnet with a locally built spectrometer operating at 46.8 MHz using the quadrupolar echo technique [55]. The typical spectrum resulted from *n* repetitions of the two-pulse sequence with 90^{o} pulse lengths of 3.95 μs, an interpulse spacing of 40 μs, and a dwell time 2 *μ*s. The delay between acquisitions was 300 ms and data were collected in quadrature with 8-CYCLOPS phase cycling. Signal averaging was performed over *n* = 10,000–40,000 scans for perdeuterated lipids and *n* = $0.5 \times 10^{6} - 1.0 \times 10^{6}$ scans for selectively labeled sphingomyelin. In samples with perdeuterated lipids, the spin-spin relaxation time, T_{2e}, was measured by varying the interpulse spacing and taking the initial slope of the echo peak signal versus echo time. In the case of PSM-d2/cholesterol samples T_{2e} was measured from the frequency domain spectrum for all orientations. For PSM-d31/cholesterol and DPPC-d31/cholesterol samples the interpulse spacing was varied from 40 to 100 *μ*s in steps of 10 *μ*s, whereas for PSM-d2/cholesterol samples this parameter was varied from 100 to 250 *μ*s in steps of 50 *μ*s.

3.5.1 Quadrupolar Echo

The free induction decay (FID) following a 90^{o} pulse decays fairly rapidly due to dephasing of the spins. The receiver electronics has a dead-time during which it cannot detect the whole FID and the first few points are lost, resulting in a distorted spectrum. The quadrupolar echo pulse sequence is used to refocus the spins such that the full FID, neglecting relaxation effects, is reproduced as an "echo" long after the receiver dead-time. The Fourier transform of this echo yields an undistorted spectrum. The two pulse sequence of the quadrupolar echo is 90_y – τ – 90_x – τ – echo. Here, a summary of the physics describing the quadrupolar echo is presented, following a density matrix treatment by Solomon [56].

The calculations presented here will be made in a frame rotating at the Larmor frequency $\omega_0 = \gamma B_0$ with the *z*-axis along the magnetic field B_0. The quadrupolar interaction leads to a frequency shift for a given nucleus, which is to first order

$$H_{\mathrm{Q}} = -a\hbar I_z^2, \tag{3.1}$$

where $a = 3e^2qQ/4\hbar$ is the value of the quadrupolar perturbation. Applying a rotating magnetic field B_1 along the *y* axis of the rotating frame for a short time Δt such that

$$\varphi = \gamma B_1 \Delta t, \tag{3.2}$$

can be described as the application of an operator R acting on the spin wave function and transforming any spin operator A into RAR^{-1}. If B_1 is large enough

(i.e. $\gamma B_1 \gg a$) then R is simply a rotation and has the explicit form $R = \exp(-i\varphi I_y)$.

The density matrix, ρ, can be used to conveniently formulate the state of the spin system right after the application of a pulse and the evolution of the system at a time *t* after the pulse. If the spin system is described by a density matrix $\rho(t)$ at a time t, the amplitude of the signal induced in the sample coil is proportional to

$$S(t) = \mathrm{Tr}[\rho(t)\, I_+], \tag{3.3}$$

where $I_+ = I_x + iI_y$. Before we apply any rf pulse, the spin system is in thermal equilibrium and applying an rf pulse will put the system off equilibrium. First, we find out the state of the spin system, $\rho(0)$, after the application of a 90°_y pulse with large rf field ($\gamma B_1 \gg a$). The density matrix of the spin system in thermal equilibrium is

$$\begin{aligned} \rho_{eq} &= \exp(-\gamma\hbar B I_z/kT) \\ &\cong 1 - (\gamma\hbar B I_z/kT). \end{aligned} \tag{3.4}$$

The first term of equation (3.4) can be dropped since it gives a signal $\mathrm{Tr}[\, I_+] = 0$. The useful part of the density matrix ρ_{eq} before we apply any rf field is then proportional to I_z:

$$\rho_{eq} \propto I_z. \tag{3.5}$$

Immediately after the 90_y pulse, the density matrix at $t = 0$ is thus

$$\rho(t = 0) = R_y \rho_{eq} {R_y}^{-1}$$

$$= \exp\left(-i\frac{\pi}{2}I_{\mathrm{y}}\right)\, I_{\mathrm{z}}\, \exp\left(i\frac{\pi}{2}I_{\mathrm{y}}\right),$$

$$\therefore \rho(0) = I_{\mathrm{x}}. \tag{3.6}$$

The evolution of the density matrix in the external magnetic field, after the application of the first pulse, will then be described as

$$\rho(t) = \exp(-iaI_{\mathrm{z}}^2 t)\, I_{\mathrm{x}}\, \exp(iaI_{\mathrm{z}}^2 t), \tag{3.7}$$

and the corresponding signal amplitude (free precession signal) is

$$S(t) = \mathrm{Tr}[\exp(-iaI_{\mathrm{z}}^2 t)\, I_{\mathrm{x}}\, \exp(iaI_{\mathrm{z}}^2 t)\, I_{+}]. \tag{3.8}$$

Expanding (3.8), one obtains

$$S(t) = \sum_{m} \langle m|I_{\mathrm{x}}|m+1\rangle \times [I(I+1) - m(m+1)]^{1/2} e^{ia(2m+1)t}. \tag{3.9}$$

The application of the second rf pulse (90_{x}) at time $t = \tau$ will rotate the density matrix, $\rho(\tau)$, by the unitary operator $R_{\mathrm{x}} = e^{-i\varphi I_{\mathrm{x}}}$. Thus, right after the second pulse we have

$$\begin{aligned}\rho'(\tau) &= R_{\mathrm{x}}\, \rho(\tau)\, {R_{\mathrm{x}}}^{-1} \\ &= R_{\mathrm{x}}\, \exp(-iaI_{\mathrm{z}}^2 \tau)\, I_{\mathrm{x}}\, \exp(iaI_{\mathrm{z}}^2 \tau)\, {R_{\mathrm{x}}}^{-1}.\end{aligned} \tag{3.10}$$

The density matrix will then evolve in the external magnetic field and the signal detected after the 90_{x} at $t > \tau$ becomes

$$\begin{aligned}S(t) &= \mathrm{Tr}\{\exp[-iaI_{\mathrm{z}}^2(t-\tau)]\, \rho'(\tau)\, \exp[iaI_{\mathrm{z}}^2(t-\tau)]\, I_{+}\} \\ &= \mathrm{Tr}\begin{Bmatrix}\exp[-iaI_{\mathrm{z}}^2(t-\tau)]\, R_{\mathrm{x}}\, \exp(-iaI_{\mathrm{z}}^2\tau)\, I_{\mathrm{x}}\, \times \\ \exp(iaI_{\mathrm{z}}^2\tau)\, {R_{\mathrm{x}}}^{-1}\, \exp[iaI_{\mathrm{z}}^2(t-\tau)]\, I_{+}\end{Bmatrix}.\end{aligned} \tag{3.11}$$

Expansion of (3.11) gives

$$S(t) = \sum_{m,m',m''} \langle m|R_{\mathrm{x}}|m''\rangle\langle m''|I_{\mathrm{x}}|m'\rangle\langle m'|\, {R_{\mathrm{x}}}^{-1}|m+1\rangle$$

$$\times [I(I+1) - m(m+1)]^{1/2} e^{ia\left[(2m+1)(t-\tau) - \left(m''^2 - m'^2\right)\tau\right]}. \qquad (3.12)$$

Now, if for particular values of t, $S(t)$ is independent of a, signals of all the nuclei are "in phase" and we get an echo. This condition happens in equation (3.12) for

$$\frac{t-\tau}{\tau} = \frac{m''^2 - m'^2}{2m+1} = \alpha. \qquad (3.13)$$

For deuterium nucleus $I = 1$, thus $S(t)$ becomes zero and there is no signal when $m = I = 1$. Therefore allowed values for m are $m = 0, -1$. Also, the value $m''^2 - m'^2 = 0$ gives a time-independent signal. The only non-vanishing matrix elements of I_{x} in equation (3.12) are obtained for $m'' - m' = \pm 1$. Therefore, the allowed values of (m, m', m'') are $(0,0,\pm 1)$ and $(-1,\pm 1,0)$, which give the value $\alpha = 1$ in equation (3.13), indicating the echo occurs at $t = 2\tau$.

3.5.2 Repetition Time (TR)

Repetition time is the time between taking successive scans. In order to gain higher signal to noise ratio (SNR) it is advantages to use as short a TR as possible and thereby collect more data, in a given amount of time. However, TR should be long enough to allow for spins to fully relax before the next pulse is scanned. If TR is shorter than spin-lattice relaxation time (T_1) the bulk magnetization does not fully return to equilibrium (z-axis) and signal is lost in the successive scans. Spins in gel and liquid crystalline phases have relatively short

T_1 relaxation times, whereas, spins with more motional restriction, such as those in crystalline solids, have longer T_1 and therefore require a longer time to relax.

In the experiments presented in this thesis, no crystalline solid phase has been observed and, thus, a TR of 300 ms seemed sufficiently long. The data acquired with this repetition time is compared with those obtained using TRs of 20 s and 50 s to characterize possible signal loss due to a shorter TR. Experiments carried out on the DPPC-d31/cholesterol and PSM-d31/cholesterol systems show that the signal amplitudes (echo-height) for data acquisition using long TR (20 s and 50 s) and short TR (300 ms) differ by 3% or less. This difference in echo-height is due to the longer relaxation time of methyl group at the end of the acyl chain.

3.5.3 Number of Scans

There is typically 40-50 mg of deuterated lipid in each of the perdeuterated samples. In the case of PSM-d31 the successive samples are made by adding cholesterol to the previous sample. Since the protocol (described in section 3.2) for making a new sample involves several weighing and transferring of the sample there is a gradual loss of perdeuterated PSM, and the SNR decreases. Increasing the number of scans can compensate for this loss since $\mathrm{SNR} \propto \sqrt{\mathrm{Number\ of\ Scans}}$. In the case of selectively deuterated sphingomyelin (PSM-d2) the number of deuterons per lipid molecule is 2, and there is only ~25 mg of lipid in each sample. Therefore, in order to obtain similar SNR as in the samples with perdeuterated lipid, the number of scans has to be increased by a factor of ~900. Typical number of scans for a sample with ~50 mg perdeuterated lipid is ~20000,

which takes 100 minutes to acquire data. Since it is not practical to spend 900×100 minutes to collect one spectrum per setting for each PSM-d2/cholesterol samples, we limited our SNR to maximum 1×10^6 scans. However, to improve the SNR in these samples ^{2}H NMR spectra are symmetrized by setting the imaginary data to zero.

3.5.4 Quadrature Detection

The electronics cannot handle the large frequencies (~ 10^6 Hz) associated with solid state NMR. During data acquisition, the signal is downshifted by subtracting off a reference frequency (typically the Larmor frequency) so that an offset is detected. Quadrature detection provides a means to distinguish between positive and negative offset frequencies and permits the phasing of the spectrum to obtain pure absorption mode lineshapes. In ^{2}H NMR experiments quadrature detection is attained by routing the signal from the receiver through two different phase sensitive detectors (PSDs), 90^o out of phase, to produce a $\cos(\omega t)$ modulated signal, commonly called the real signal, and a $\sin(\omega t)$ modulated signal, which is commonly called the imaginary signal. Linear combination of these two signals produces a complex signal, the Fourier transform of which produces a resonance line at a single frequency that can be phased to give a pure absorption mode lineshape.

3.5.5 Phase Cycling

8-CYCLOPS (CYCLically Ordered Phase Sequence) phase cycling [57] removes spectral artifacts created by non-ideal conditions in the NMR electronics. These

artifacts are caused by imperfections in the 90^{o} pulses, DC offset, gain mismatch, and phase error in the receiver amplifiers. Phase cycling eliminates these artifacts by changing the transmitter phase in the sequence 0, 90, 180, 270. This involves alternating pulses used in the sequence between (x,y), (y,-x), (-x,-y), (-y,x), (x,-y), (-y,-x), (-x,y), (y,x). The computer combines the real and imaginary spectra from each channel for each step of the sequence to generate the final phase cycled spectrum. In this process the signals add, but the artifacts cancel.

Chapter 4: Analysis

4.1 Moment Analysis

The *n*th moment of a symmetric ^{2}H NMR spectrum is defined as

$$M_n = \frac{1}{A}\int_0^\infty \omega^n f(\omega) d\omega, \tag{4.1}$$

where $f(\omega)$ is the function describing the spectral lineshape, ω is the angular frequency shift from Larmor frequency, and

$$A = \int_0^\infty f(\omega) d\omega, \tag{4.2}$$

is half the area of the spectrum. The first moment (M_1) measures the average spectral width and therefore tells us how broad a spectrum is. Since spectra are centered on the Larmor frequency, each pair of deuterons gives rise to a Pake doublet that extends symmetrically on both negative and positive frequency shifts. We calculate M_1 by averaging over both sides of the spectrum,

$$M_1 = \frac{1}{A}\int_{\omega=-x}^{x} |\omega| f(\omega) d\omega, \tag{4.3}$$

$$A = \int_{\omega=-x}^{x} f(\omega) d\omega.$$

In calculating M_1 from the experimental spectrum, we choose x so that the frequency range $-x$ to x contains the entire spectrum and the spectral intensities at $\omega = x$ and $\omega = -x$ (shoulders of the spectrum) disappear into the baseline,

and integrate over each side of the spectrum separately and add the absolute values of the two.

4.2 Order Parameters

The bilayer structure imposes constraints on lipid acyl chain motion, leading to a characteristic profile in the orientational order along the chain. Carbons near the head group undergo more restricted motions and exhibit a higher degree of order, whereas those closer to the end of the chain, i.e. close to the methyl group, have much more freedom and are characterized by lower order. In other words, the local order parameter is a measure of the local "rigidity" of the lipid chain.

The local orientational order parameter of deuterons on the *i*-th carbon, $S_{\mathrm{CD}}(i)$, is defined by

$$S_{\mathrm{CD}}(i) = \frac{\langle 3\cos^2\theta_i - 1\rangle}{2}, \tag{4.4}$$

where θ_i is the angle between the C−D bond at the *i*-th carbon position and the acyl chain axis of symmetry of the motions, and the angular brackets denote the time average. S_{CD} is proportional to the quadrupolar splitting, $\Delta\nu_{\mathrm{Q}}$, and can therefore be measured from the ^{2}H NMR spectra:

$$\Delta\nu_{\mathrm{Q}} = \chi_{\mathrm{Q}}\, S_{\mathrm{CD}}, \tag{4.5}$$

where $\chi_{\mathrm{Q}} = (3e^2qQ/4h)$ is magnetic susceptibility representing the quadrupolar coupling constant (126 kHz for the C−D bond).

If deuterons attached to the same carbon experience the same chemical environment, the deuterons contribute to the area of the same peak. Otherwise, the deuterons are inequivalent and they show up as two well-resolved peaks each with half the area of the peak of the equivalent deuterons. In this study, we have observed that the deuterons on C2 and C3 of the palmitoyl chain of PSM-d31 and DPPC-d31 (sn2) are inequivalent. This is due to their proximity to the "kink" conformation that influences the geometric order parameter of C2 and C3 deuterons. This effect is less pronounced for C3 deuterons.

If the molecules undergo rapid axially symmetric reorientation the first moment is proportional to the average of the quadrupolar splitting along the chain or, equivalently, of the Carbon-Deuteron order parameter,

$$M_1 = \frac{4\pi}{3\sqrt{3}} \chi_{\mathrm{Q}} \langle S_{\mathrm{CD}} \rangle. \tag{4.6}$$

The C−D order parameters can be used to estimate the length of the lipid chains through the relation [58, 59]

$$\langle L \rangle = 1.25 \left\{ \frac{N}{2} + \sum_i S_{CD}^i \right\}, \tag{4.7}$$

where *N* is the number of carbon-carbon bonds in the lipid chain and the sum is over all carbons (except the carbonyl) with C-D bond order parameters S_{CD}^i. In the all-trans configuration, all of the C-D bond order parameters are equal to 0.5 and thus the chain length is just *L* = 1.25*N*.

The smoothed order parameter profiles are extracted from the dePaked spectra using an established procedure [60], which assumes that the local order parameter decreases monotonically with the carbon position. While this assumption is not entirely correct, it does describe the general trend accurately.

4.3 De-Pake-ing ^{2}H NMR Spectra

For a sample, such as an MLV, in an external magnetic field, $\boldsymbol{B}_0$, the quadrupolar interaction depends on the orientation relative to $\boldsymbol{B}_0$. In the case of an axially symmetric reorientational motion, this dependence typically involves $P_2(\cos\theta) = \frac{1}{2}(3\cos^2\theta - 1)$ with the angle θ between the magnetic field and the symmetry axis of the interaction. This scales the interaction by a factor between 1 and −0.5 (zero at the "magic angle") and the resulting spectrum, for each carbon position, is a Pake doublet lineshape: a superposition of contributions from all possible orientations present in the sample. The essential consequence of the highly symmetrical nature of the fast motions in lipid bilayers is that a spectroscopic observable ω (quadrupolar splitting) is related to some generalized time averaged anisotropy parameter x, through $P_2(\cos\theta)$ scaling:

$$\omega(x,\theta) = 4\pi\chi_{\mathrm{Q}}\, S_{\mathrm{CD}} P_2(\cos\theta) = xP_2(\cos\theta). \qquad (4.8)$$

For a fixed θ, e.g., for a lipid bilayer squeezed between flat glass plates, the observed pattern of quadrupolar splitting provides a direct measure of the order parameter profile. Extracting the same information from a "powder" sample is considerably more difficult. If the sample contains multiple deuterons the powder spectrum is a superposition of Pake doublets and the overlapping of these broad

doublets makes it even more difficult to extract structural and dynamical information, such as S_{CD}, about the membrane. When all orientations in a powder are equally probable (random orientational distribution function $p(\theta) \propto \sin\theta$) then the standard "de-Pake-ing" technique [61, 62] can be used to dePake (deconvolute) a powder spectrum into its 0^o oriented counterpart and thus to extract the order parameter profile.

A random orientational distribution in a powder sample is realized when ordering due to the presence of an external magnetic field is negligible. However, the magnetic susceptibility of lipid bilayers is anisotropic,

$$\Delta\chi = \chi_{\parallel} - \chi_{\perp} < 0. \tag{4.9}$$

When a small domain of a bilayer of area *A*, thickness *d*, and bilayer normal $\vec{n}$ is placed in a strong external magnetic field $\vec{B}$, a magnetic moment is induced, which then interacts with the field. The resulting torque [63]

$$\vec{\tau} = \Delta\chi Ad\left(\vec{B}.\vec{n}\right)\left(\vec{B}\times\vec{n}\right), \tag{4.10}$$

orients the domain preferentially so that $\vec{n} \perp \vec{B}$ is favored. Because of the quadratic dependence on the strength of the external magnetic field, the effect on the distribution of bilayer domain orientations at high fields is considerable. Such ordering can distort the interpretation of NMR lineshapes, their moments, and the relaxation times. In particular, extraction of the orientational order profile is strongly affected if the standard dePakeing procedure is applied to partially oriented samples.

An experimental technique known as the spherically supported vesicles [64] can be used to avoid the orientational ordering in liposomes placed in a high magnetic field. Alternatively, we have used a well-established numerical method that is capable of extracting the oriented spectra, and thus the order parameter profiles, from the NMR spectra of partially oriented lipid samples. Here, we present a summary of the technique and for more details the reader is referred to [63, 65].

In general, a system has more than a single inherent time averaged anisotropy (more than a single order parameter) and thus it is appropriate to introduce the anisotropy distribution function $g(x)$, which contains all of the physical information of interest. Clearly, for a system that can be adequately described by a single anisotropy parameter, e.g., anisotropy of the chemical shift for a spin-(1/2) system, $g(x)$ is a δ-function. On the other hand, since a powder sample contains contributions from all the orientations a single fixed anisotropy parameter x corresponds to a continuous lineshape function, $s_x(\omega)$, in the frequency domain. To determine $s_x(\omega)$, it is essential to consider also the orientation distribution function $p(\theta)$, which represents the probability of encountering bilayer normal at an angle θ with respect to the external magnetic field. For an oriented sample, the orientation distribution function reduces to $p(\theta) = \delta(\theta)$ and the corresponding ^{2}H NMR lineshape is simply $s_x(\omega) = \delta(|\omega| - x)$. Clearly, the position ω of the spectral line is a direct measure of the anisotropy (order parameter). Once the anisotropy and orientation distribution

functions are defined, the powder spectrum can be described as a mapping $g(x),\ p(\theta) \longrightarrow S(\omega)$:

$$S(\omega) = \int g(x)\left[p(\theta)\frac{\partial\theta}{\partial\omega}\right]\mathrm{d}x, \quad \theta = \theta(x,\omega) \tag{4.11}$$

$$= \int p(\theta)\left[g(x)\frac{\partial x}{\partial\omega}\right]\mathrm{d}\theta \quad x = x(\theta,\omega). \tag{4.12}$$

The first expression is a $g(x)$-weighted superposition of lineshape functions, one for each anisotropy *x*; a classic example of a lineshape function would be a powder pattern of a single chemical shift anisotropy in ^{31}P NMR. The second expression is a $p(\theta)$-weighted superposition of spectra from the individual orientations that constitute the powder sample, one for each orientation *θ*. For reasons that will become clear it is convenient to introduce the kernel function $C(x,\omega)$ and rewrite equation (4.11) as

$$S(\omega) = \int_{-\infty}^{\infty} g(x)C(x,\omega)\,\mathrm{d}x, \tag{4.13}$$

$$C(x,\omega) = \begin{cases} p(\theta)\dfrac{\partial\theta}{\partial\omega}, & \text{for } -x/2 < \omega \le x \\ 0, & \text{otherwise.} \end{cases} \tag{4.14}$$

Using the scaling relation (4.8), the lineshape can be expressed as

$$p(\theta)\frac{\partial\theta}{\partial\omega} = -\frac{p[\theta(x,\omega)]}{[2(x-\omega)(x+2\omega)]^{\frac{1}{2}}}. \tag{4.15}$$

If $p(\theta)$ is known $C(x,\omega)$ can be determined and the anisotropy distribution $g(x)$ can be extracted from the powder spectrum using

$$S(\omega) = -\int_{-\infty}^{\infty} g(x) \frac{p[\theta(x,\omega)]}{[2(x-\omega)(x+2\omega)]^{\frac{1}{2}}} \mathrm{d}x \qquad -\frac{x}{2} < \omega \leq x. \tag{4.16}$$

The numerical procedure of extracting an oriented spectrum $g(x)$ from a powder spectrum $S(\omega)$ through equation (4.16) is precisely the case of dePakeing. If a uniform random orientation distribution, $p(\theta) = \sin\theta$, is assumed then (using the scaling relation (4.8)) the well-known lineshape function is obtained: $C(x,\omega) = [3x(x+2\omega)]^{-1/2}$ for $-x/2 < \omega \leq x$ and $C(x,\omega) = 0$ otherwise. And, for a single quadrupolar splitting the so-called Pake doublet lineshape takes the form $C(x,\omega) + C(-x,\omega)$. For random orientation distribution the dePakeing algorithm reduces to numerically solving the following equation for $g(x)$

$$S(\omega) = \int_{-\infty}^{\infty} \frac{g(x)}{[3x(x+2\omega)]^{\frac{1}{2}}} \mathrm{d}x \qquad -\frac{x}{2} < \omega \leq x. \tag{4.17}$$

A discrete set of experimental data, S_j^{σ}, is always incomplete, i.e., is known at a limited number of frequency sampling points ω_j, and is affected by the noise

$$S_j^{\sigma} = S_j + \sigma\sigma_j\varepsilon_j \qquad j = 1, \ldots, m. \tag{4.18}$$

The ε_j are Gaussian random variables, the σ_j are defined by the noise model, σ is a noise scaling factor, and the "exact data" $S_j = S(\omega_j)$ are completely determined by $g(x)$ through Eq. (4.17). Numerical analysis of noisy data provides only approximations for the distribution function, $\tilde{g}(x)$. Equation (4.17) is a Fredholm integral equation of the first kind and thus belongs to the class of so-called inverse ill-posed problems [66]. That is, for any set of noisy data $\{S_j^{\sigma}\}$,

there are many possible approximations for $\tilde{g}(x)$ with equally good fits to the input data (their least-squares residues are not distinguishable). Almost all of those approximations are in fact wrong, as can be demonstrated by using the Riemann-Lebesque theorem [67]. For this reason, simple least-squares or linear programming algorithms are not appropriate for dealing with such integral equations.

The numerical approximation of $g(x)$ from powder spectra was first carried out successfully by M. Bloom *et al*. [61] using an iterative algorithm. The procedure was applicable to symmetric quadrupolar and to simple chemical-shift powder spectra. It was generalized by Sternin *et al*. [62] for the analysis of asymmetric doublets. While the iterative method is the pioneer work in dePakeing it has some drawbacks: mainly, the signal-to-noise ratio decreases substantially when mapping the powder spectrum to the approximated $\tilde{g}(x)$. Whittall *et al.* [68] applied inverse-theory methods for the first time and achieved significant improvement. They successfully implemented two techniques: the nonnegative least-squares algorithm, NNLS, by Lawson and Hanson [69] and the calculation of least-squares approximation by using a discrete regularization technique based on singular-value decomposition, SVD, [70, 71]. With these techniques, they could extract $\tilde{g}(x)$ from frequency-domain spectra as well as from the corresponding time-domain signals. The non-negativity constraint and the discrete regularization both lead to an increase of stability and reliability of the results compared to the iteration method. Nonetheless, the fundamental

problems due to the ill-posed character of the Fredholm integral equation of the first kind, Eq. (4.17), could not be resolved.

However, the Tikhonov regularization technique [66, 72] is known to provide reliable solutions of such integral equations by minimizing the least-squares error with respect to $g(x)$ under additional constraints, e.g., a certain degree of smoothness of $g(x)$. Successful dePakeing of powder spectra has already been achieved by this method [73]. For *m* input data points, the regularization algorithm minimizes the following expanded least-squares expression with respect to $g(x)$:

$$\psi[g(x),\lambda] = \sum_{j=1}^{m} \frac{1}{\sigma_j}\left(S_j^{\sigma} - \int_{-\infty}^{\infty} g(x)C(x,\omega_j)\,dx\right)^2 + \lambda\|g''\|^2, \qquad (4.19)$$

subject to $g(x) \geq 0$. The first term in Eq. (4.19) is the usual least-squares term, which guarantees compatibility of the fit with the data. The Tikhonov regularization approach introduces the second term, which controls the smoothness of the approximation. Here λ is the regularization parameter, and g'' denotes the second derivative of the distribution function $g(x)$. A good estimate for λ is essential for the quality of the solution. Too small values for λ result in artificial, physically meaningless structures in $\tilde{g}(x)$, whereas too large a λ tends to oversmooth the shape of $\tilde{g}(x)$ and to suppress information. Among several methods established to determine the regularization parameter λ the self-consistency (SC) method developed by Honerkamp and Weese proved to be the most powerful one in many numerical algorithms related to Fredholm integral equations [74, 75, 76, 77]. The essence of SC method is to estimate the

regularization parameter uniquely from the experimental noise, thereby to guarantee that the approximation $\tilde{g}(x)$ is in the vicinity of the true distribution function $g(x)$. In other words, the numerical strategy is that the fit proceeds until the statistics of the misfit is equal to the statistics of the noise distribution in the baseline of the spectrum. Once the optimum value of the regularization parameter is determined from the SC method, minimizing the misfit, $\psi[g(x), \lambda]$, yields $\tilde{g}(x)$.

For magnetically partially oriented bilayers one needs to re-express the kernel function $C(x, \omega)$, in terms of x and ω, for non-spherical (non-random) orientation distribution and then the regularization dePaking algorithm, as explained above, can be used to estimate the oriented spectrum $\tilde{g}(x)$. Several studies on lipid membranes [78, 79, 80] have shown that multilamellar vesicles undergo magnetically induced ellipsoidal deformations in high magnetic field. In [78] the first freeze-etch electron microscopy data obtained from DPPC/cholesterol samples that were frozen directly in the NMR magnet at field strength of 9.4 Tesla. These data clearly show that the MLVs adopt an ellipsoidal shape in the magnetic field. The ellipsoidal orientation distribution can be modeled as [63]

$$p(\theta) \propto \sin\theta \times [1 - (1 - \kappa_{\mathrm{E}}) \cos^2 \theta]^{-2}. \qquad (4.20)$$

Here κ_{E} is the square of the ratio of the semiaxes, i.e., $\kappa_{\mathrm{E}} = 1$ means spherical symmetry and $\kappa_{\mathrm{E}} > 1$ describes an ellipsoidal deformation, with the long axis parallel to the magnetic field. Now calculation of the dePaked spectrum becomes numerically more expensive since κ_{E} is introduced as the second fitting

parameter in the minimization problem, Eqn. (4.19). First, a reasonable range of κ_{E} is considered, and then for each κ_{E} value the misfit functional $\psi[g(x),\lambda]$ is minimized. The minimum value of the standard deviation of the misfit corresponds to the κ_{E} value that provides the best fit. Once the optimum κ_{E}, and hence optimum λ, is known the dePaked spectrum $\tilde{g}(x)$ is estimated.

Here we present an example of the ellipsoidal deformation of pure PSM-d31 MLD in a magnetic field strength of 7 Tesla. The spectrum $S(\omega)$, collected at 47^{o}C, consists of 4096 data points and extends between -250 and +250 kHz, the kernel $C(x,\omega)$ is a 4096×820 matrix, and the dePaked spectrum $\tilde{g}(x)$ is estimated between -100 to +100 kHz as a 820×1 vector. The dePaked spectrum, the fit to the powder spectrum, and the misfit (the discrepancy between the data and the fit) obtained from the iterative method is shown in Figure 4-1. The reported unphysical negative intensities in the dePaked spectrum indicates that random orientation of the domains in the magnetic field is not an appropriate model for sphingomyelin membrane. The inadequacy of $p(\theta) = \sin\theta$ model can clearly be observed in the form of systematic features in the misfit. The standard deviation of this misfit, $\sigma_{\mathrm{misfit}} \approx 1.8 \times 10^{-3}$, is nearly 15 times greater than that of the noise in the baseline of the data, $\sigma_{\mathrm{noise}} \approx 1.23 \times 10^{-4}$.

Further, we applied the Tikhonov regularization algorithm with an ellipsoidal model for the orientation of liposomes in the external magnetic field and the results are presented in Figure 4-2. The square of the ratio of the semiaxes, κ_{E}, was varied from 1.0 to 10.0 in steps of 0.1 and the numerical inversion, i.e. minimization of $\psi[g(x),\lambda]$, was performed using Snowpatch cluster

on WestGrid (Western Canada Research Grid is a grid-enabled system for the high performance computing, collaboration and scientific visualization). The program executed in about 20 seconds for each κ_{E} value and the minimum quadratic misfit function $\psi[\kappa_E]$ obtained for $\kappa_{\mathrm{E}} = 7.0 \pm 0.1$, corresponding to the ratio of semiaxes equal to ~2.6 (see the inset in Figure 4-2). Then, the optimum regularization parameter and the noise level were estimated to be $\lambda \cong 0.899 \times 10^4$ and $\sigma \cong 0.186 \times 10^{-3}$.

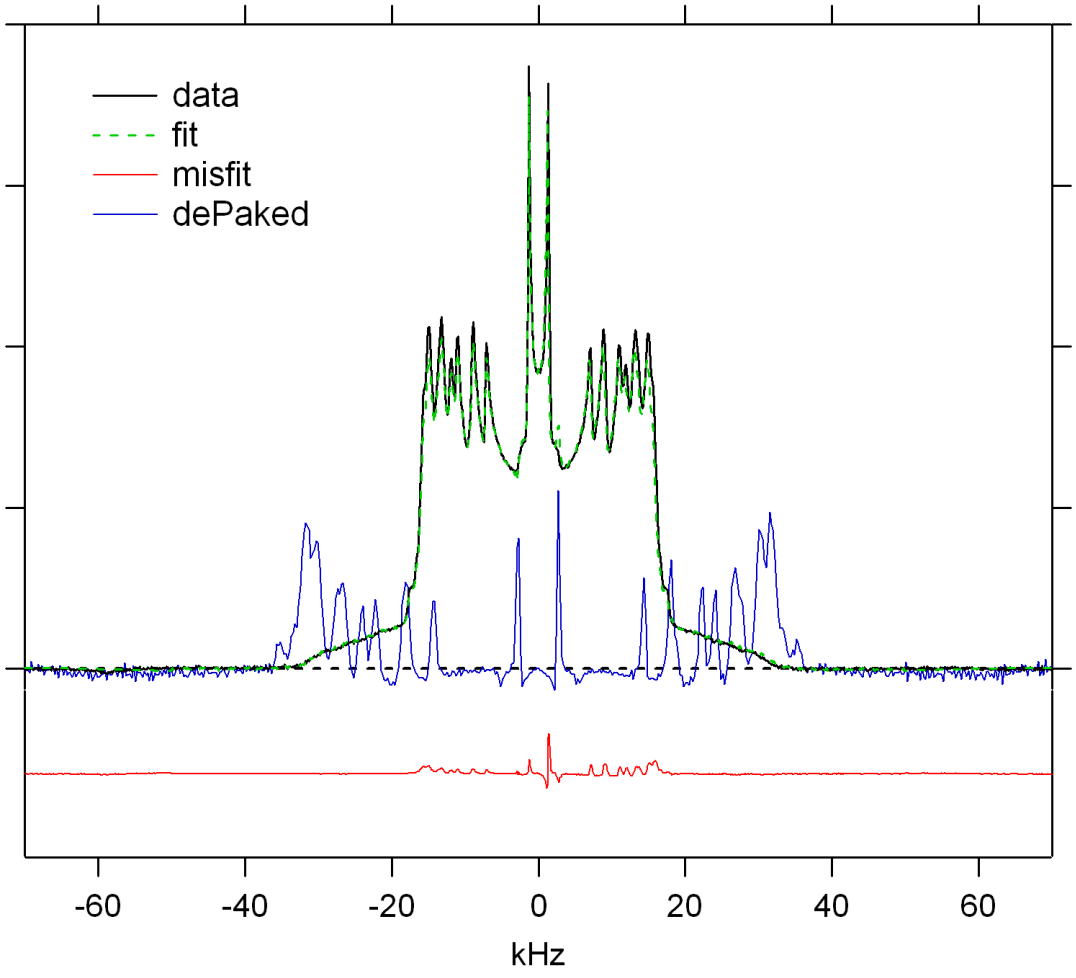

Figure 4-1: DePakeing of a ^{2}H NMR spectrum based on a random orientational distribution model, using iterative algorithm.

First clear observation is that going from powder spectrum to dePaked spectrum, unlike in the iterative method, the signal to noise ratio is not decreased. Also, the reported misfit is shown 20 times larger and clearly the systematic difference between the input data and the fit curve is essentially eliminated. The standard deviation of the misfit is $\sigma_{\mathrm{misfit}} \approx 1.54 \times 10^{-4}$, which is very close to that of the noise. However, the estimated dePaked spectrum shows unphysical positive amplitudes, indicating that the deformation of liposomes in the magnetic field is not adequately described by an ellipsoidal model. One can speculate that the random orientation and ellipsoidal deformation models correspond to two extremes.

Following the procedure in [65], we employed a mix orientation model: an elliptical distribution of Eq. (4.20) as well as a spherically symmetric term:

$$p(\theta) \propto \{R \sin\theta + (1-R)\sin\theta \times [1-(1-\kappa_{\mathrm{E}})\cos^2\theta]^{-2}\}. \qquad (4.21)$$

Now calculations become even more expensive since the relative contribution of the two components was introduced as the third fit parameter. The results are presented in Figure 4-3 for the minimum misfit function corresponding to $R = 28 \pm 2\%$ spherical, $1 - R = 72 \pm 2\%$ ellipsoidal distribution, as well as $\kappa_E = 5.8 \pm 0.1$ for the elliptical part. The misfit $\times 20$ shows no systematic features and its standard deviation is again close to that of the noise. Also, the estimated dePaked spectrum does not exhibit unphysical positive/negative amplitudes.

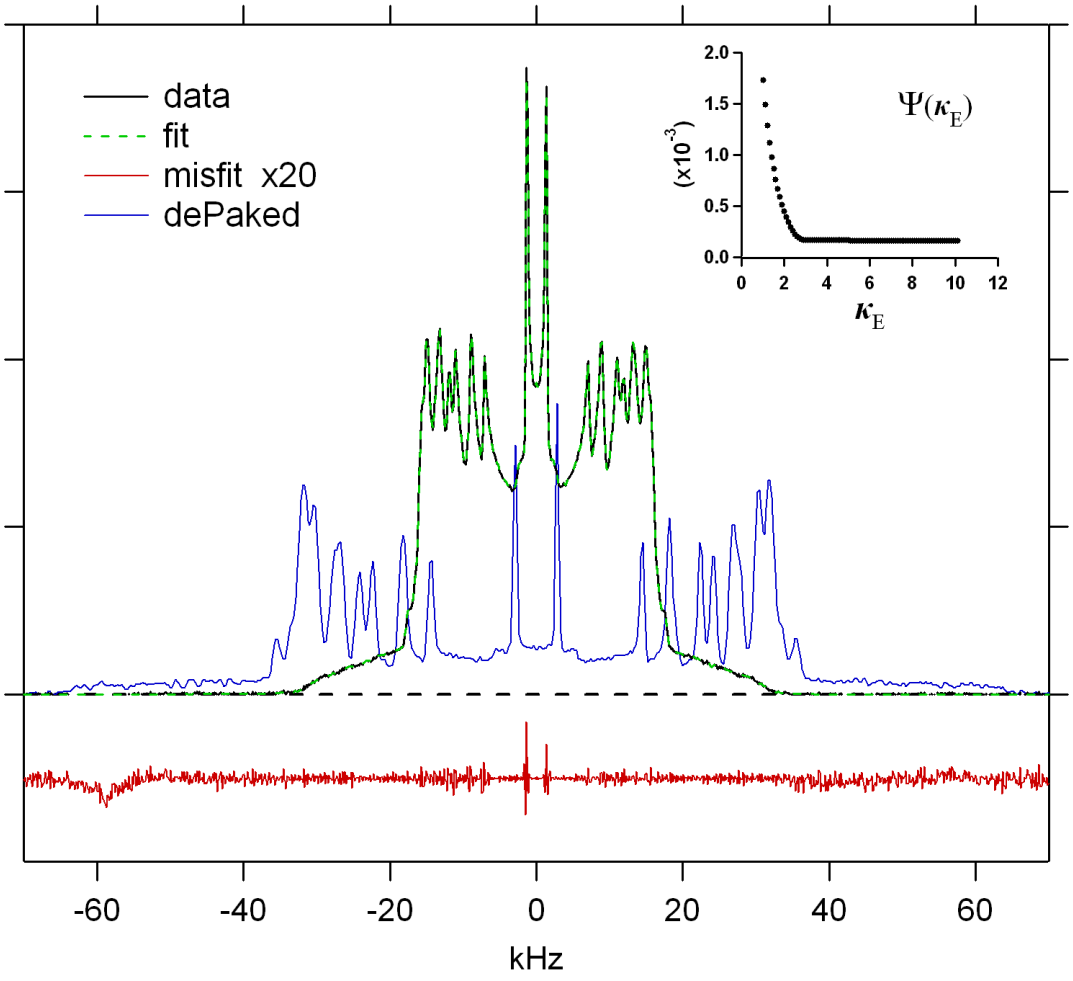

Figure 4-2: DePakeing of a ^{2}H NMR spectrum based on an ellipsoidal orientational distribution model, using Tikhonov regularization algorithm. The inset shows the standard deviation of the misfit as a function of κ_E.

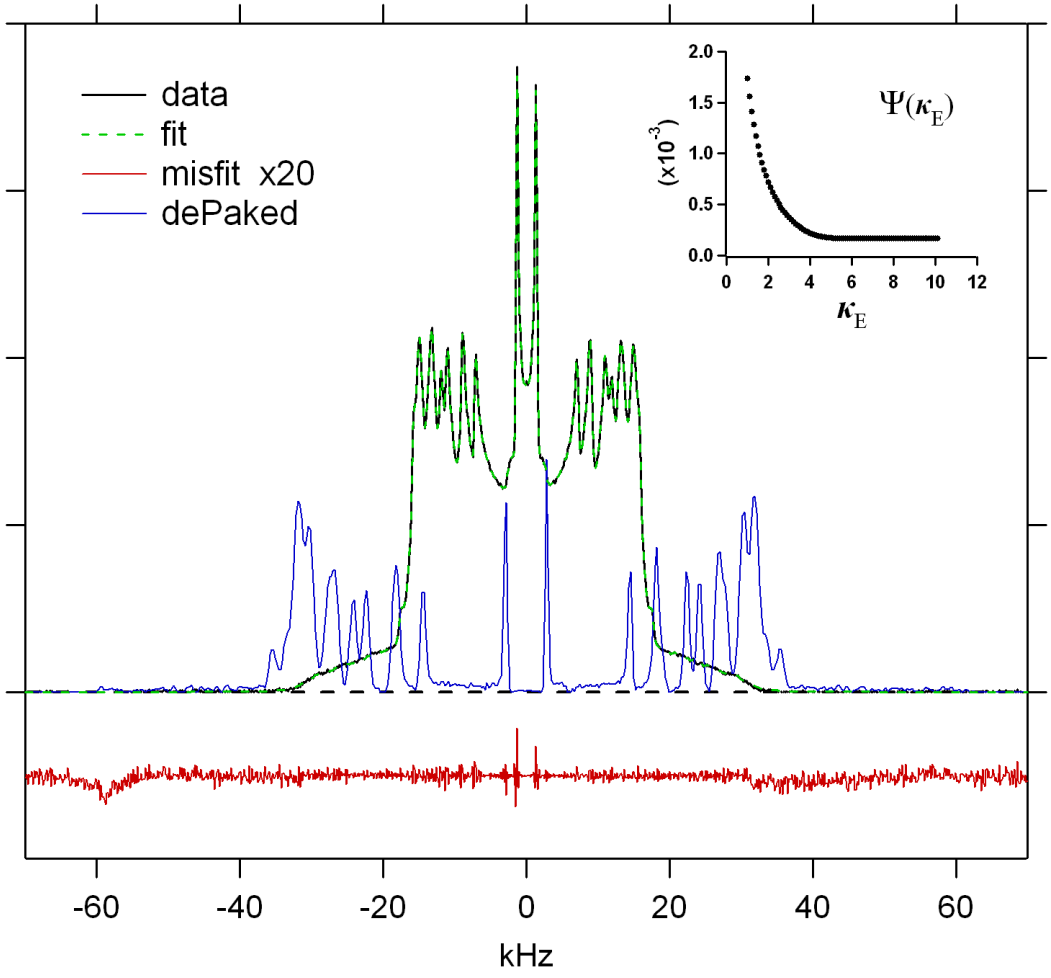

Figure 4-3: DePakeing of a ^{2}H NMR spectrum based on a mixed orientational distribution model, using Tikhonov regularization algorithm. The inset shows the standard deviation of the misfit as a function of κ_E.

4.4 Spectral Subtraction

According to the Gibbs phase rule, the temperature-composition phase diagram of a two-component system can have regions of two-phase coexistence. Spectral subtraction, also known as ^{2}H NMR difference spectroscopy, can be carried out in phase coexistence regions to determine the phase boundaries [10]. Spectra from two samples with different compositions at the same temperature *T* are needed. The spectral subtraction method is valid for any two-phase region as long as certain assumptions hold. The spectra of the two phases have to be sufficiently different that one can easily distinguish and carry out the subtraction procedure. The exchange of labeled lipid between two kinds of domains must be slow on the NMR timescale so that it can be neglected. In addition, the domain must be sufficiently large, so that the signal from the lipid on the boundary of the domains is negligible.

^{2}H NMR experiments on binary systems, such as PSM-d31/cholesterol, show that these conditions are satisfied in the region of the phase diagram where gel and liquid ordered phases coexist (**so**+**lo**). In the following derivations we use subscript “g” to refer to the “gel” or “**so**” phase and subscript “f” to refer to the “fluid” or “**lo**” phase. The partitioning of the sample between these two types of domains is given by the lever rule. For example, for a sample of composition x_i at a temperature *T***,** the fluid fraction is given by

$$\alpha_\mathrm{i}(T) = \frac{x_\mathrm{i} - x_\mathrm{g}(T)}{x_\mathrm{f}(T) - x_\mathrm{g}(T)}, \tag{4.22}$$

and the gel fraction is $1-\alpha_{\mathrm{i}}(T)$. In this equation x_{g} and x_{f} are the cholesterol concentrations at the **so** and **lo** phase boundaries. It follows from Eqn. (4.22) that

$$1-x_{\mathrm{i}}=\alpha_{\mathrm{i}}(1-x_{\mathrm{f}})+(1-\alpha_{\mathrm{i}})\big(1-x_{\mathrm{g}}\big), \tag{4.23}$$

and therefore

$$1=\alpha_{\mathrm{i}}\frac{(1-x_{\mathrm{f}})}{(1-x_{\mathrm{i}})}+(1-\alpha_{\mathrm{i}})\frac{\big(1-x_{\mathrm{g}}\big)}{(1-x_{\mathrm{i}})}, \tag{4.24}$$

where $1-x_{\mathrm{i}}$ is the lipid concentration of the sample, and $1-x_{\mathrm{f}}$ and $1-x_{\mathrm{g}}$ are the lipid concentrations of the fluid- and gel-phase domains, respectively. The fraction of the lipid in the fluid-phase domains is then

$$f_{\mathrm{i}}=\alpha_{\mathrm{i}}\frac{1-x_{\mathrm{f}}}{1-x_{\mathrm{i}}}, \tag{4.25}$$

and the second term of Eqn. (4.24) (or $1-f_{\mathrm{i}}$) gives the gel lipid fraction**.** Within the two-phase region, the ^{2}H NMR spectrum S consists of different amounts of endpoint spectra characteristic of the two phases in equilibrium:

$$S(x_{\mathrm{A}},T)=f_{\mathrm{A}}S_{\mathrm{f}}(x_{\mathrm{f}},T)+(1-f_{\mathrm{A}})S_{\mathrm{g}}\big(x_{\mathrm{g}},T\big), \tag{4.26}$$

$$S(x_{\mathrm{B}},T)=f_{\mathrm{B}}S_{\mathrm{f}}(x_{\mathrm{f}},T)+(1-f_{\mathrm{B}})S_{\mathrm{g}}\big(x_{\mathrm{g}},T\big), \tag{4.27}$$

where x_{A} and x_{B} are the cholesterol concentrations of two lipid/cholesterol MLDs, f_{A} and f_{B} are the fractions of fluid lipid in the two samples, and S_{g} and S_{f} are the end-point spectra characteristic of solid phase and liquid phase domains, respectively, at the solid and liquid phase boundaries. The endpoint spectra can be obtained by linear decomposition of the composite spectra, using Eqns. (4.26) and (4.27): Given two area-normalized ^{2}H NMR spectra $S(x_{\mathrm{A}},T)$ and $S(x_{\mathrm{B}},T)$; the

solid (or liquid) spectrum can be obtained by subtracting a fraction K (or K') of one spectrum from the other as follows;

$$S(x_{\mathrm{A}},T) - K\,S(x_{\mathrm{B}},T) = (f_{\mathrm{A}} - Kf_{\mathrm{B}})S_{\mathrm{f}}(x_{\mathrm{f}},T) + (1 - K - f_{\mathrm{A}} + Kf_{\mathrm{B}})S_{\mathrm{g}}(x_{\mathrm{g}},T), \quad (4.28)$$

$$S(x_{\mathrm{B}},T) - K'\,S(x_{\mathrm{A}},T) = (f_{\mathrm{B}} - K'f_{\mathrm{A}})S_{\mathrm{f}}(x_{\mathrm{f}},T) + (1 - K' - f_{\mathrm{B}} + K'f_{\mathrm{A}})S_{\mathrm{g}}(x_{\mathrm{g}},T). \quad (4.29)$$

We obtain the gel phase end-point spectrum when the first term in Eqn. (4.28) vanishes, i.e.

$$f_{\mathrm{A}} - Kf_{\mathrm{B}} = 0 \quad \longrightarrow \quad K = \frac{f_{\mathrm{A}}}{f_{\mathrm{B}}} < 1, \quad (4.30)$$

$$S_{\mathrm{g}}(x_{\mathrm{g}},T) = \frac{1}{1-K}[S(x_A,T) - K\,S(x_B,T)]. \quad (4.31)$$

And we obtain the fluid phase end-point spectrum when the second term in Eqn. (4.29) vanishes:

$$1 - K' - f_B + K'f_{\mathrm{A}} = 0 \quad \longrightarrow \quad K' = \frac{1 - f_{\mathrm{B}}}{1 - f_{\mathrm{A}}} < 1, \quad (4.32)$$

$$S_{\mathrm{f}}(x_{\mathrm{f}},T) = \frac{1}{1-K'}[S(x_B,T) - K'\,S(x_{\mathrm{A}},T)]. \quad (4.33)$$

Finally, from Eqns. (4.22), (4.25), (4.30), and (4.32), we can solve for the end-point concentrations:

$$x_{\mathrm{g}} = \frac{(1 - x_{\mathrm{B}})x_{\mathrm{A}} - K(1 - x_{\mathrm{A}})x_{\mathrm{B}}}{(1 - x_{\mathrm{B}}) - K(1 - x_{\mathrm{A}})}, \quad (4.34)$$

$$x_{\mathrm{f}} = \frac{(1 - x_{\mathrm{A}})x_{\mathrm{B}} - K'(1 - x_{\mathrm{B}})x_{\mathrm{A}}}{(1 - x_{\mathrm{A}}) - K'(1 - x_{\mathrm{B}})}. \tag{4.35}$$

The spectral subtraction method explained above assumes that both phases have the same relaxation time T_{2e}, which is not true in our case. Depending on the temperature, the **lo** phase has a T_{2e} two to six times larger than the **so** phase T_{2e} and therefore the **so** component decays faster than the **lo** component (the signal $\propto e^{-t/T_{2e}}$). Thus, at any given quadrupolar echo time 2τ, the ^{2}H NMR spectrum will contain a smaller **so** component S_s than is representative of the sample. Due to this T_{2e} effect f_{A} and f_{B} in Eqs. (4.30) and (4.32), which should be denoted as $f_{\mathrm{A}}(t = 2\tau)$ and $f_{\mathrm{B}}(t = 2\tau)$, do not reflect the actual fraction of fluid lipid in the samples. Thus, the K and K' (which should be denoted as $K(t = 2\tau)$ and $K'(t = 2\tau)$, respectively) determined from the spectral subtraction will not be correct, leading to a deviation of x_g and x_{f} from the actual values. To incorporate this T_{2e} effect, corrected f_{A} and f_{B} values (i.e., $f_A(t = 0)$ and $f_{\mathrm{B}}(t = 0)$) are calculated by extrapolating the height of the respective echo signal back to $t = 0$ using the measured T_{2e} for a given temperature, and then the corrected K and K' values (i.e., $K(t = 0)$ and $K'(t = 0)$) can be derived and expressed in terms of the experimentally determined K and K' (i.e., $K(t = 2\tau)$ and $K'(t = 2\tau)$), and T_{2e}s. Assuming the gel component of a mixed spectrum will have decayed by an extra factor R relative to the liquid ordered component, then [81]

$$\begin{aligned} K(t = 0) &= K(t = 2\tau) \times C, \\ K'(t = 0) &= K'(t = 2\tau)/C, \end{aligned} \tag{4.36}$$

where the coefficient *C* is given by

$$C = \frac{1 + f_A\left(\frac{1-R}{R}\right)}{1 + f_B\left(\frac{1-R}{R}\right)}. \tag{4.37}$$

Using Eqns. (4.34) and (4.35) with these corrected K and K' values, the T_{2e}-corrected values of x_{g} and x_{f} are obtained.

Chapter 5: Results and Discussion

In this chapter, ^{2}H NMR results will be presented and discussed in two parts. The first half will focus on perdeuterated lipid/cholesterol membranes and the pertinent phase diagrams will be mapped. The latter half of the chapter will be devoted to the study of the orientation dependence of T_2 relaxation time and its influence on the nano-domain structure of PSM/cholesterol using selectively deuterated sphingomyelin.

5.1 Perdeuterated Lipid/cholesterol

5.1.1 Distinct Phases are Observed

Depending on temperature and composition, both PSM-d31/cholesterol and DPPC-d31/cholesterol MLDs can exist in three distinct phases. These are the gel or solid-ordered (**so**) phase, liquid-disordered (**ld**) phase, and the liquid-ordered (**lo**) phase. The ^{2}H NMR spectra of these phases have unique characteristics which can be used to map phase boundaries and regions of phase coexistence. Figure 5-1 shows the spectra representative of these three phases for PSM-d31/cholesterol and DPPC-d31/cholesterol membranes, respectively. The spectra in Figure 5-1 A and A' are typical of the membrane **ld** phase. The spectrum is a superposition of Pake doublets; each is contributed from a labelled carbon along the chain and is a powder pattern with a quadrupolar splitting representative of the local carbon-deuterium bond order parameter, S_{CD}. The

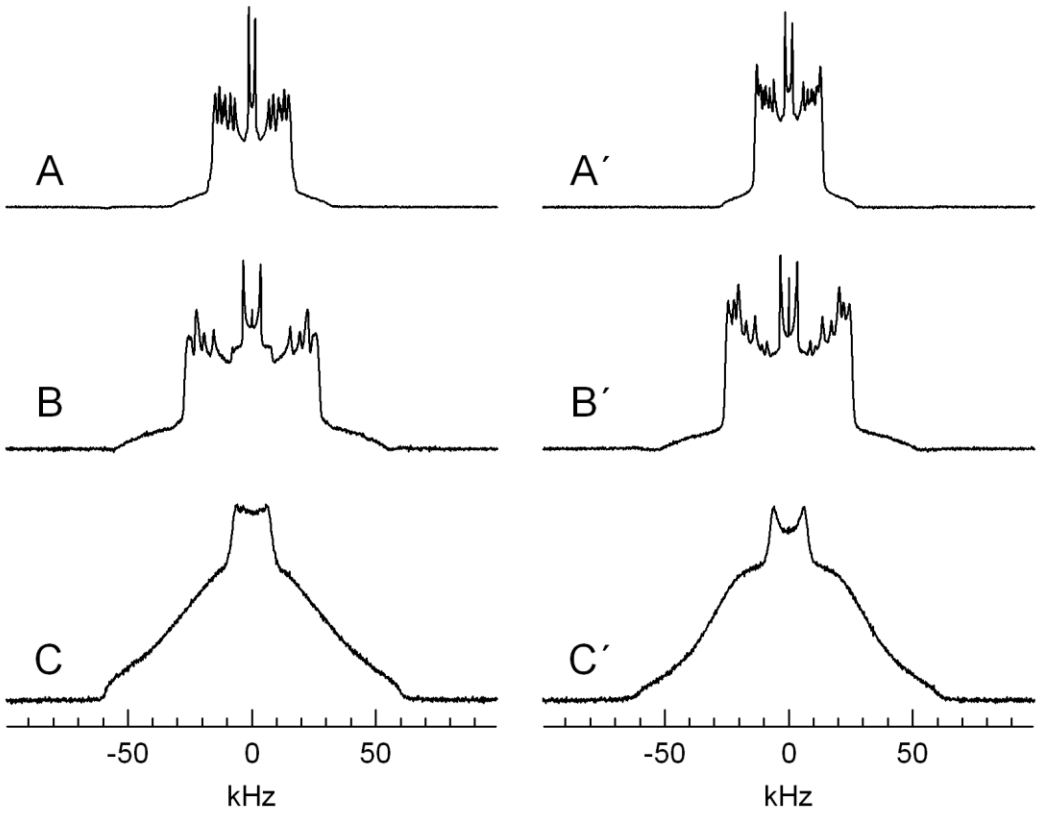

Figure 5-1: ^{2}H NMR spectra representative of three phases:

(A) & (A') typical ld phases above 41ºC; (B) & (B') lo phases with 40 mole% cholesterol at 48ºC; and (C) & (C') so phases, below 39ºC, of the PSM-d31 & DPPC-d31 membranes, respectively.

lipid chains have a relatively high population of gauche conformers and gauche-trans isomerisation is very rapid. The lipid molecules also undergo rapid axially symmetric reorientation about the bilayer normal [82, 83] and rapid lateral diffusion [84]. In the ld phase lipid chains are loosely packed laterally within the bilayer. Figure 5-1 B and B' show the spectra representative of the **lo** phases. The **lo** phase spectrum has a line shape qualitatively similar to that of the **ld** phase: The spectrum is a superposition of Pake doublets indicating that the acyl

chains undergo rapid axially symmetric reorientation about the bilayer normal, [85, 86]. However, the average spectral width in the **lo** state is much broader than that of the **ld** state, nearly 1.7 times larger for PSM-d31 and 1.9 times larger for DPPC-d31, respectively. This means that the quadrupolar splitting for each position on the chain is considerably larger in the **lo** phase than in the **ld** phase and, thus, lipid chains are highly conformationally ordered with a reduced population of gauche conformers. The chains approach the all-trans conformation at low temperatures [10]. As a consequence **lo** phase hydrocarbon chain packing is much stronger than in the **ld** phase, and the rate of lateral diffusion is significantly reduced [84]. Figure 5-1 C and C' show the spectra characteristic of pure so phase membrane. Deuterons in **so** membranes do not undergo rapid axially symmetric motion on the NMR timescale since the acyl chains are closely packed. The significantly slower motions in the **so** phase lead to the characteristic bell shape of this phase [87, 88].

5.1.2 Phase Transitions

The first moment, M_1, is determined from the average spectral width, as described in section 4.1. Labelled lipids in each phase state within a given membrane possess a distinct ^{2}H NMR spectrum and thus a distinct M_1 value. Phase changes can be detected by examining the spectra or M_1 as a function of temperature or composition. For instance, a large variation of M_1 with temperature can be used to pinpoint phase transition temperatures in the membrane. Figure 5-2 A and B show M_1 as a function of temperature for all PSM- d31/cholesterol and DPPC-d31/cholesterol MLDs, respectively. The gel

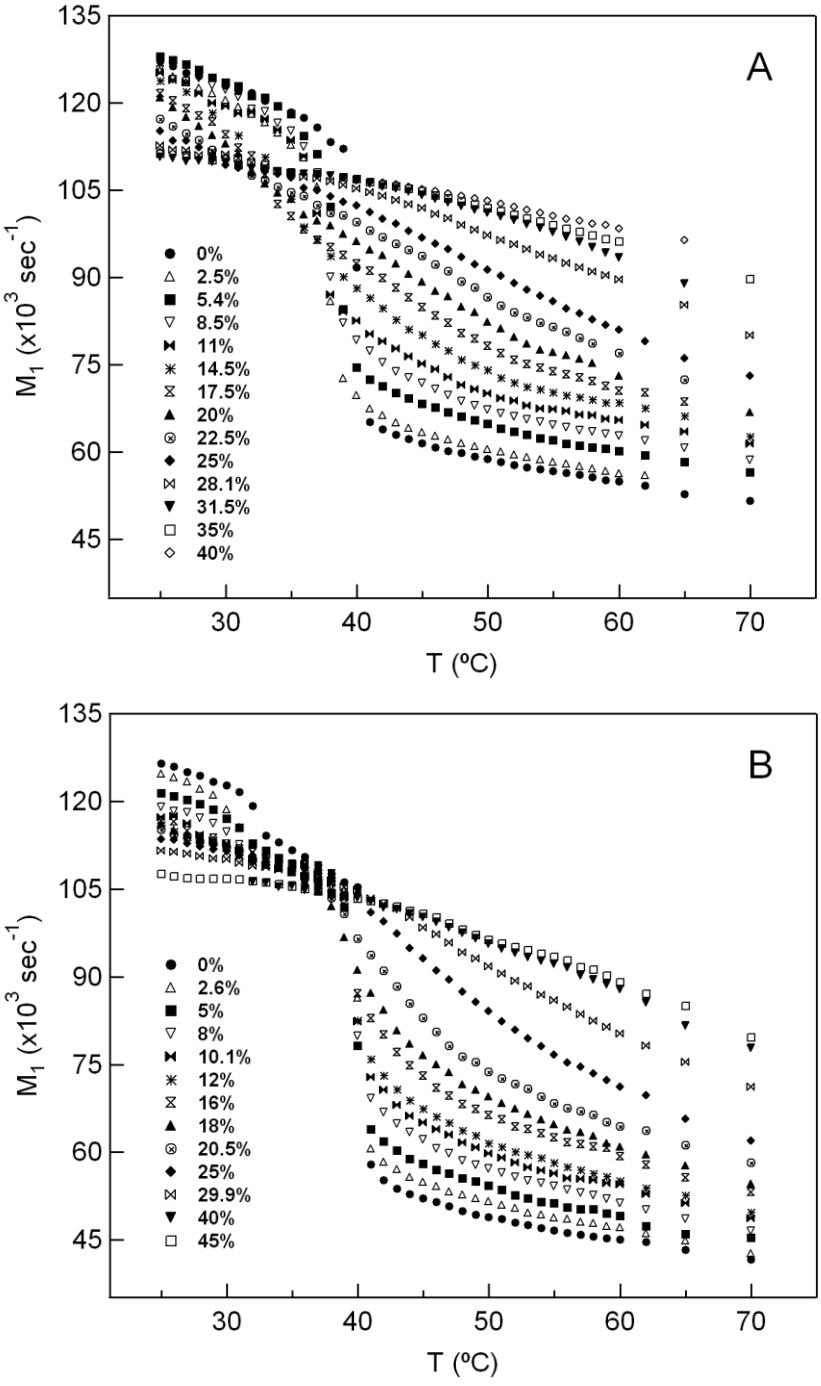

Figure 5-2: The temperature dependence of M_1 for (A) PSM-d31/cholesterol and (B) DPPC-d31/cholesterol at various cholesterol concentrations.

phase of pure DPPC-d31 dispersions exhibits a pre-transition from a rippled phase ($\mathbf{L_{\beta'}}$) to a nonrippled, tilted phase ($\mathbf{P_{\beta'}}$) near 32^{o}C. Also, in the absence of cholesterol, both PSM-d31 and DPPC-d31 undergo main transitions at 40^{o}C from the **so** phase to the **ld** ($\mathbf{L_{\alpha}}$) phase. Adding cholesterol modifies both the **ld** and **so** phases of the lipid membranes. The $M_1(T)$ curve plunges less dramatically at T_m as more cholesterol is added: below T_m $M_1(T)$ decreases with increasing cholesterol concentration, whereas above T_m $M_1(T)$ increases with increasing cholesterol concentration. M_1 is proportional to the average order parameter in the liquid crystalline phase, therefore adding cholesterol increases the phospholipid chain ordering above T_m.

5.1.3 Phase Boundaries at low Cholesterol Content: so/(so+ld)/ld

As shown in Figure 5-3 A, pure PSM-d31 MLDs undergo a sharp phase transition near 40°C. The spectra obtained below 39°C are characteristic of a **so** phase membrane and those obtained above 41°C represent the **ld** phases. The spectrum collected at 40°C is composed of both **so** and **ld** components. The **so** component in such a **so+ld** spectrum can be traced by magnifying the "shoulders" of the spectrum. The shoulders of **so** and **ld** spectra extend to ~ ±60 kHz and ~ ±30 kHz, respectively (see Figure 5-1). Therefore, signal between 30 and 60 kHz (or between −30 and −60 kHz) is an indication of the **so** component. Spectra obtained above 41°C show only noise in this region, thus they contain no **so** component. Figure 5-3 B displays the temperature dependence of spectra for the 94.6:5.4 PSM-d31/cholesterol membranes. The spectrum obtained at 37^{o}C

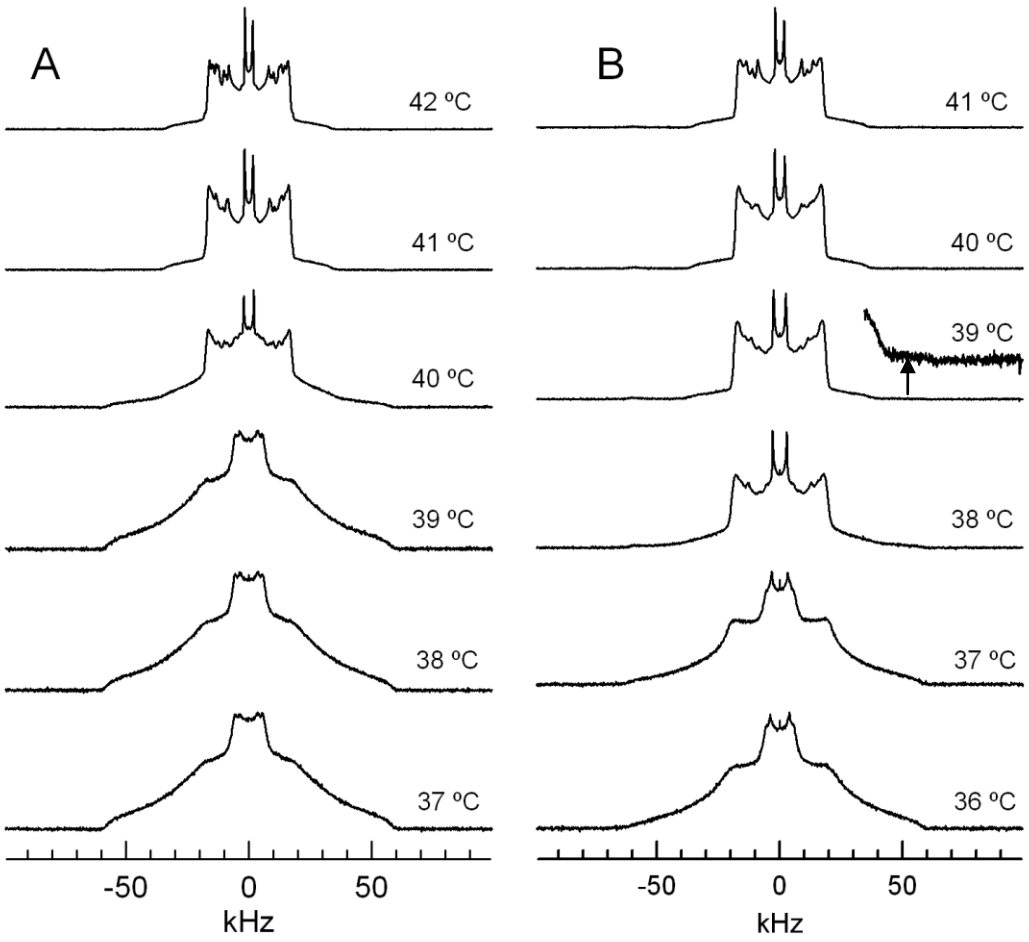

Figure 5-3: ^{2}H NMR spectra of (A) pure PSM-d31 and (B) 94.6:5.4 PSM-d31/cholesterol as a function of temperature.

displays both **so** and **ld** components, but with the **so** component dominating. The emergence of the 90^o edges near ±19 kHz confirms the existence of the **ld** component (the onset of the transition). The 39^{o}C spectrum also contains both **so** and **ld** components but the **ld** component dominates (the end of the transition). A trace of residual **so** component is visible, illustrated by an arrow in Figure 5-3 B. Similar spectral analysis (and the M_1 *vs.* temperature plot) shows

that for MLDs containing 2.5 and 5.4 mole% cholesterol there are temperatures where the **so** and **ld** phases co-exist and, thus, the transition between these phases occurs over a broader range than for pure PSM-d31.

5.1.4 Phase Boundaries at Higher Cholesterol Content and Low Temperature: so/(so+lo)/lo

Figure 5-4 shows the spectrum of PSM-d31/cholesterol as a function of cholesterol concentration at 31°C (i.e., below T_m). The **so** phase spectra are apparent in spectra for samples containing up to 8.5 mol% cholesterol. For the 11 mol% cholesterol sample, a very small lo component appears in the **so** spectrum. The residual **lo** component can be detected by the emergence of peaks near ±19 and ±23 kHz. These peaks are more obvious in the 14.5 mol% sample. The coexistence of **so** and **lo** phases indicates that cholesterol induces **lo** domains in the PSM-d31 bilayers. As the concentration is increased within the two-phase region the fraction of fluid phase increases. Thermodynamically, this process corresponds to the growth of macroscopic fluid phase domains at the expense of gel phase domains. In the presence of 25 mol% cholesterol PSM-d31 seems to display an pure **lo** spectrum. However, whether the **so** component has totally disappeared from this spectrum is not clear. Examining the shoulders of the spectrum as we did for the **so**+**ld** spectrum is difficult in this case, as the shoulders of **so** and **lo** spectra both extend to ±60 kHz (see Figure 5-1). As the cholesterol concentration reaches 31.5 mol% and higher, the spectra are consistent with **lo** phase PSM-d31 MLDs. Therefore, Figure 5-4 implies a **so**/**so**+**lo** phase change occurring between 8.5 and 14.5 mol% and a **so**+**lo**/**lo**

phase change between 22.5 and 28 mol% cholesterol. Further analysis is required to accurately measure these phase boundaries.

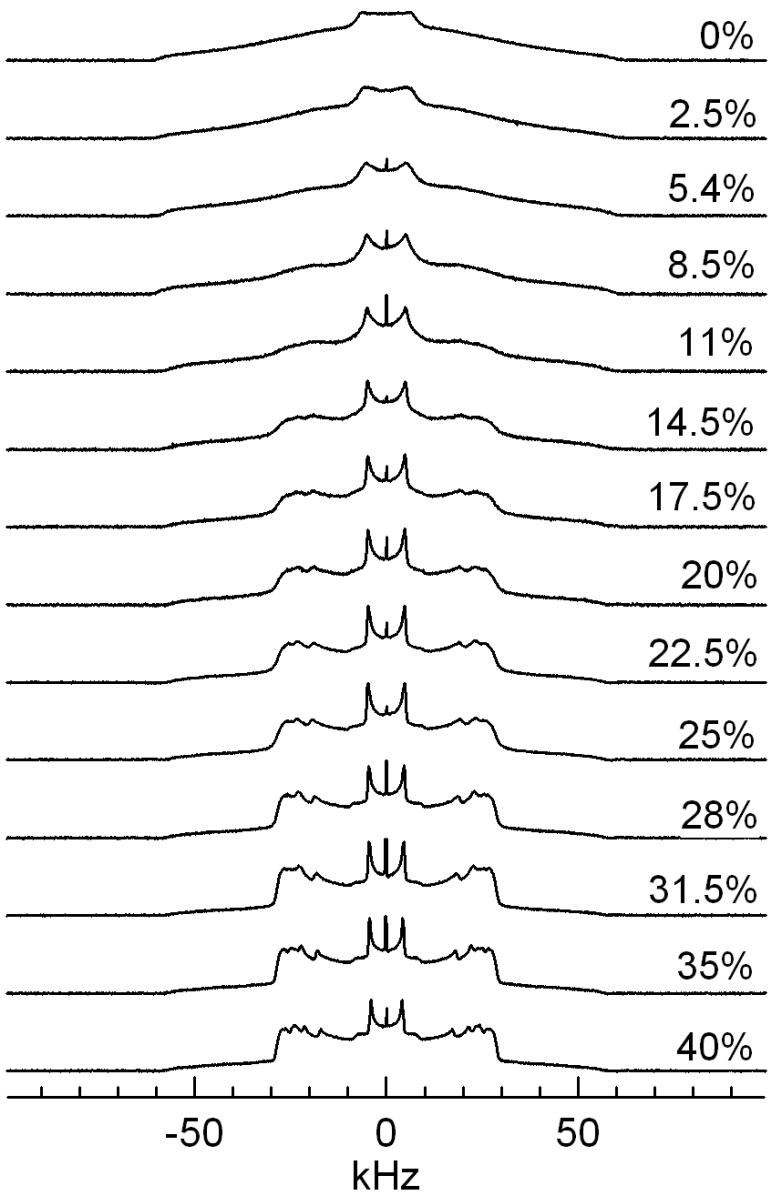

Figure 5-4: ^{2}H NMR spectra of PSM-d31/cholesterol as a function of cholesterol concentration at T = 31°C.

The ^{2}H NMR spectrum of PSM-d31/cholesterol dispersion within a two-phase region will be a superposition of its distinguishable components, provided that the domains are sufficiently large and exchange of the lipid molecules between the two domains is slow on the NMR time scale. The widths of the features within the **so** and **ld** spectra cover a range of from about 1 to 100 kHz, resulting in a range of time scales from about 10 μs to 1 ms. The sharpest feature in the spectrum, the fluid phase methyl group resonance, has a T_{2e}~1 ms. Motions faster than, or on the order of, this time scale can influence the shape of the spectrum. The decay time for the quadrupolar echo, T_{2e}, can be a prime cause for line broadening if $1/T_{2e}$ is greater than the contribution of the magnet inhomogeneity to the line width. The spectral subtraction approach proves robust in separating experimental spectra of MLDs within the **so**+**lo** region into their end-point components.

Figure 5-5 and Figure 5-6 illustrate spectral subtraction procedure at 32^{o}C using normalized spectra of PSM-d31/cholesterol dispersions with 11 and 22.5 mol% cholesterol, Figure 5-5 A and B. We refer to the 11 mol% cholesterol membrane as "**so**-rich" and the 22.5 mol% cholesterol membrane as "**lo**-rich". By subtracting 24% of the **so**-rich spectrum from the **lo**-rich spectrum, we obtain the difference spectrum shown in Figure 5-5 (D). The value K' = 0.24 gives the **lo** phase end-point mole fraction x_f = 0.255 denoting the **so**+**lo**/**lo** boundary. This difference spectrum, renormalized in Figure 5-6 (B), is compared with the normalized experimental spectrum obtained at 31^{o}C for 25 mol% cholesterol,

Figure 5-6 (A). The difference between the spectra in Figure 5-6 (A) and (B) is shown in Figure 5-6 (C).

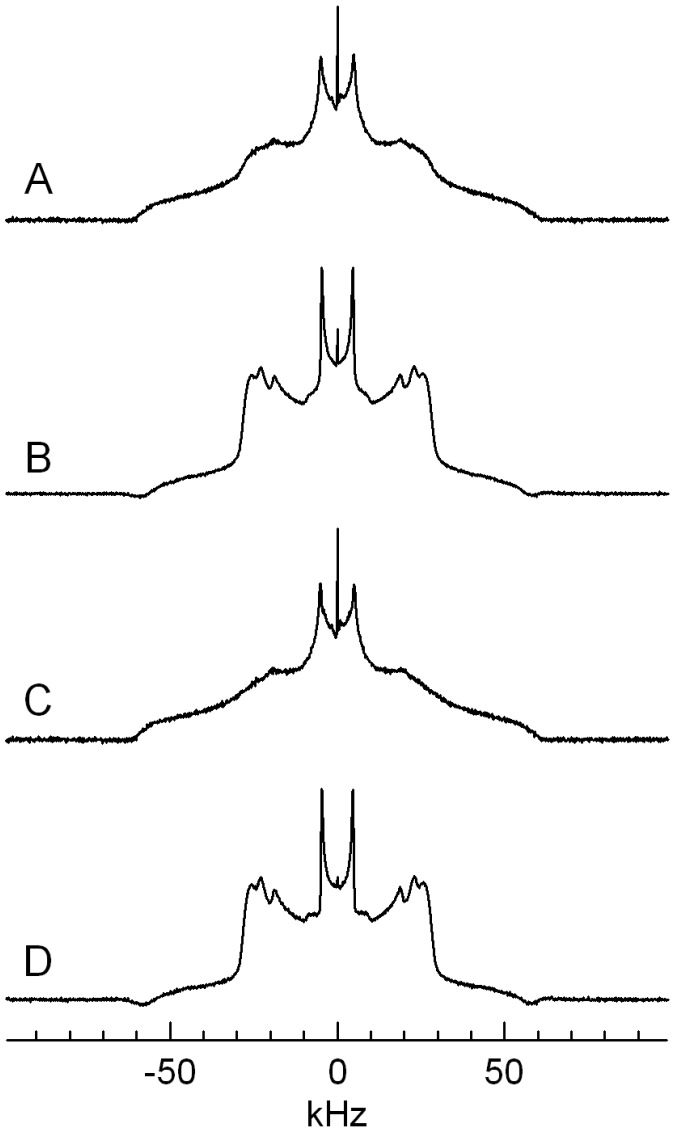

Figure 5-5: ^{2}H NMR spectral subtraction at 32ºC.

(A) and (B) experimental spectra of 11 mole% and 22.5 mole% cholesterol, respectively; (C) the spectrum in (A) minus 0.17 times that in (B); (D) the spectrum in (B) minus 0.24 times that in (A). All spectra are normalized in area.

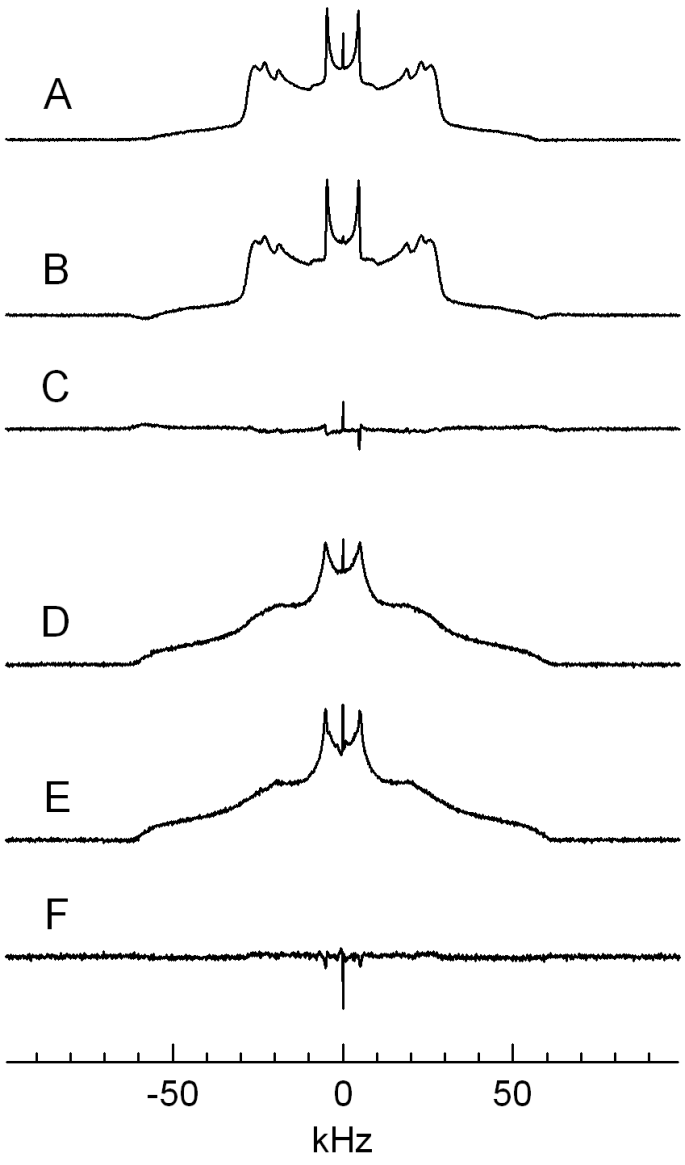

Figure 5-6: Comparison of the end-point difference spectra with experimental spectra at 32ºC.

(A) the spectrum of the 25 mol % cholesterol sample; (B) the end-point difference spectrum obtained from Figure 5D; (C) the difference between the spectrum in A and that in B; (D) the spectrum of the 8.5 mol% cholesterol sample; (E) the end-point difference spectrum obtained from Figure 5C; (F) the difference between the spectrum in D and that in E. All spectra (except those in (C) and (F)) are normalized in area.

Clearly, there is excellent agreement between the end-point spectrum obtained by spectral subtraction and the spectrum of the 25 mol% sample. If we subtract 17% of **lo**-rich spectrum from the **so**-rich spectrum, then we obtain the **so** phase end-point spectrum shown in Figure 5-5 (C), corresponding to a cholesterol mole fraction of x_s = 0.082. This difference spectrum, after normalization (Figure 5-6 (E)), is compared to the experimental spectrum obtained for the 8.5 mol% sample at 31^{o}C (Figure 5-6 (D)). The difference between the end-point spectrum and the 8.5 mol% spectrum is shown in Figure 5-6 (F). Again, the agreement between the two is promising. It is difficult to determine precisely how much of a spectrum like that in Figure 5-5 (B) should be subtracted from one like that in Figure 5-5 (A), and this uncertainty is reflected in the error in determining the coefficients K = 0.17 ± 0.03 and K' = 0.24 ± 0.04. At each temperature, we have collected spectra for 5 or 6 compositions in the so+lo region and, ideally, we could have formed various pair-wise decompositions and compared the end points obtained as in [89]. However, in DPPC/chol and PSM/chol the spectra corresponding to membranes differing in cholesterol by less than 7.5 mol% are not easily distinguishable and decomposing such spectra is difficult. That leaves us with only two (or three) convenient pairs of sample compositions, at each temperature, to be used for the subtraction analysis.

As was discussed in section 4.4, the spectral subtraction procedure assumes that the **so** and **lo** phases have the same relaxation time, T_{2e}. Figure 5-7 shows that this is not true for PSM-d31/cholesterol; the **lo** phase has a T_{2e} two to six times longer than that of the **so** phase, depending on the temperature.

Thus the **so** component decays faster than the **lo** component and is underrepresented in the quadrupolar echo spectrum of a membrane containing both phases. Note that 5.4 and 35 mol% cholesterol compositions are used to measure relaxation times of the **so** and **lo** phases, respectively. The values of the end-points compositions, x_s and x_f, with and without T_{2e} correction are listed in Table 5-1. At each temperature there is a significant shift in the **so**+**lo**/**lo** boundary to higher cholesterol concentrations, ranging from 2.1 to 2.9 mol%. This shift is less dramatic for DPPC-d31/cholesterol, maximum ~1.2 mol%. Furthermore, for both PSM-d31/cholesterol and DPPC-d31/cholesterol a relatively small shift in the **so**/**so**+**lo** boundary is observed, ranging from 0.3 to 1.8 mole%.

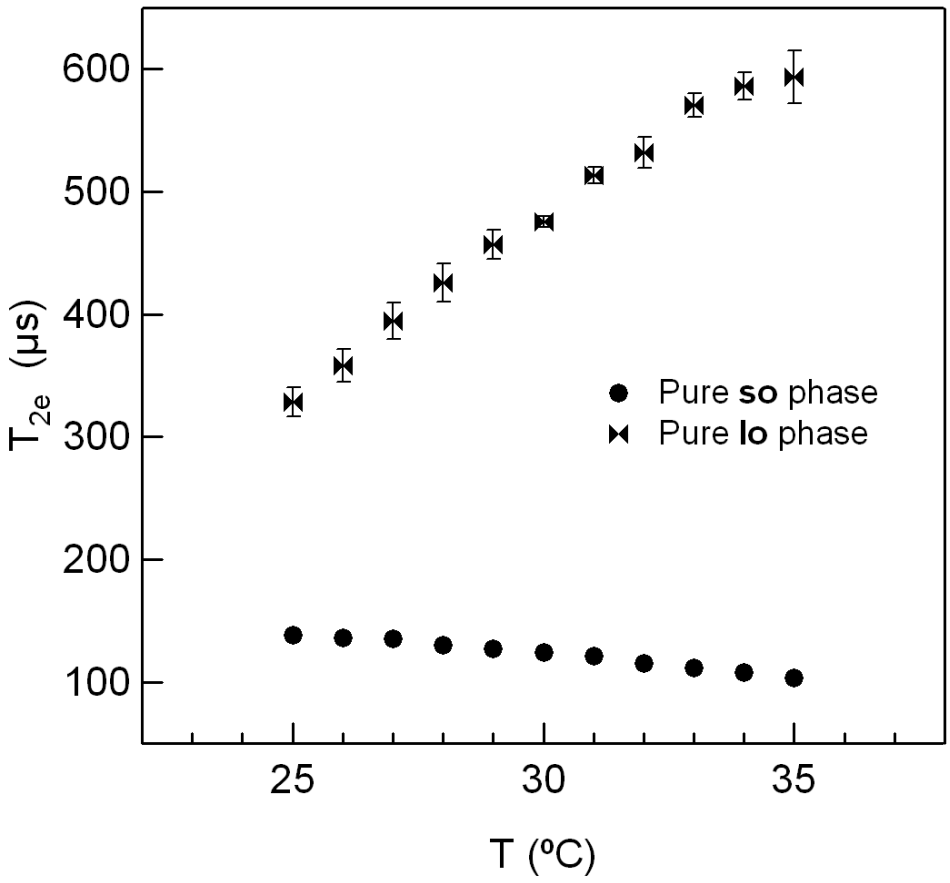

Figure 5-7: T_{2e} as a function of temperature for PSM-d31/cholesterol membranes with 5.4 mol% cholesterol (pure so phase) and 35 mole% cholesterol (pure lo phase).

Table 5-1: Comparison of the x_s and x_f Values and Those with T_{2e} Corrections

	No Correction		With T_{2e} Correction	
T (°C)	x_s	x_f	x_s	x_f
27	9.7 ± 0.5	27.3 ± 0.8	10 ± 0.5	30.2 ± 1.1
29	9.2 ± 0.4	26.4 ± 0.5	9.8 ± 0.5	29.2 ± 0.8
31	9 ± 0.5	25.7 ± 0.7	9.7 ± 0.5	28.3 ± 0.9
33	8 ± 0.6	25.3 ± 0.6	9.3 ± 0.5	27.8 ± 0.8
35	6.9 ± 0.7	24.9 ± 0.6	8.7 ± 0.6	27 ± 0.8

5.1.5 Phase Boundaries at Higher Cholesterol Content and High Temperature: ld/(ld+lo)/lo

Adding cholesterol changes the **ld** phase of the PSM-d31 membrane. This can be qualitatively observed by examining spectra of PSM-d31/cholesterol dispersions at a temperature above T_m as a function of cholesterol concentration (Figure 5-8, T = 47°C). Up to 8.5 mol% cholesterol the spectra exhibit the well-resolved "sharp" peaks associated with **ld** phase membranes. With increasing cholesterol concentration the average spectral width continues to increase and the individual peaks broaden. For cholesterol concentrations between 11 and 25 mol%, we interpret this broadening in terms of lipid diffusion between **ld** and **lo** domains with a rate faster than the NMR time scale. This implies that the PSM-d31/cholesterol membrane is in a heterogeneous phase state: **ld** and **lo** domains coexist. Around 28 mol% cholesterol, the individual peaks become sharper and remain sharp at higher cholesterol concentrations.

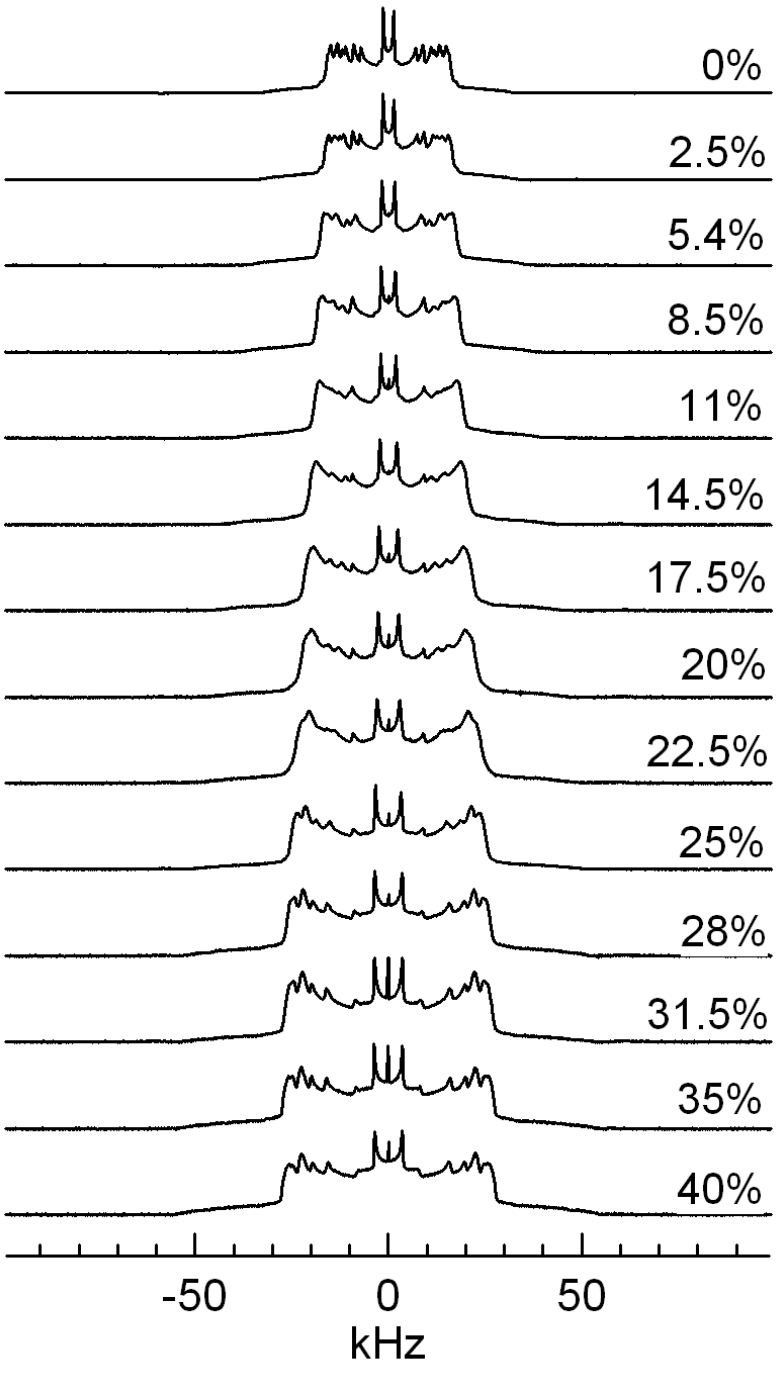

Figure 5-8: ^{2}H NMR spectra of PSM-d31/cholesterol as a function of cholesterol concentration (mole %) at T = 47ºC.

The spectra obtained for PSM-d31 membranes containing 31.5 mol% cholesterol or more are typical **lo** phase spectra, with an average spectral width significantly larger than that of the **ld** phase. Therefore, cholesterol induces **lo**-phase domains in PSM-d31 bilayers. With this inspection of powder spectra it is not obvious whether the PSM-d31 membrane with 28 mol% cholesterol is in a pure **lo** phase.

Further analysis is required to pinpoint the boundaries between the **ld** or **lo** phases and the **ld**+**lo** domain coexistence region. In Figure 5-8 we have plotted M_1 as a function of cholesterol concentration for several temperatures between 41^{o}C and 65^{o}C. The first moment of a ^{2}H NMR spectrum measures the average order parameter; therefore Figure 5-9 shows the increase of the average order parameter with increasing cholesterol concentration for various temperatures above T_m. The average order parameter of MLDs containing coexisting **lo** and **ld** domains is expected to be most sensitive to increasing cholesterol concentration because a proportion of **ld** phase will be converted to the much more ordered lo phase upon cholesterol addition. For **lo**-phase MLDs the effect of added cholesterol will be less pronounced. The M_1 (cholesterol) curves exhibit two distinct behaviors, as cholesterol concentration increases: below 28 mol% cholesterol the average order parameter increases rapidly, whereas above 28 mol% cholesterol it increases slowly or levels off.

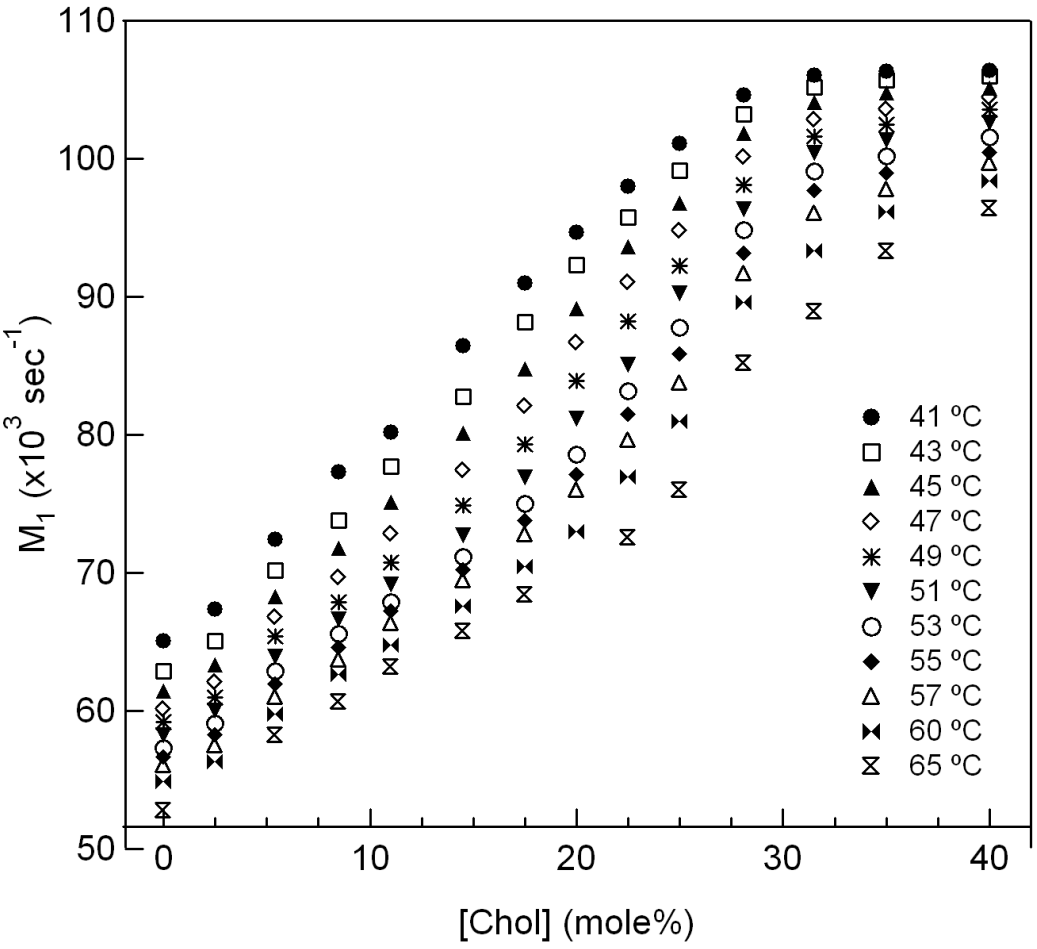

Figure 5-9: First moment (M_1) of PSM-d31/cholesterol spectra as a function of cholesterol concentration for various temperatures.

This plateau indicates that the PSM-d31 acyl chain has reached its maximum cholesterol-induced order. The NMR spectra suggest that at these temperatures the 75:25 PSM-d31/cholesterol MLD has coexisting **ld**+**lo** phases whereas the 68.5:31.5 DPPC-d31/cholesterol MLD is in the **lo** phase. Therefore,

the changes of slope in the M_1 (cholesterol) curve suggest a (**ld**+**lo**)/**lo** boundary near 28 mol% cholesterol. To determine this boundary, we drew a line through the points between 17.5 and 25 mol% cholesterol (or 20 and 28 mol%) and fitted another line to the points between 31.5 and 40 mol% cholesterol. The (**ld**+**lo**)/**lo** boundary is then obtained from the intercept of the two lines. An alternative approach to map the (**ld**+**lo**)/**lo** boundary is to examine the behaviour of the order parameter of a specific carbon-deuteron bond. Figure 5-10 shows the quadrupolar splitting of carbon 12 on the acyl chain of PSM-d31 as a function of cholesterol composition at 47^{o}C. The (**ld**+**lo**)/**lo** boundaries obtained as the temperature is varied are in very good agreement with those obtained through the analysis of M_1. In principle there should be a similar change in the slope of M_1 at low cholesterol concentrations, reflecting crossing the **ld**/(**ld**+**lo**) phase boundary. However, up to 50^{o}C no change in slope is observed. For higher temperatures, this slope change becomes obvious and the **ld**/(**ld**+**lo**) boundary can be determined. The two cholesterol concentrations corresponding to the slope changes come together as the temperature is raised indicating that the **ld**/(**ld**+**lo**) and (**ld**+**lo**)/**lo** boundaries are starting to merge. At 65^{o}C there is a narrow **ld**+**lo** region between 25 and 28 mol% cholesterol, suggesting that this temperature is close to the critical point of the PSM-d31/cholesterol membrane. For all temperatures below 55^{o}C the **ld**/(**ld**+**lo**) phase boundary has been determined by direct examination of the dePaked spectra. DePakeing the powder spectra allows one to observe variations in spectral width and sharpness of individual peaks more clearly.

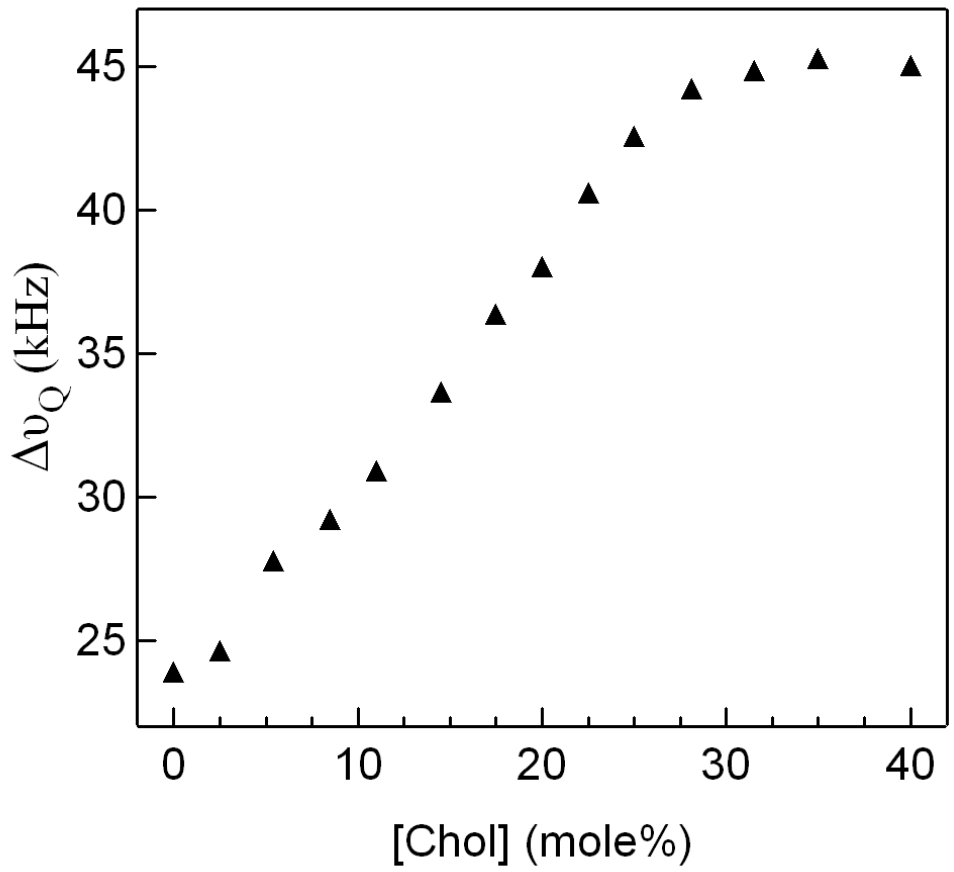

Figure 5-10: Quadrupolar splittings of carbon 12 on palmitoyl chain of PSM-d31/cholesterol membranes for various cholesterol concentrations, at T = 47ºC.

Figure 5-11 shows the dePaked spectra as a function of cholesterol concentration at 47^{o}C. Up to 8.5 cholesterol mol% the spectral lines are sharp. From 11 to 28 mol% cholesterol the spectral width increases rapidly and the dePaked spectra are blurry. They become sharp again at cholesterol concentrations 31.5 mol% and above. The “blurriness” is interpreted to mean that the PSM-d31/cholesterol membranes are in the heterogeneous domain coexistence region of the phase diagram. Thus, the **ld**/(**ld**+**lo**) phase boundary lies between 8.5 and 11 mol% cholesterol and the (**ld**+**lo**)/**lo** phase boundary between 28 and 31.5 mol% cholesterol.

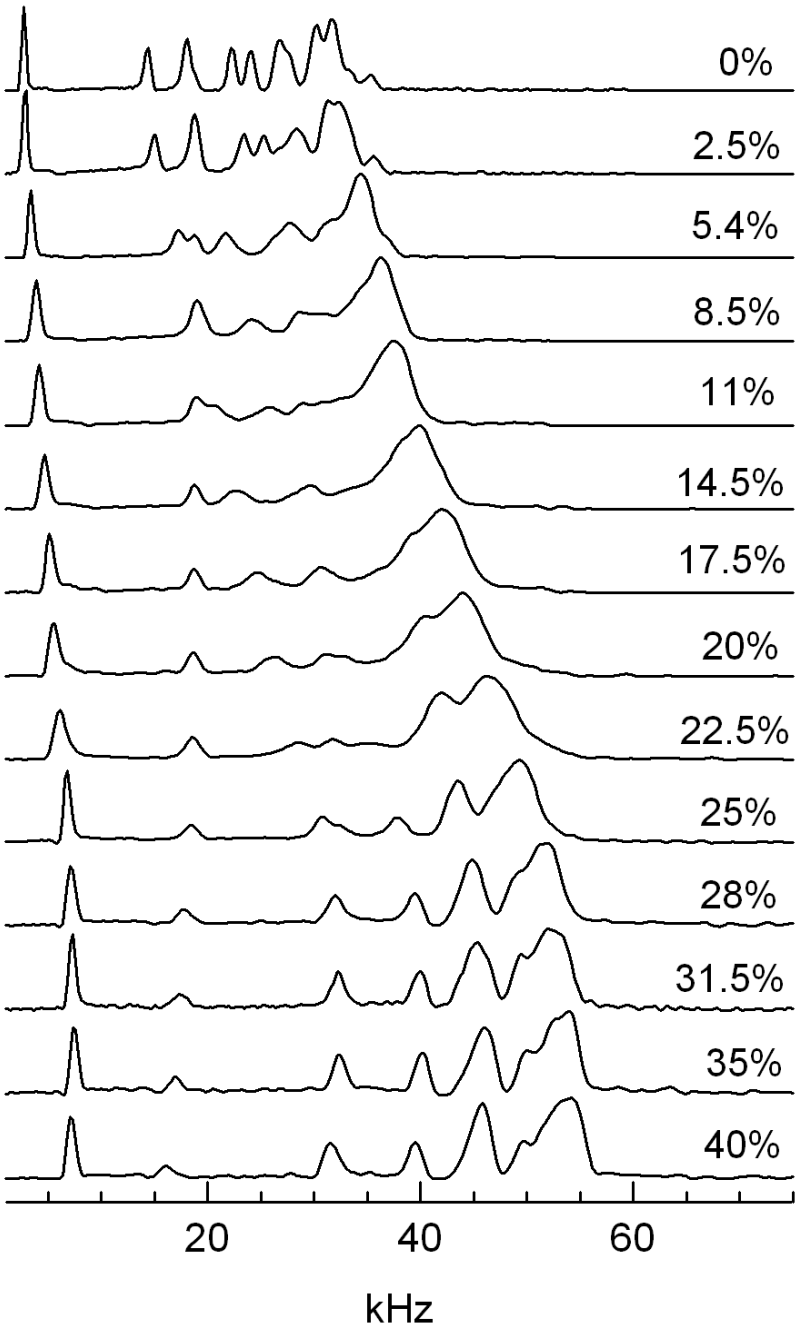

Figure 5-11: The dePaked spectra of PSM-d31/cholesterol as a function of cholesterol concentration at T = 47ºC.

5.1.6 Phase Diagrams

The partial phase diagrams for PSM-d31/cholesterol and DPPC-d31 (sn-2 perdeuterated)/cholesterol determined from the analysis of ^{2}H NMR spectra for various temperatures and cholesterol compositions, as discussed above, are shown in Figure 5-12. We have identified two regions of two-phase coexistence, one region of two-liquid-domains coexistence and a three-phase line in both lipid/cholesterol systems. The region of gel and liquid-crystalline phase coexistence lies in a narrow temperature range just below the melting point of pure lipids, at 39.5^{o}C, in DPPC-d31/cholesterol membranes and 3 degrees below the melting point, at 37^{o}C, in PSM-d31/cholesterol membranes. In both membranes, the **so/ld** region covers cholesterol concentration range from 0 to about 8 mol%. The boundaries of this two-phase region, open triangles, are estimated by the inspection of the powder spectra as a function of temperature, Figure 5-3, and tracing the residual gel component as the temperature is raised. The boundaries of gel and liquid-ordered phase coexistence region, open squares, are mapped using the well-established spectral subtraction method, described in detail in section 4.4 and illustrated in Figure 5-12. The **so**+**lo** phase coexistence region lies below 39^{o}C and extends between 9 mol% cholesterol and 26–30 mol% cholesterol in DPPC-d31/cholesterol system. For PSM-d31/cholesterol MLDs, this region lies below 37^{o}C and extends between 9 mol% cholesterol and 27–31 mol% cholesterol. The solid triangles, obtained from the onset of the transition in the $M_1(T)$ curves for MLDs with high cholesterol concentrations, Figure 5-2, are consistent with the data obtained from spectral subtraction. The **ld**/(**ld**+**lo**) boundary (solid diamonds) are determined from the

line broadening, characteristic of **ld**+**lo** heterogeneities, in the dePaked spectra described in Figure 5-11. The (**ld**+**lo**)/**lo** boundary is determined from the changes of slope in the M_1 versus cholesterol concentration curves (Figure 5-9) and the data agrees with the boundary obtained by examining the changes in the cholesterol-dependent dePaked spectra discussed in Figure 5-11. In the DPPC/cholesterol phase diagram, below 55^{o}C, the **ld**+**lo** region is between 7-16 mol% cholesterol and 26-32 mol% cholesterol. For PSM/cholesterol, this region is between 8-16 mol% and 28-30 mol% cholesterol. The upper bound of the **ld**+**lo** phase coexistence region lies in the vicinity of 65^{o}C in the PSM-d31/cholesterol phase diagram, as was discussed above, and higher than 65^{o}C in the DPPC-d31/cholesterol phase diagram. It follows from the $M_1(T)$ plots that the **so** to **ld** transition for DPPC-d31/cholesterol MLDs containing 8–20 mol% cholesterol occurs at constant temperature T_m = 39.5 ± 0.5^{o}C, implying the existence of a **so**+**ld**+**lo** three-phase line in the phase diagram separating the **so**+**lo** and **ld**+**lo** regions. The phase diagram suggests that the three phase line might be extended to 22.5 mol% cholesterol but the data for this composition does not exist to support that. The three phase line for the PSM-d31/cholesterol phase diagram is at T_m = 37 ± 0.5^{o}C and lies between 8.5 and 22.5 mol% cholesterol.

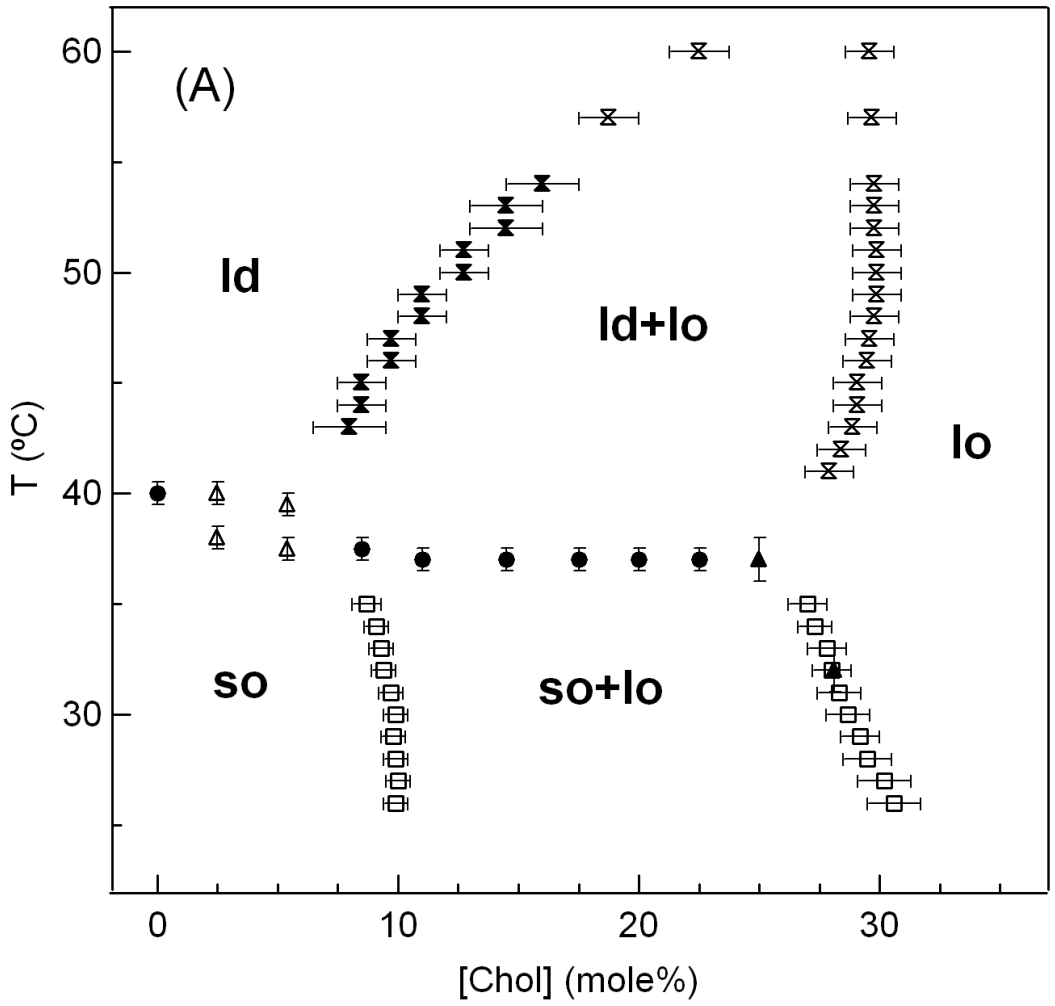
(A)
ld
ld+lo
lo
so
so+lo
T (°C)
60
50
40
30
0
10
20
30
[Chol] (mole%)

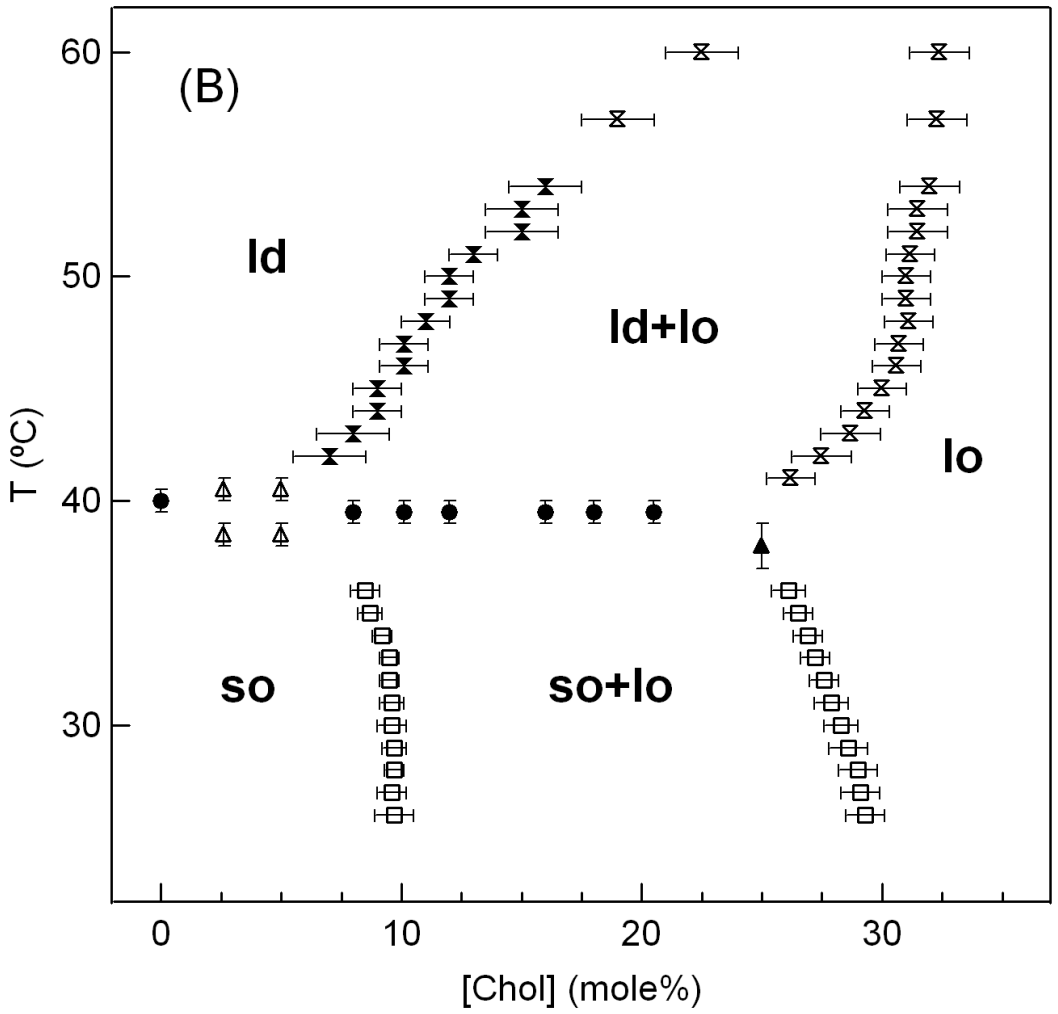

Figure 5-12: Partial phase diagram of the (A) PSM-d31/cholesterol and (B) DPPC-d31/cholesterol membranes.

Midpoint of the transition from M_1(T) curves (Fig. 5-2) (●); onset or end of transition obtained by inspection of the spectra versus temperature (Fig. 5-3) (△); obtained from the spectral subtraction (□); obtained from M_1(cholesterol) curves (Fig. 5-9) (⧖); obtained by inspection of the depaked spectra versus cholesterol concentration (Fig. 5-11) (⧗).the onset of transition in M1(T) curves for MLDs having cholesterol concentrations of 25 or 28.1 mol% in PSM/cholesterol and 25 mol% in DPPC/cholesterol (▲).

We now compare the partial phase diagram of sn-2 chain labelled DPPC-d31/cholesterol with that of DPPC-d62/cholesterol by Vist and Davis [10]. Both diagrams contain a three-phase line and three two-phase regions. For DPPC-d62 the main phase transition temperature is two degrees lower, at 38^{o}C due to both chains being perdeuterated, and correspondingly in the presence of cholesterol the **so**+**ld** region and the three-phase line are at lower temperatures. To compare the **so**/(**so**+**lo**)/**lo** boundaries, we consider our spectral subtraction results without the correction due to transverse relaxation time, since this effect is missing in the DPPC-d62/cholesterol study. The **so**/(**so**+**lo**) boundary lies close to 9 mol% for DPPC-d31/cholesterol and around 7.5 mol% for DPPC-d62/cholesterol, which are consistent within error. However, the (**so**+**lo**)/**lo** boundaries are quite different. The (**so**+**lo**)/**lo** boundary of DPPC-d62/cholesterol occurs around 22.5 mol% and is nearly vertical, indicating that the formation of **lo** domains in the **so** membrane depends only slightly on temperature. However, the (**so**+**lo**)/**lo** boundary of DPPC-d31/cholesterol is about 5 mol% higher and slopes from 26 mol% at 36^{o}C toward 29 mol% at 26^{o}C, meaning that the composition of **lo** domains depends on temperature. The **ld**/(**ld**+**lo**) and (**ld**+**lo**)/**lo** boundaries of DPPC-d62/cholesterol are partially determined from the upper limit of the broad component of the DSC traces and the sharpening of the resonances at high cholesterol concentrations, respectively. Limited data points are available for full comparison between the two studies. The **ld**/(**ld**+**lo**) boundary of the DPPC-d62/cholesterol extends from 10 mol% cholesterol at 39^{o}C to 20 mol% cholesterol at 43^{o}C, whereas, the (**ld**+**lo**)/**lo** boundary extends

from 22.5 mol% cholesterol at 39^{o}C to 25 mol% cholesterol at 41.5^{o}C. Therefore, the **ld**+**lo** region of the DPPC-d62/cholesterol covers a smaller range of temperature and composition than those of DPPC-d31/cholesterol or PSM-d31/cholesterol.

We also compare the partial phase diagram of DPPC-d31/cholesterol (or PSM-d31/cholesterol) with that of *sn*-1 chain labelled DPPC-d31/ergosterol determined by Hsueh *et al.* [11]. The overall phase diagrams are very similar except for one major difference. The (**ld**+**lo**)/**lo** boundary in DPPC-d31/cholesterol covers a broader range of cholesterol mol% and lies at slightly higher temperatures. A much more obvious difference between these two systems is that the **ld**+**lo** coexistence region extends to very high temperatures, above 65^{o}C, for DPPC-d31/cholesterol, whereas the critical point in DPPC-d31/ergosterol is found near 54^{o}C.

5.1.7 Order Parameter Profile

^{2}H NMR spectra of PSM-d31/cholesterol membranes, shown in Figure 5-1, are much broader than those of DPPC-d31/cholesterol membranes in both the **ld** and **lo** phases, indicating that the lipid molecules in the two systems have different packing properties. To quantitatively discuss these differences we have calculated the order parameter profiles, S_{CD}, along the acyl chains of both lipid/cholesterol membranes in fluid phases for various cholesterol concentrations. Figure 5-13 shows order parameter profiles of PSM-d31/cholesterol MLDs for various cholesterol compositions at 47^{o}C. In pure PSM-d31 membrane S_{CD} is about 0.26 in the plateau region near the head-group and

drops significantly to about 0.02 for methyl group at the end of the chain. Adding cholesterol orders the membrane with different rates in **ld**, **ld**+**lo**, and **lo** regions of the phase diagram. The average order parameter, excluding the C2 deuterons, increases from 0.195 to 0.230 in the ld phase when 8.5 mol% cholesterol is added to pure PSM-d31. By adding nearly the same amount of cholesterol to PSM-d31/cholesterol 85.5:14.5 membrane in the **ld**+**lo** region the average S_{CD} increases from 0.259 to 0.308. In the lo phase the average order

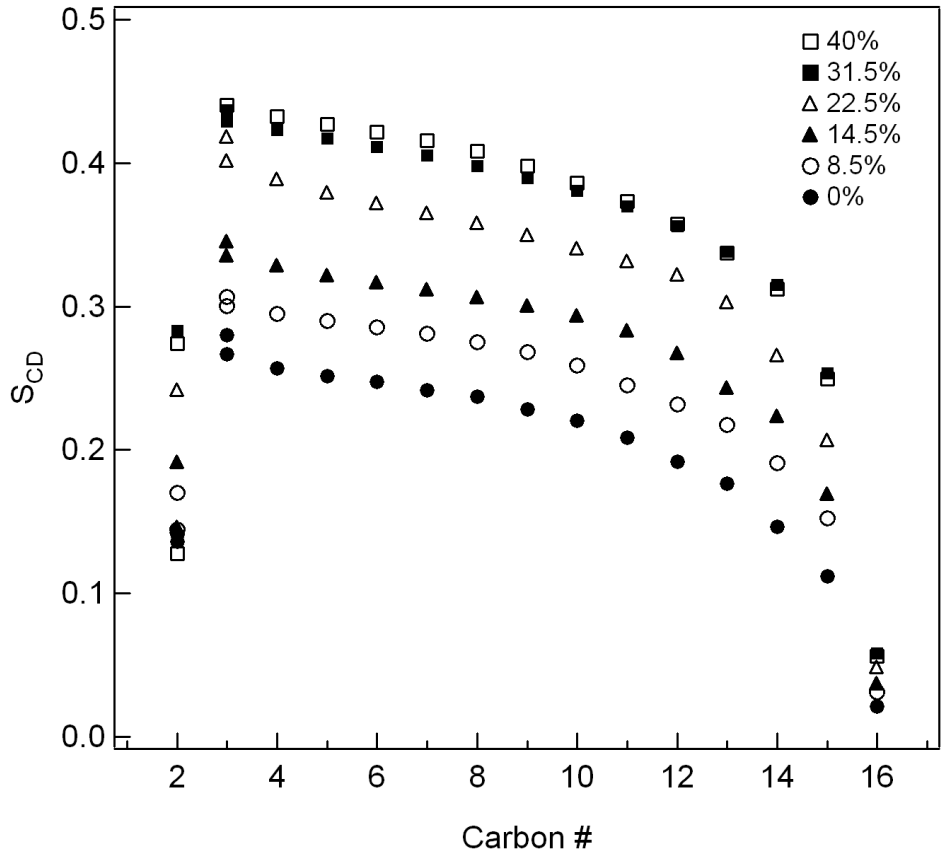

Figure 5-13: Smoothed order parameter profiles of PSM-d31/cholesterol for various cholesterol concentrations at T = 47ºC.

parameter increases by a small amount, from 0.343 to 0.348, when same amount of cholesterol, 8.5 mol%, is added to PSM-d31/cholesterol 68.5:31.5 membrane. Thus, cholesterol is most effective in ordering the PSM-d31/cholesterol membrane in the two-liquid domain coexistence region. This is consistent with the observed slope change in $M_1(T)$ plot, Figure 5-2. A. Bunge *et al.* [90] have published order parameter data for PSM-d31/cholesterol at 40^{o}C, which is two degrees above their reported main phase transition temperature, 38^{o}C. We compared our results at 42^{o}C, two degrees above the PSM-d31 T_m in this work, with their reported average ordered parameter and found good agreement. Figure 5-14 shows the order profile of PSM-d31/cholesterol compared with that of DPPC-d31/cholesterol for 0, 20, and 40 mol% cholesterol at 47^{o}C. In the absence of cholesterol, PSM ($<S_{CD}>$ = 0.195) is significantly more ordered than DPPC ($<S_{CD}>$ = 0.169). This result supports the hypothesis of intermolecular hydrogen bonding within the PSM bilayer mediated by the free hydroxyl group of adjacent PSM molecules [91]. Figure 5-14 also shows that when cholesterol is added to pure lipids the PSM-d31/cholesterol membrane is still more ordered than DPPC-d31/cholesterol but the difference in the order parameter becomes smaller as cholesterol concentration is increased. For instance, for carbon C10 on the acyl chain the differences between S_{CD} of PSM-d31/cholesterol and that of DPPC- d31/cholesterol are as follows: for pure lipids ΔS_{CD} = 0.221-0.191 = 0.03 (PSM 15.7% more ordered than DPPC), for lipids with 20 mol% cholesterol ΔS_{CD} = 0.323-0.298 = 0.025 (8.4% more ordered) and for membranes with 40 mol% cholesterol ΔS_{CD} = 0.386-0.365 = 0.021

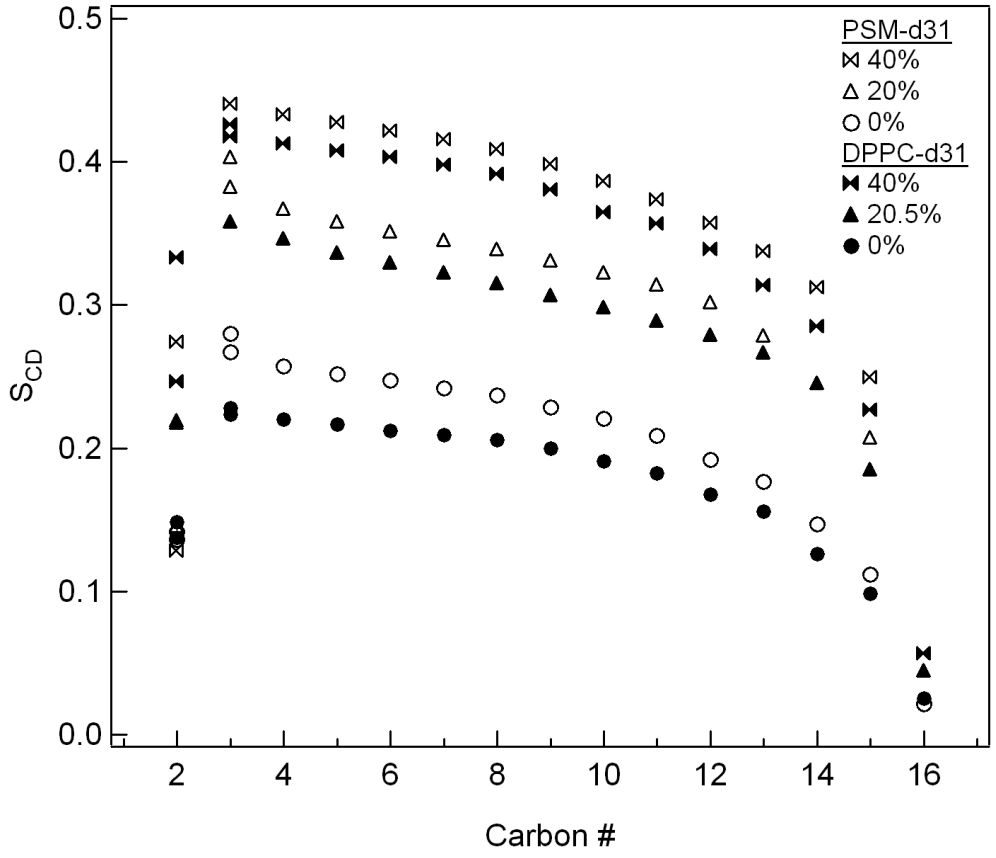

Figure 5-14: Smoothed order parameter profiles of MLDs composed of PSM-d31/cholesterol and DPPC-d31/cholesterol for various cholesterol concentrations T = 47ºC.

(5.7% more ordered). This trend is consistent with the M_1 (cholesterol) curve as illustrated in Figure 5-15, at 47^{o}C. It should be emphasized that the kink conformation has unique characteristics that are observed in quadrupolar splittings of C2 and C3 deuterons. Figure 5-13 shows that the C3 deuterons in PSM-d31/cholesterol have different quadrupolar splittings and thus they are inequivalent. This can also be observed in the dePaked spectra of pure PSM-d31 and PSM-d31 with low cholesterol compositions (Figure 5-11). A similar feature

is observed in DPPC-d31/cholesterol but the difference in quadrupolar splitting of the C3 deuterons is smaller than that in PSM-d31/cholesterol. The C2 deuterons display a unique behaviour in both PSM-d31/cholesterol and DPPC/cholesterol (Figure 5-14). Not only the two C2 deuterons are inequivalent but also they have different (smaller) geometrical order parameters compared to the deuterons on the rest of the acyl chain. The dePaked spectra of PSM-d31/cholesterol (Figure 5-11) shows that the quadrupolar splitting of the C2 deuteron, unlike that of the rest of the acyl chain, drops slightly when cholesterol is added to the PSM-d31 membrane. This quadrupolar splitting changes from about 19 kHz in pure PSM-d31 to about 16 kHz in PSM-d31 with 40 mol% cholesterol. This means that one of the C2 deuterons undergoes a distinct conformational change as cholesterol is added to either PSM-d31 or DPPC-d31.

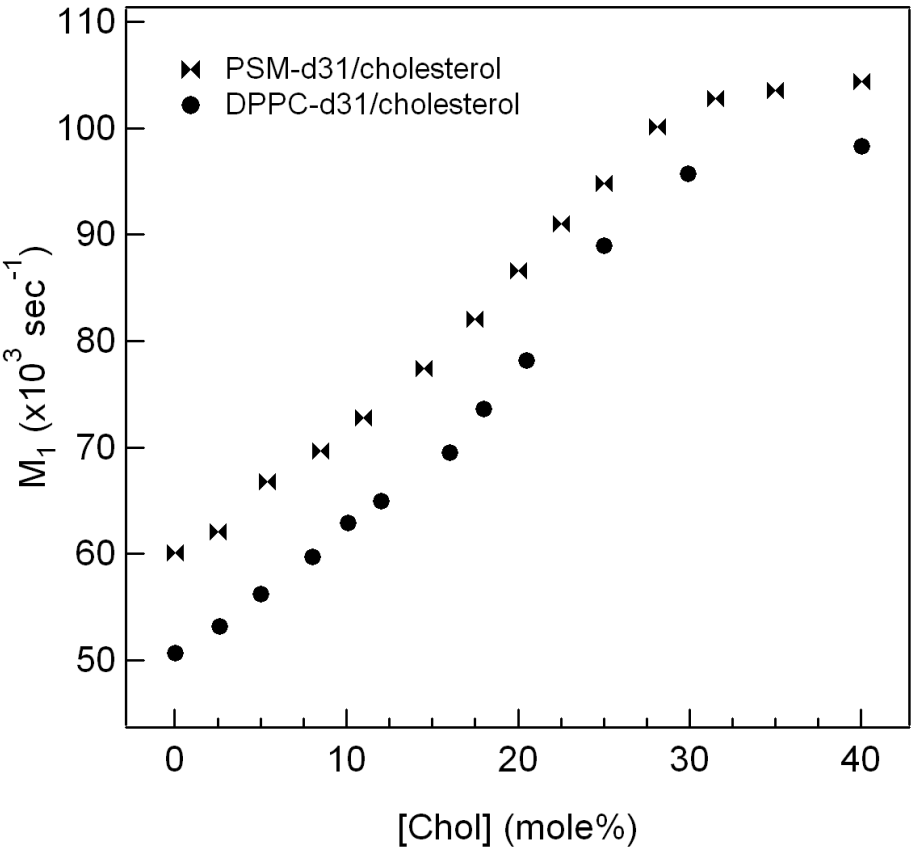

Figure 5-15: M_1 as a function of cholesterol concentration for PSM-d31 and DPPC-d31 MLDs at T = 47ºC.

5.1.8 Domain Size in ld+lo Region

Within the **ld**+**lo** coexistence region the ^{2}H NMR spectra of the two phases show the axial symmetry of molecular motions, but they differ in average value of quadrupolar splittings. For example, in the spectra of PSM at 47^{o}C the largest quadrupolar splitting changes from 39.4 kHz at 11 cholesterol mol% to 53.5 kHz at 28.1 mol%. This difference in quadrupolar splitting translates into a spectroscopic time scale of about 70 μs. The translational diffusion constant *D* for PSM/cholesterol close to the middle of the two-phase region is about $1.8 \times 10^{-12}\, m^2/s$ at 47^{o}C [84]. Using the relation,

$$(\langle \Delta x^2 \rangle)^{1/2} = (4\mathrm{D}\tau)^{1/2}. \qquad (5.1)$$

We estimate that a lipid can diffuse a root mean squared distance of about 22 nm during our NMR time scale. If the domains in the **ld**+**lo** region are smaller than, or of the order of, this characteristic distance, then the NMR experiment will see an averaged spectrum, and the spectral subtraction technique will not be able to separate the spectrum into two components. Our observation of line broadening of the spectra which occur within this region is suggestive of nanoscale separation between cholesterol-rich and cholesterol-poor regions, as was proposed for cell membranes [92], and of the exchange averaging mechanism. Such small length scales are consistent with the lack of observation of micron-sized phase-separated domains in binary phospholipid/cholesterol giant unilamellar vesicles [93].

We now estimate the size of the domains involved in this **ld**+**lo** nanoscale phase coexistence by applying the method commonly used to understand A↔B

chemical exchange, replacing chemical shifts by quadrupolar splitting [11]. The lipid exchange time is

$$\tau = 1/2k_{-1}, \tag{5.2}$$

where k_{-1} is the rate constant characterizing lipid exchange between **lo** and **ld** domains (k_{-1} is assumed to be equal to k). This rate constant is obtained from [94]

$$1/T_{2,\mathrm{obs}} = f_{\mathrm{A}}/T_{2\mathrm{A}} + f_B/T_{2B} + \left[\left({f_A}^2{f_B}^2\right)4\pi^2(\Delta\delta_{\mathrm{AB}})^2\right]/k_{-1}, \tag{5.3}$$

In this equation f_{A} and f_{B} are fractions of total labelled lipid in the **ld** and **lo** domains, respectively, and $\Delta\delta_{\mathrm{AB}} = \Delta\delta_{\mathrm{A}} - \Delta\delta_{\mathrm{B}}$ is the difference of the quadrupolar splittings in the two states

$$\Delta\delta_{\mathrm{AB}} = \Delta\nu_{\mathrm{Q,lo}} - \Delta\nu_{\mathrm{Q,ld}}, \tag{5.4}$$

where $\Delta\nu_{\mathrm{Q,lo}}$ and $\Delta\nu_{\mathrm{Q,ld}}$ are the quadrupole splittings of doublets of a particular carbon for the **lo** and **ld** spectra, respectively. In both PSM/cholesterol and DPPC/cholesterol, the only isolated doublets for all cholesterol compositions are the methyl and one of the C2 deuterons. However, none of these peaks are reliable for this calculation. It is well-known that the methyl resonance has distinctly long T_1 and T_2 relaxation times, resulting in an inaccurate measurement of its width. In addition, dePaked spectra in Figure 5-11 show that the C2 deuteron in PSM-d31/cholesterol system undergoes distinct conformational changes due to its proximity to the kink, thereby its quadrupolar splitting stays more or less the same as cholesterol concentration is raised. Our best option is

the C15 peak since it is either well separated or overlaps with only one other peak, in which case it can be separated by multi-peak fitting.

The rate constants $T_{2,\mathrm{obs}}$, $T_{2\mathrm{A}}$, and T_{2B} can be obtained from the linewidths $\Delta\nu$ of individual peaks:

$$1/T_{2,\mathrm{obs}} = \pi\,\Delta\nu_{\mathrm{ld+lo}},$$

$$1/T_{2,\mathrm{A}} = \pi\,\Delta\nu_{\mathrm{lo}},$$

$$1/T_{2,\mathrm{B}} = \pi\,\Delta\nu_{\mathrm{ld}}, \qquad (5.5)$$

where $\Delta\nu_{\mathrm{ld+lo}}$, $\Delta\nu_{\mathrm{lo}}$, and $\Delta\nu_{\mathrm{ld}}$ are the widths at half maximum height of the individual C15 peaks in the depaked **ld**+**lo**, **lo**, and **ld** spectra, respectively.

The calculation of domain size within the **ld**+**lo** region is based on the labelled lipid diffusing between the two domains. In principle, both the lipid and cholesterol diffuse in the coexistence region. A study on the lateral diffusion of DPPC and cholesterol by ^{1}H pulsed field gradients (PFG) magic angle spinning (MAS) NMR spectroscopy [95] revealed that the diffusion constants of DPPC and cholesterol are very close. For example, in a DPPC-d62 sample with 20 mol% cholesterol at 47 ^{o}C, $D = 7.5 \times 10^{-12}\ m^2/s$ for DPPC and $D = 9.0 \times 10^{-12}\ m^2/s$ for cholesterol. This study also shows that, depending on the cholesterol composition, the DPPC diffusion constant [95] is 4-6 times larger than that of sphingomyelin [84].

An example of the parameters required to estimate the *rms* distance $(\langle \Delta x^2 \rangle)^{1/2}$, in DPPC/cholesterol, PSM/cholesterol, and DPPC/ergosterol [11] are listed in Table 5-2. This comparison shows that the diffusion constant has a

significant influence on the calculated domain size. The reported result by Hsueh *et al.* [11] is more than twice that of DPPC/cholesterol. The main discrepancy arises from the quadrupolar splitting of the **ld** and **lo** states, $\Delta\delta_{Q,ld}$ and $\Delta\delta_{Q,lo}$, used in Eq. 5.3. We used the full splitting in the dePaked spectra, corresponding to the 0^o splitting in the powder spectra, since the T_2 relaxation times are estimated from the linewidths in the dePaked (0^o orientation) spectra. In DPPC/ergosterol study, Hsueh *et al.* used half of the quadrupolar splitting as measured from the dePaked spectra. We also compare our results with the work by Veatch *et al.* [96] where they estimated domain sizes of ~80 nm in dioleoylphosphatidylcholine/DPPC (1:1) + 30 mol% cholesterol membranes displaying liquid/liquid coexistence at 25^oC.

Table 5-2: Parameters used in Eqns. 5.1 and 5.3 and the estimated length scale characterizing the ld/lo domains, at *T* = 47 °C.

Parameters and result	DPPCd31/cholesterol	PSMd31/cholesterol	DPPCd31/ergosterol
Cholesterol mol%	20.5	20	20
D	7.5×10^{-12} m^2/s	1.8×10^{-12} m^2/s	10^{-11} m^2/s
f_A	0.44	0.45	0.52
f_B	0.56	0.55	0.48
$1/T_{2A}$	3.4 $(ms)^{-1}$	3.4 $(ms)^{-1}$	3.8 $(ms)^{-1}$
$1/T_{2B}$	5.7 $(ms)^{-1}$	4.5 $(ms)^{-1}$	3.2 $(ms)^{-1}$
$1/T_{2,obs}$	7.6 $(ms)^{-1}$	6.8 $(ms)^{-1}$	7.1 $(ms)^{-1}$
$\Delta\upsilon_{Q,lo}$	56.2 kHz	64.4 kHz	26.7 kHz
$\Delta\upsilon_{Q,ld}$	33.6 kHz	34.6 kHz	13.9 kHz
$\Delta\delta_{AB}$	22.6 kHz	29.8 kHz	12.8 kHz
$(<\Delta x^2>)^{1/2}$	6 nm	2.2 nm	13 nm

The root mean squared distance $(\langle\Delta x^2\rangle)^{1/2}$ traveled by lipid molecules before they sense **lo/ld** heterogeneity is plotted as a function of cholesterol concentration in Figure 5-16. The domain size in the **ld/lo** region is estimated to be $2\times(\langle\Delta x^2\rangle)^{1/2}\approx 5\,\mathrm{nm}$ in PSM-d31/cholesterol and $2\times(\langle\Delta x^2\rangle)^{1/2}\approx 12\,\mathrm{nm}$ in DPPC/cholesterol. It seems that close to the **ld/lo** boundaries the domains become significantly large. However, this is a consequence of the behaviour of

Eqn. (5.3) when the fraction of **ld** or **lo** approaches zero ($1/k_{-1}$ diverges). The number of molecules constituting a domain is not known since we have no information on domain shape. If we make a simple assumption that the domains are circular then the number of DPPC lipids constituting an **ld** domain close to the middle of **ld**+**lo** region is on the order of 50, since each lipid occupies approximately 0.60 nm^2 (Seelig [97]; Levine & Wilkins [98]). This corresponds to ~ 5 cholesterol and ~ 45 lipid molecules.

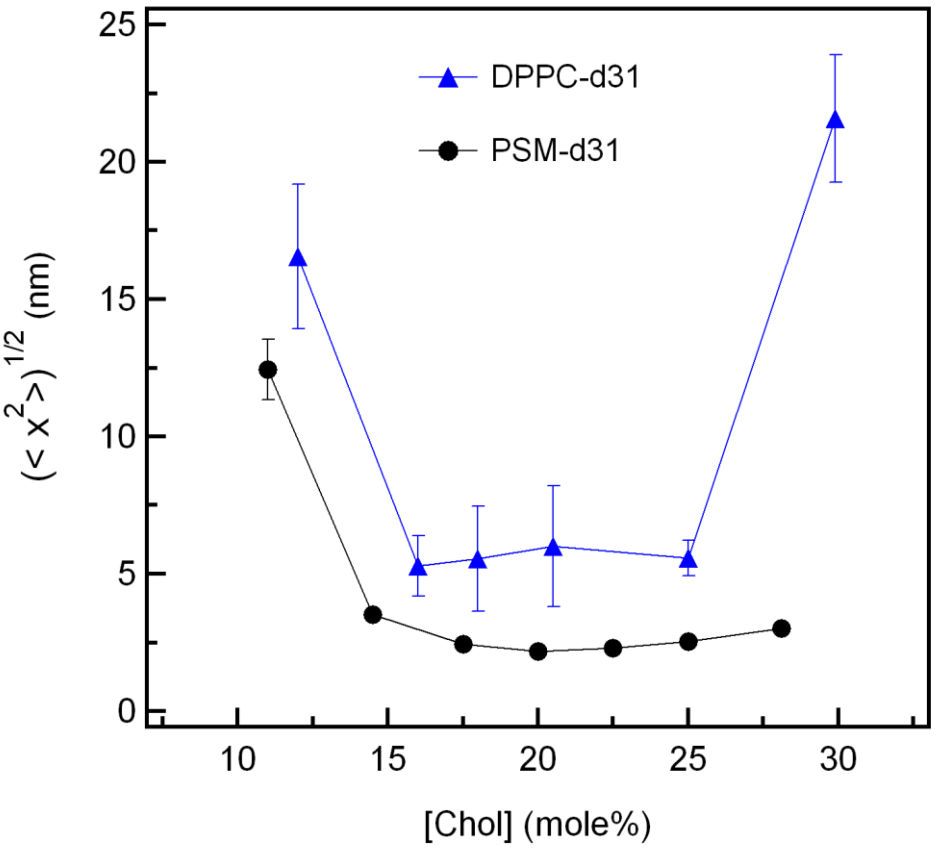

Figure 5-16: The root mean square distance diffused by lipid molecules within the ld/lo domains membranes for various cholesterol compositions, at T = 47ºC.

Table 5-3 shows the length scale $(\langle \Delta x^2 \rangle)^{1/2}$ in PSM-d31 with 20 mol% cholesterol for several temperatures. This result indicates that the domain size is independent of the temperature.

Table 5-3: The ld/lo domain length scale of PSM-d31 for various temperatures, cholesterol composition = 20 mol%.

T (^{o}C)	$(\langle \boldsymbol{\Delta x^2} \rangle)^{\boldsymbol{1/2}}$
47	2.2 ± 0.2
50	2.4 ± 0.5
53	2.7 ± 0.5
57	2.3 ± 0.9

Fluorescence microscopy methods have not been able to detect phase separation in binary DPPC-cholesterol mixtures that have been inferred from ^{2}H NMR studies. However, micron-sized immiscible phase separated liquid domains are observed by fluorescence in ternary mixtures. The line-broadening observed in DPPC/cholesterol [10], DPPC/ergosterol [11], and the binary mixtures studied in this work was attributed to a diffusion-limited exchange of lipids between domains of the coexisting liquid phases.

The “condensed complex” model provides an alternative interpretation to describe phase diagrams and, in particular, domain formation (line broadening) in binary mixtures of cholesterol-DPPC and ergosterol-DPPC. The condensed complex model is a thermodynamic model that attributes the composition-

dependent NMR line broadening to the kinetics of complex formation between these sterols and the DPPC [99]. Ternary mixtures of DPPC/cholesterol/DOPC form micron-sized immiscible liquid domains easily observed with fluorescence microscopy. The immiscibility can be modeled in terms of an intermolecular attractive interaction and a repulsive interaction. The attractive interaction is between cholesterol and DPPC, leading to a complex formation. The (mean field) repulsive interaction is between the complex and DOPC, leading to immiscibility. The model provides a semi-quantitative description of the DPPC/cholesterol/DOPC phase diagram and involves no phase separation of DPPC/cholesterol, or other binary pairs. The chemical kinetics of complex formation and dissociation can account for the ^{2}H NMR line broadening attributed to the nano-scaled domains coexistence. At a given temperature there are two parameters used to model the phase diagram: the equilibrium constant, K_{eq}, and the critical temperature, T_C, of the binary DOPC/Complex pair (representing mean-field repulsion). The calculated first moment of the ^{2}H NMR spectra in DPPC/ergosterol using the parameters in the model fits well to the experimental data [11].

A more recent study on ternary mixtures of DPPC/cholesterol/DiPhyPC using a model of condensed complexes predicts phase separation in binary DPPC/cholesterol mixtures [27]. This study assumes immiscibility between the complex and DiPhyPC to model the closed miscibility loop found in the ternary mixture. This study also assumes immiscibility between complex and DPPC to generate phase separation in the binary DPPC/cholesterol mixture. There are

three parameters used in this study: the equilibrium constant K_{eq}, and the critical temperatures of complex/DPPC and complex/DiPhyPC binary pairs. The rotation of tie-lines orientation in ternary mixtures of DPPC/cholesterol/DiPhyPC from parallel to roughly perpendicular with respect to the DPPC/cholesterol axis results in phase separation in binary DPPC/cholesterol mixtures.

It seems that dynamic “condensed complexes” are a useful way of modeling the phase diagram and, in particular, describing the line-broadening in the **ld**/**lo** region. However the choice of model parameters makes a big difference; one shows results that are consistent with the results presented in this work while the other predicts the possibility of micron-sized **ld**/**lo** phase separation in binary mixtures.

5.2 Selectively Deuterated PSM/cholesterol

The constructed phase diagrams in both PSM-d31/cholesterol and DPPC-d31/cholesterol have shown **ld** + **lo** phase coexistence regions, however macroscopic coexistence of the two fluid phases does not occur. Instead, we observed nano-domain structures consistent with the ^{2}H NMR spectral line-broadening in the **ld** + **lo** region. The size of the domains was estimated by means of fast exchange (in a ^{2}H NMR sense) of lipids between **ld** and **lo** domains. The spin-spin relaxation time used in the calculation is estimated from the linewidth of a well-resolved peak in the dePaked spectra, at a given temperature (Eqns. 5.5). However, by analyzing the depaked spectrum, information from all orientations of the lipid long axis, which constitutes the powder pattern, is averaged. As was pointed out by Professor Harden

McConnell [private communication], this may obscure the results used to characterize domain size. Furthermore, the *rms* distance diffused by lipid molecules within the **ld/lo** domains is sensitive to the difference of the quadrupolar splittings, $\Delta\delta_{\mathrm{AB}}$, in the two pure states (Eqns. (5.1), (5.2), and (5.3)):

$$(\langle \Delta x^2 \rangle)^{1/2} \propto \frac{1}{\Delta\delta_{AB}} \tag{5.6}$$

This difference in the quadrupolar splitting (or, equivalently, the order parameter) of a peak varies along the acyl chain, as shown on Figure 5-13. For example, for the methyl resonance $\Delta S_{\mathrm{CD}} = 0.03$ whereas for carbon 4 on the plateau region of order parameter profile $\Delta S_{\mathrm{CD}} = 0.14$. One can establish the estimation of domain size based on a peak in the plateau region, where the parameter $\Delta\delta_{\mathrm{AB}}$ levels off, but all the resonances in this region are composite peaks and separating them by fitting to Gaussians will introduce large errors to the parameter. Selectively deuterated sphingomyelin, labeled at C9 of the N-linked palmitoyl chain, is used to accurately measure the orientation dependence of T_2 relaxation time and accordingly estimate domain size as a function of orientation.

5.2.1 PSM-d2/cholesterol MLDs

Figure 5-17 (A) shows the spectra obtained for pure C9 deuterated PSM. Below 39^{o}C, the membrane is in the gel phase and the ^{2}H NMR spectra display the “bell-shape” characteristic of this phase. The spectra above 43^{o}C are “Pake-doublets”, which are characteristic of liquid-crystalline spectra for two deuterons. At 41^{o}C, the spectrum displays mainly gel phase with a small residual **ld**

component. First moment of the spectra as a function of temperature, Figure 5-17 (B), shows that PSM-d2 undergoes a fairly sharp transition from **so** to **ld** phase around 42^{o}C. This is two degrees higher than the main phase transition temperature for perdeuterated PSM. It is well-known that each chain perdeuteration decreases the transition temperature by nearly two degrees [100]. The M_1 plot indicates that the transition temperature of PSM-d2, measured by ^{2}H NMR, is close to that of non-deuterated PSM.

The constructed phase diagram of PSM-d31/cholesterol membrane is used as a guide to carefully choose the appropriate cholesterol compositions for the calculation of the domain size. At 47^{o}C, the **ld**+**lo** domain coexistence region extends from 9.75 ± 1 to 29.6 ± 1 mol% cholesterol. Therefore, cholesterol compositions of 5.4% and 35% are made to obtain pure **ld** and **lo** phase spectra respectively. The minimum domain size in PSM-d31/cholesterol is found to be near the middle of **ld**+**lo** region, where the membrane is most heterogeneous. Therefore, 20 mol% is chosen for cholesterol composition to obtain the spectrum of two-liquid domains.

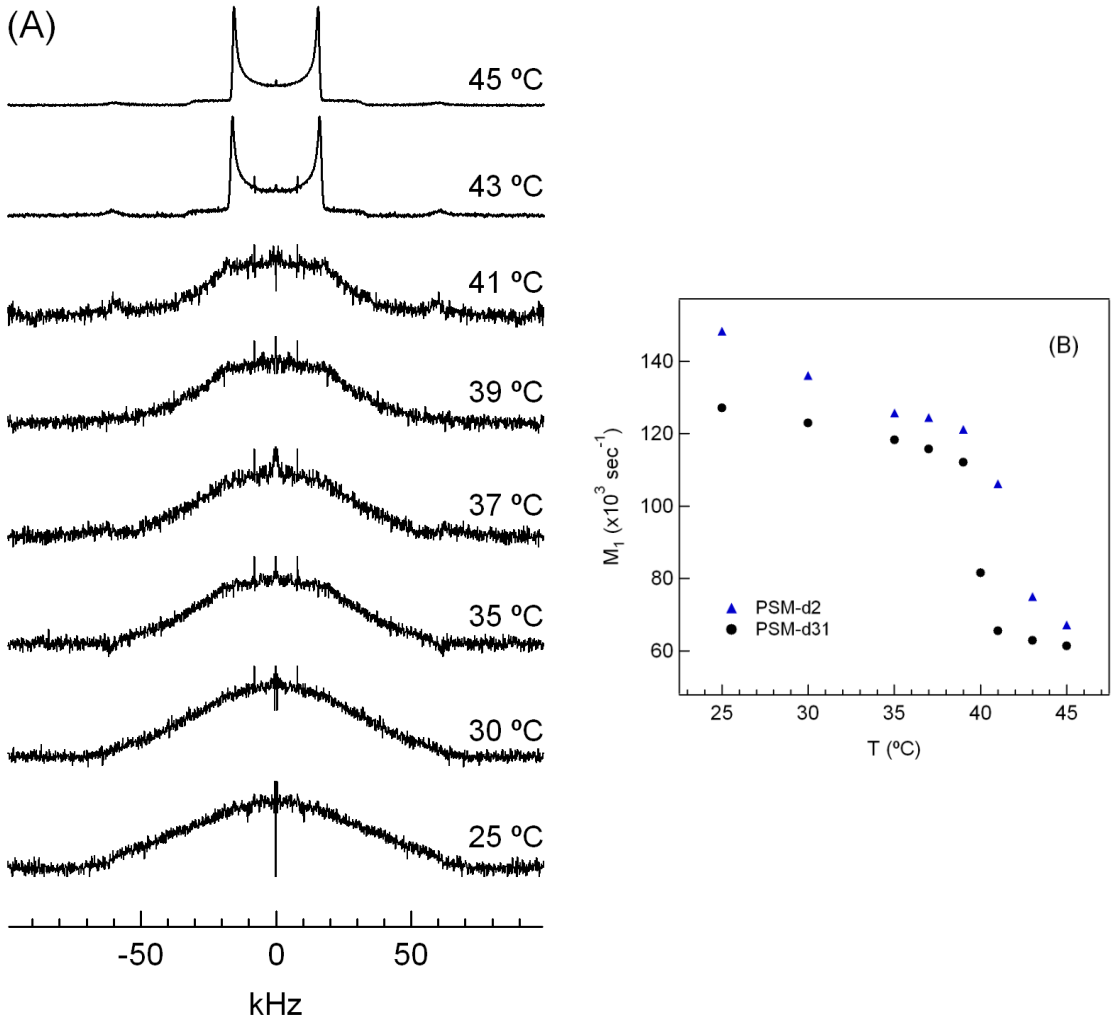

Figure 5-17: (A) ^{2}H NMR spectra of pure C9 deuterated PSM as a function of temperature, and (B) First moment (M_1) of PSM-d2 spectra compared to that of PSM-d31 as a function of temperature.

The ^{2}H NMR spectra of pure **ld** phase, pure **lo** phase, and **ld**+**lo** phase domains are displayed in Figure 5-18.

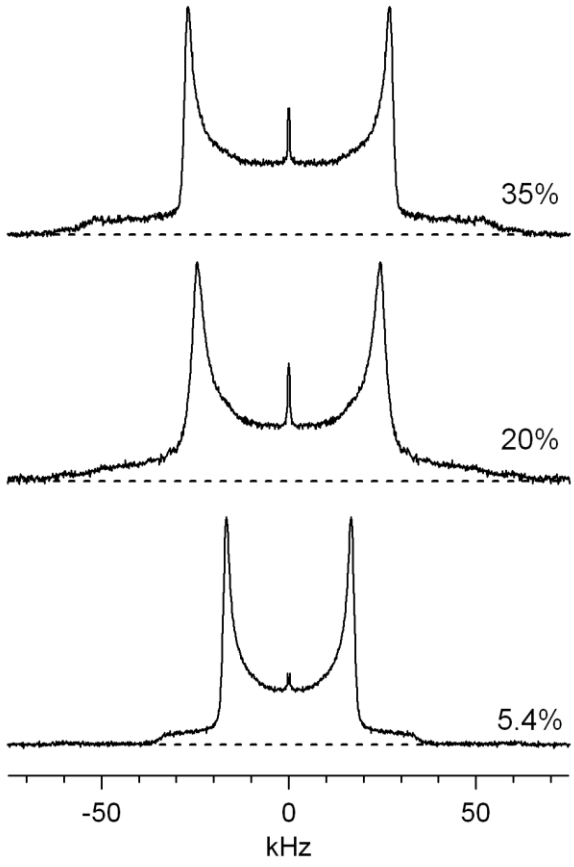

Figure 5-18: ^{2}H NMR spectra of PSM-d2 with 5.4 (pure ld phase), 20 (ld+lo phase), and 35 (pure lo phase) mol% cholesterol, at T = 47ºC.

5.2.2 Orientation Dependence of T_2 Relaxation Time

The NMR spectra obtained for PSM-d2/cholesterol membranes at T = 47^{o}C are Pake doublets characteristic of the axially symmetric reorientations about the bilayer normal. Each point on such a spectrum corresponds to an orientation of bilayer normal with respect to the magnetic field. The x-axis of a spectrum represents the frequency shift from the Larmor frequency (for simplicity we denote it as ω) which can be mapped into the orientation, θ_n, through the following scaling relation:

$$\omega = 2\omega_{90}|P_2(\cos\theta_n)|, \tag{5.7}$$

where ω_{90} is the frequency of 90^o edges of the spectrum. Various orientations are shown on Figure 5-19. The shoulders of the Pake doublet extend from 0^o to ~35^o orientations. The 90^o orientations have the maximum intensity and the center of the doublet (zero frequency) corresponds to the magic angle, 54.7^o. On the other hand, any frequency between zero and that of the 90^o edges will be mapped into two orientations by taking + or – sign of $|P_2(\cos\theta_n)|$ in Eqn. 14. Schematically, a Pake doublet can be viewed as a superposition of two half-Pake doublets. Therefore, intensity in (54.7^o – 90^o) region is composed of two different intensities; each corresponds to its own orientation, with a distinct T_2 relaxation time. In measuring T_2 in this region, the amplitude vs. echo time graph should theoretically be fitted to two exponentials, each for the relaxation time of one of the orientations. However, such behavior is not observed and the fit converges to only one exponential, suggesting that the longer T_2 dominates the amplitude. We measured T_2 relaxation time by varying the interpulse spacing from 100 to 250 μs

in steps of 50 µs. It might be possible to detect the shorter T_2 component, too, if the measurements are started from a shorter interpulse spacing (e.g. 40 µs) and continued for small increments up to 250 µs. Since data acquisition for a selectively deuterated lipid is very time-consuming large amount of lipid sample is required for this purpose.

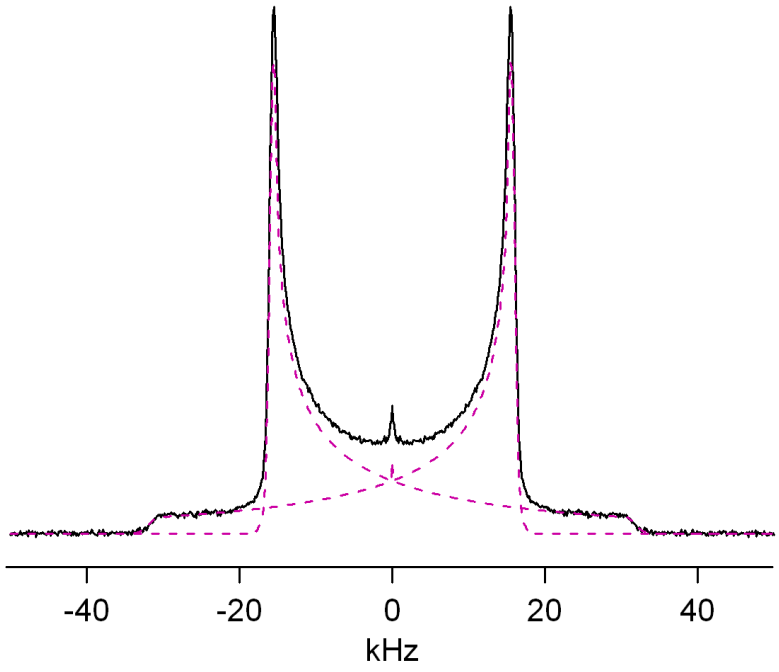

Figure 5-19: Pake-doublet of pure PSM-d2 membrane, at T = 45ºC.

Some amplitudes of the doublet have contributions from two different orientations; each corresponds to a half-Pake doublet (dashed lines).

Due to poor signal-to-noise ratio the amplitude of the spectrum, for each setting (interpulse spacing), is the result of an average over 5 degrees of orientation. For example, the amplitude assigned to 5^o is an average between 2.5^o and 7.5^o. Figure 5-20 (A) shows T_2 relaxation time of the pure PSM-d2 as a function of orientation. The 90^o edges have a relaxation time of nearly 600 µs whereas for low intensity shoulders T_2 is as short as 200 µs. Similar trend for the orientation dependence of T_2 relaxation time is observed for PSM-d2/cholesterol MLDs, Figure 5-20 (B). However, the variation in T_2 between 0^o and 90^o orientations is smaller when cholesterol in added to the PSM-d2 membrane. The membrane in the **ld** phase (5.4% cholesterol) has a longer T_2 relaxation time than in the **lo** phase (35% cholesterol), consistent with the reduced conformational freedom, i.e. higher order parameters, of the **lo** phase. In the **ld**+**lo** region the membrane is most heterogeneous and therefore the shortest T_2 is obtained for 20% cholesterol.

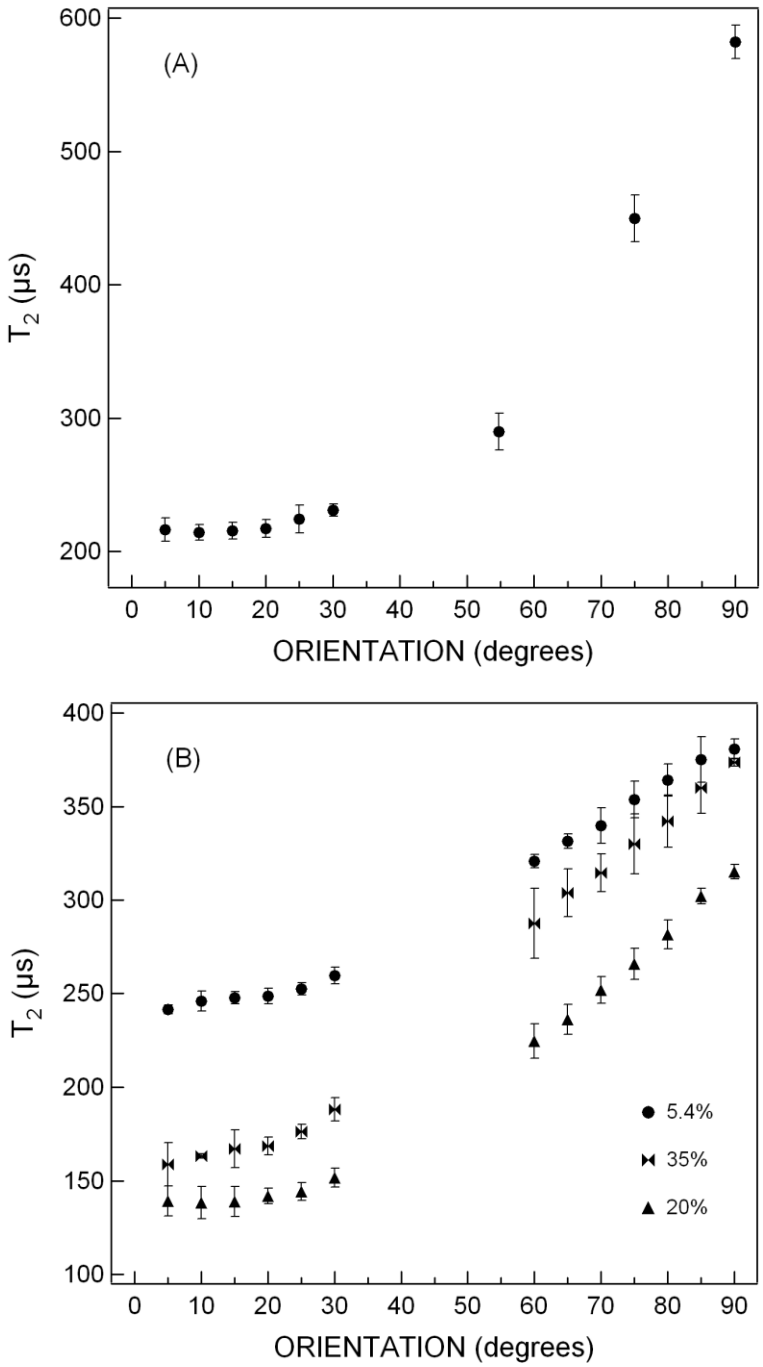

Figure 5-20: Orientation dependence of the T_2 relaxation time, $T_2(\theta_n)$.

(A) pure PSM-d2, at T = 45ºC, and (B) PSM-d2 MLDs with cholesterol concentrations corresponding to the ld, ld+lo, and lo regions of the phase diagram, at T = 47ºC.

5.2.3 ld+lo Nano-Domains Revisited

The *rms* distance diffused by PSM-d2 molecules within the **ld**/**lo** domains can be estimated as a function of orientation, θ_n. It follows from equations 5.1, 5.2, and 5.3 that

$$(\langle \Delta x^2 \rangle)^{1/2} = \left[2\mathrm{D} \left(\frac{1}{T_2^{\mathrm{ld+lo}}} - \frac{f_{\mathrm{lo}}}{T_2^{\mathrm{lo}}} - \frac{f_{\mathrm{ld}}}{T_2^{\mathrm{ld}}} \right) \right]^{1/2} \times \frac{1}{(f_{\mathrm{lo}} f_{\mathrm{ld}}) 2\pi \left(\Delta\delta_{\mathrm{ld,lo}} \right)}, \qquad (5.8)$$

where $T_2^{\mathrm{ld+lo}}$, T_2^{lo}, and T_2^{ld} are experimentally determined relaxation times, Figure 5-20 B, f_{ld} and f_{lo} are fractions of total labelled lipid in the **ld** and **lo** domains, respectively, and $\Delta\delta_{\mathrm{ld,lo}}$ is the difference in the quadrupolar splitting of pure **lo** (30% cholesterol) and **ld** (5.4% cholesterol) phases, measured from the doublets as a function of orientation (Figure 5-18). The parameter $\Delta\delta_{\mathrm{ld,lo}}$ becomes very small close to the magic angle and has a singularity at $\theta_n = 54.7°$ since, regardless of cholesterol composition, the quadrupolar splitting is zero at the magic angle. Thus, Eq. 5.9 is not appropriate to estimate the domain size close to the magic angle. At T = 47^{o}C, the **ld**/(**ld**+**lo**) and (**ld**+**lo**)/**lo** boundaries are at 9.75 ± 1 and 29.6 ± 1 mol% cholesterol, respectively (Figure 5-12). Therefore for 20% cholesterol in the **ld**+**lo** region we have $f_{\mathrm{lo}} = 0.45$ and $f_{\mathrm{ld}} = 0.55$. The diffusion coefficient is about $1.8 \times 10^{-12}\, m^2/s$ at 47^{o}C [3]. Figure 5-21 shows the *rms* distance diffused by PSM-d2 molecules within the **ld**/**lo** domains, as a function of orientation. For orientations where Eq. 5.9 can appropriately estimate $(\langle \Delta x^2 \rangle)^{1/2}$ small values (< 4 nm) of the *rms* distance is obtained (corresponding to a domain size of less than 8 nm). The result obtained near 0^o orientation ($(\langle \Delta x^2 \rangle)^{1/2} \approx 2.5\ \mathrm{nm}$) perfectly agrees with that obtained for perdeuterated PSM

with 20 mol% cholesterol, as shown in Figure 5-16 ($(\langle \Delta x^2 \rangle)^{1/2} \cong 2.2\ \mathrm{nm}$). It turns out that the choice of carbon 15 in the dePaked spectra of PSM-d31/cholesterol membranes leads to a correct estimate of the domain size.

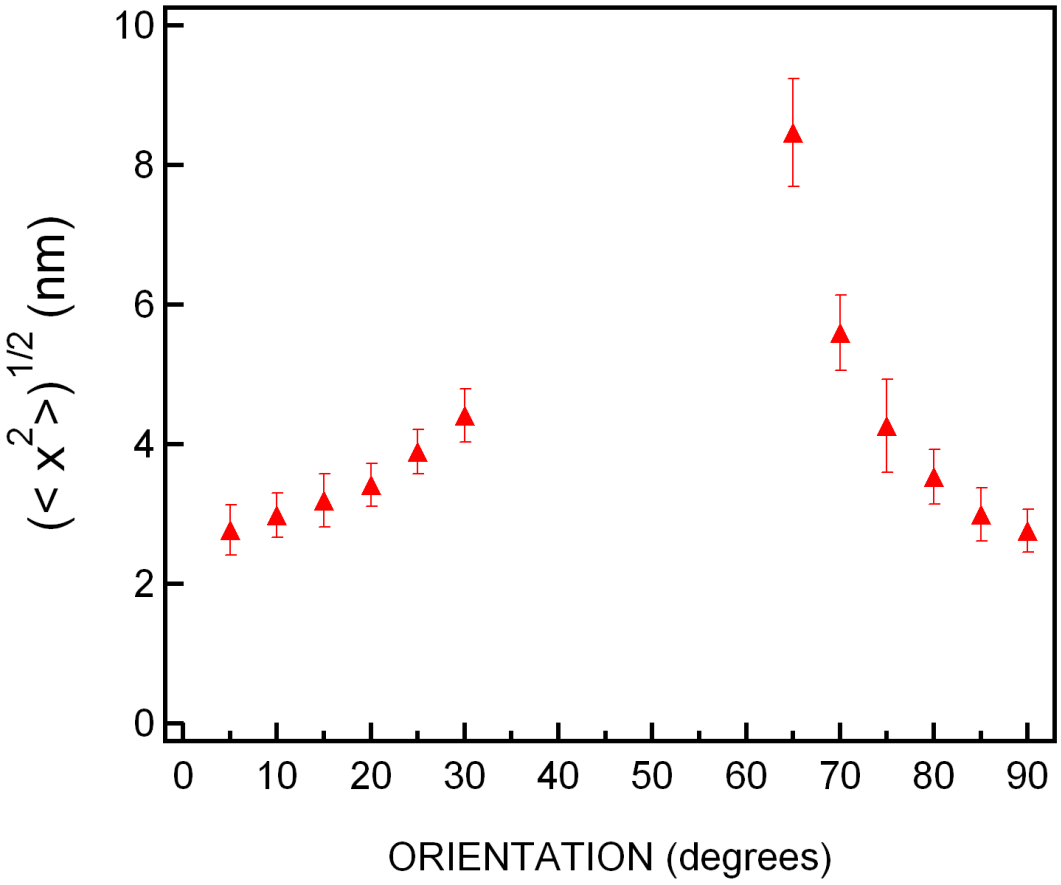

Figure 5-21: The root mean square distance diffused by PSM-d2 molecules within the ld/lo domains membranes for 20% cholesterol composition, at T = 47ºC.

5.2.4 Phenomenological Theory of the Orientation Dependence of T_2

A phenomenological theory, first determined by M. Bloom [46, 47], was discussed in section 2.4.2 and the following orientation dependence for T_2 relaxation time is obtained:

$$\frac{1}{T_2} = A + B\sin^2\theta_n\cos^2\theta_n + C[P_2(\cos\theta_n)]^2. \tag{5.9}$$

A theory for contributions of thermally induced curvature fluctuations to the transverse relaxation rate (i.e. the *B* coefficient) is described in [49]. In this theory, the curvature fluctuations are expressed in terms of a spectrum of curvature modes of wavelengths λ_q having correlation times τ_{cq} and *B* is expressed as a product of the form $\langle(\delta\theta_q)^2\rangle\ \tau_{cq}$. Furthermore, the *B* coefficient, Eq. 2.37, is given by

$$B = 9(\omega_{\mathrm{Q}}S_{\mathrm{CD}})^2\frac{k_BT}{4\pi\kappa_c}\ln\left(\frac{\lambda_M}{\lambda_m}\right)\tau_{c\theta_n}. \tag{5.10}$$

The major uncertainty is *B* in the damping mechanism. While $\langle(\delta\theta_q)^2\rangle$ can be obtained reliably from thermodynamic considerations and the equipartition theorem, τ_{cq} should depend sensitively on factors such as the degree of hydration, tension, and the multi-layer character of the membranes, that, in turn, depend on the method of preparation and the thermal history of the membrane. Within the range of uncertainty of these factors, it is concluded that the predicted values of T_2 due to this mechanism could easily fall in the observed range of ~ 100 to 1000 μs typically found for ^{2}H NMR in membranes [49]. A second mechanism, associated with order-director fluctuations [101], has been proposed

for a $\sin^2\theta_n\cos^2\theta_n$ contribution to R_2^S. It might be possible that both contribute to R_2^S, with curvature fluctuations being of greater importance for spins located in the head-group and the order-director fluctuations for spins located on the chains.

The contributions of area (or equivalently thickness) fluctuations to R_2^S are given by the *C* coefficient of Eq. 5.10. They can be described by a similar theory based on sinusoidal modes of area fluctuations which take into account an empirical or theoretical connection between S_{CD} and membrane area A. Rewriting Eq. 2.38, the C coefficient is expressed as

$$C = \left[\left(\partial S_{CD}/\partial A\right)_{\theta_n}\right]^2 \left(\frac{k_B T}{K_a}\right) \tau_{cA}. \tag{5.11}$$

In order to calculate C one can model the hydrophobic region of a fluid membrane as an incompressible fluid and make use of the empirical relationship between bilayer thickness x, its maximum value in the fluid phase x_m (or, alternatively, the corresponding membrane area $A = \langle A \rangle$ with its maximum value Am) and the average chain order parameter *S* [6]

$$\frac{A_m}{A} = \frac{x}{x_m} = \alpha S + \beta, \text{with} \;\; 0.5\alpha + \beta = 1. \tag{5.12}$$

The order parameter profile corresponding to the variation of S_{CD} with chain position has been found to have a universal form for a given value of S [102, 103] so that one can express $\partial S_{CD}/\partial A$ in Eqn. (5.12), for a given S, in terms of the experimentally measurable coefficients $E_{CD} = \partial S_{CD}/\partial S$ as follows:

$$\frac{\partial S_{CD}}{\partial A} = E_{CD}\frac{\partial S}{\partial A} = -E_{CD}\frac{A_m}{A^2\alpha}. \tag{5.13}$$

We also make the assumption that fluctuations in area are relaxed by spatial diffusion so that

$$\tau_{cA} = p\frac{A}{D}, \tag{5.14}$$

where D is the translational diffusion coefficient and p is a dimensionless coefficient of order unity. Using Eqns. (5.12), (5.13), (5.14), and (5.15), one obtains

$$C = pE_{\mathrm{CD}}^2\omega_{\mathrm{Q}}^2\left(S + \frac{1}{\alpha} - 0.5\right)^2\left(\frac{k_BT}{DK_a}\right). \tag{5.15}$$

Figure 5-22 shows Eq. 5.10 fit to the inverse of T_2 relaxation time. The coefficients A, B, and C obtained from the fit are listed in Table 5-4. The small errors in the coefficients reflect the quality of the fit. It is clear that both the curvature fluctuations and area (or thickness) fluctuations contribute to the orientation dependence of T_2, with the curvature fluctuations (the coefficient B) having a bigger influence. The ratio of B/C decreases from ~ 3 for pure lipid to ~ 2.1 for PSM-d2/cholesterol membrane in the lo phase (35% cholesterol). This indicates that when cholesterol is added to the membrane, fluctuations in the thickness of the bilayer have bigger effect on the orientation dependence of T_2 relaxation time.

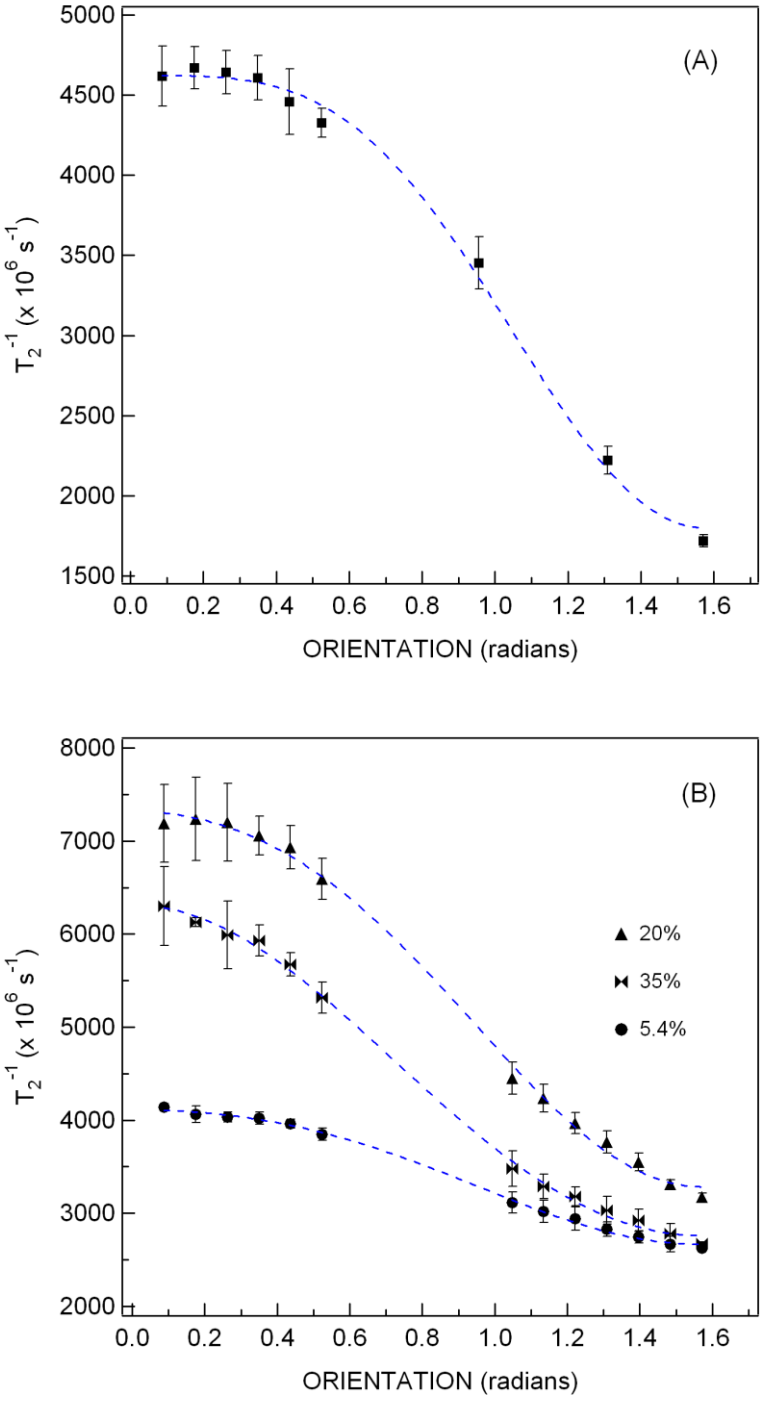

Figure 5-22: Inverse of the T_2 relaxation time in Figure 5-20, fitted to equation 16, for (A) pure PSM-d2 and (B) PSM-d2 MLDs with 5.4, 20, and 35 mol% cholesterol.

Table 5-4: The coefficients A, B, and C obtained from T_2 relaxation times fitted to equation (5.10).

	A	B	C	B/C
Pure PSM-d2	861.41 ± 84.1	11238 ± 431	3762.1 ± 98.6	3
PSM-d2+5.4% Cholesterol	2184.6 ± 19.4	4956.2 ± 130	1929.8 ± 26.3	2.6
PSM-d2+20% Cholesterol	1940.2 ± 61.4	13731 ± 412	5380.1 ± 83.4	2.6
PSM-d2+35% Cholesterol	1577 ± 44.8	10175 ± 301	4736.8 ± 60.9	2.1

Now, using experimentally determined *B* values we can estimate the effective surface-undulation correlation time, $\tau_{c\theta}$. First we need to determine the parameters in Eq. 5.11. Experimental values are $T = 320\,\mathrm{K}$ and $\omega_{\mathrm{Q}} = 2\pi \times 1.26 \times 10^{5}\mathrm{s}^{-1}$. Parameters measured from the ^{2}H NMR spectra are $S_{\mathrm{CD}} = 0.25$ for pure PSM-d2 at 45^{o}C, $S_{\mathrm{CD}} = 0.265, 0.388, \mathrm{and}\ 0.427$ for PSM-d2 MLDs with 5.4, 20, and 35 mol% cholesterol, at 47^{o}C, respectively. Parameters known from elsewhere [49] includes the ratio of the long and short wavelength cutoff for the surface undulations is $\lambda_M/\lambda_m = 20$ and $\kappa_c \approx 5 \times 10^{-20}$J.

Substituting all these values in equation (5.11) the coefficient *B* becomes $7.43 \times 10^9\ s^{-2}\ \tau_{c\theta}$ for pure PSM-d2, at 45^{o}C. and $8.34 \times 10^9\ \mathrm{s}^{-2}\ \tau_{c\theta}$, $17.89 \times 10^9\ \mathrm{s}^{-2}\ \tau_{c\theta}, \mathrm{and}\ 21.66 \times 10^9\ \mathrm{s}^{-2}\ \tau_{c\theta}$ for PSM-d2 MLDs with 5.4, 20, and 35 mole% cholesterol, at 47^{o}C, respectively.

Equating these to the experimentally determined *B* values from the fit, we obtain: $\tau_{c\theta} = 1.5\,\mu s, 0.6\,\mu s, 0.8\,\mu s, \text{and } 0.5\,\mu s$ for PSM-d2/cholesterol membranes with 0%, 5.4%, 20%, and 35% cholesterol.

This surface-undulation correlation time is significantly smaller than the NMR time-scale. During this time a PSM molecule in the fluid phase diffuses a distance of the order of ~ 12 Å. In a study on DPPC-d2, deuterated in the α-CH2 position of the polar head group [104], the effective surface-undulation correlation time of $\tau_{c\theta} \approx 45\,\mu s$ is obtained. This result was interpreted as indicating the presence of frozen-in surface undulations, along which molecules diffuse, on the NMR time-scale ($\tau_{\mathrm{NMR}} \sim \tau_{c\theta}$). Furthermore, this result illustrates the extreme softness of biological materials. The softness of biological materials is due primarily to the fluidity of the lipid-bilayer core of cell membranes, one consequence of which is the small curvature energy of cell membrane (e.g. for DPPC in the fluid phase $\kappa_c \approx 5 \times 10^{-20}$J, which is only about an order of magnitude greater than $k_B T$ at room temperature). During $\tau_{c\theta} \approx 45\,\mu s$, a DPPC molecule in the fluid phase diffuses a distance of ~ 300 Å or more. This distance diffused in the NMR time-scale defines an effective NMR length scale. The main discrepancy between this result and ours lies in the order parameter. For DPPC-d2 deuterated on the headgroup the reported order parameter is $S_{\mathrm{CD}} = 0.05$, which is 5-8 times smaller than the S_{CD} of the PSM-d2 deuterated on the acyl chain. This comparison suggests that the curvature fluctuation mechanism is not appropriate to solely describe the orientation dependence of T_2, due to $\sin^2\theta\cos^2\theta$ contribution, for spins located on the chains. An alternative

mechanism, associated with order-director fluctuations [101], should be tested for a $\sin^2\theta\cos^2\theta$ contribution to R_2^S for spins on the chains.

Chapter 6: Conclusions

We have mapped and compared partial phase diagrams of PSM-d31/cholesterol and DPPC-d31/cholesterol solely from the ^{2}H NMR measurements. The overall phase diagrams are very similar. They exhibit both **so**+**lo** and **ld**+**lo** coexistence regions with a clear three-phase line separating them. We have located and characterized the **ld**+**lo** domain coexistence region to great accuracy. Our observation of **ld**+**lo** domain coexistence provides evidence that two liquid crystalline phases can coexist even in model membranes containing no proteins. Thus, rafts in cell membranes may be strongly influenced by lipid/lipid interactions. We estimated distances between **ld**/**lo** domain interfaces in PSM/cholesterol and DPPC/cholesterol to be ~ 2.5 nm and ~ 5 nm, respectively. Such dimensions are of the order of ‘‘rafts’’ in cell membranes [105]. These domains are very small, thus it is hard to imagine that they are “phases”. We have also compared the ordering effect of cholesterol in PSM and DPPC. In the liquid crystalline phase, pure PSM is significantly more ordered than DPPC but this difference diminishes as cholesterol is added. This implies that it takes less cholesterol to promote an **lo** phase in PSM than in DPPC. In other words, cholesterol orders PSM chains more effectively to form an **lo** phase than DPPC chains. This is consistent with our observation that, above 45^{o}C, the **ld**+**lo**/**lo** boundary in PSM/cholesterol phase diagram forms at lower (by ~ 2 mol%) cholesterol concentration than in DPPC/cholesterol phase diagram. Therefore,

cholesterol is more effective in PSM membranes than in DPPC at inducing chain conformational order. Furthermore, we re-estimated the **ld**/**lo** domain size by measuring the orientation dependence of T_2 relaxation time in PSM-d2, selectively deuterated at C9 on the acyl chain, and obtained similar results as in the PSM-d31/cholesterol membrane. This removes any ambiguities in the domain size calculation based on dePakeing ^{2}H NMR powder spectra and measuring T_2 relaxation time indirectly from the linewidth. T_2 relaxation times fit very well to the phenomenological theory, suggesting that both order-director and area (or thickness) fluctuations are possible mechanisms responsible the orientation-dependence of the transverse relaxation time.

6.1 Future Work

The phase behaviour of the sphingomyelin/cholesterol model membrane has been understood to an unprecedented level through the use of ^{2}H NMR techniques. Regions of the phase diagram where two phases coexist have been studied in detail. In particular, the formation of two liquid-phase domains has been identified and the **ld**/**lo** domain size was estimated to great accuracy. However, there are some ambiguities in the phase diagram yet to be cleared up: What is the shape of **ld**/**lo** domains (e.g. circular, stripes)? Is a domain characterized by a length scale of less than 10 nm consistent with a phase? If these domains are too small to constitute true phase separation in the **ld**+**lo** region, what is the meaning of the 3-phase line? A three-phase line is a partition between the **so**/**lo** region, where macroscopic phase separation is observed in the NMR sense, and the **ld**/**lo** region, where the two “phases” do not separate

and, instead, a fast NMR exchange between the two “nano-domains” is observed. The observed line broadening rather than complete phase separation in the **ld/lo** region and the existence of a three-phase line seems to be in contradiction with the Gibbs phase rule, which dictates that there must be macroscopic phase separations above and below the three-phase line.

The outer leaflet of plasma membrane is mostly composed of sphingomyelin, POPC, and cholesterol. The next logical step in the study of raft formation is to do experiments on ternary mixtures of PSM/POPC/cholesterol. This ternary system has already been studied to some extent by fluorescence microscopy techniques [16]. Now that we know quite well about the details of the PSM/cholesterol binary system, ^{2}H NMR can be used to study the ternary system more thoroughly and get more insight into the complex behaviour of lipid raft in cell plasma membrane.

BIBLIOGRAPHY

[1] Gorter, E., and F. Grendel. 1925. *J. Exptl. Med*. 41:439–443.

[2] Danielli, J. F., and H. Davson. 1934. *J. Cell. Comp. Physiol*. 5:495–508.

[3] Pietzsch, J. http://www.nature.com/horizon/livingfrontier/background/figs/membrane_f2.html.

[4] Singer, S. H., and G. L. Nicolson. 1972. *Science, Wash*. 175:720–731

[5] Ipsen, J. H., G. Karlström, O. G. Mourtisen, H. Wennerström, and M. J. Zuckermann. 1987. *Biochim. Biophys. Acta.* 905 (1):162–172.

[6] Ipsen, J. H., O. G. Mouritsen, and M. Bloom. 1990. *Biophys. J.* 57:407–412.

[7] Bloom, M., E. Evans, O. G. Mouritsen. 1991. Physical properties of the fluid lipid-bilayer: a perspective. *Quart. Rev. Biophys*. 24:293–397.

[8] Boggs, J. M. 1987. *Biochim. Biophys. Acta.* 906:353–404.

[9] Koenig, S. H., Q. F. Ahkong, R. D. Brown, M. Lafleur, M. Spiller, E. Unger, and C. Tilcock. 1992. *Magnetic Resonance in Medicine.* 23:275–286.

[10] Vist, M., and J. H. Davis. 1990. Phase equilibria of cholesterol/DPPC mixtures: ^{2}H nuclear magnetic resonance and differential scanning calorimetry. *Biochemistry.* 29:451–464.

[11] Hsueh, Y. W., K. Gilbert, C. Trandum, M. Zuckermann, and J. Thewalt. 2005. The Effect of Ergosterol on Dipalmitoylphosphatidylcholine Bilayers: A Deuterium NMR and Calorimetric Study. *Biophys. J*. 88:1799–1808.

[12] Nielsen, M. Numerical Studies of Ising Models Defined on a Random Lattice as Applied to the Phase behavior of Lipid Bilayer Systems. 1999. Ph. D. Thesis. McGill University.

[13] Zachowski, A. 1993. *Biochem. J.* 294:1–14 review.

[14] Ahmed, S. N., D. A. Brown, E. London. 1997. *Biochem*. 36 (36):10944–10953.

[15] Simons, K., E. Ikonen. 1997. *Nature.* 387:569–572.

[16] Veatch, S. L., and S. L. Keller. 2005. Miscibility phase diagrams of giant vesicles containing sphingomyelin. *Phys. Rev. Lett.* 94(14):148101.

[17] De Almeida, R. F. M., A. Fedorov, and M. Prieto. 2003. *Biophys. J*. 85 (4):2406–2416.

[18] Veatch, S. L., P. Cicuta, P. Sengupta†, A. Honerkamp-Smith, D. Holowka, and B. Baird. 2008. *ACS Chem. Biol.* 3 (5):287–293.

[19] Sahl, S. J., M. Leutenegger, M. Hilbert, S. W. Hell, and C. Eggeling. 2010. *PNAS*. 107 (15):6829–34

[20] Davis, J. H., J. J. Clair, and J. Juhasz. 2009. *Biophys. J*. 96:521–539.

[21] Veatch, S. L., O. Soubias, S. L. Keller, K. Gawrisch. 2007. *PNAS*. 104:17650–17655.

[22] Ali, M. R., K. H. Cheng, and J. Huang. 2007. *PNAS.* 104 (13):5372–5377.

[23] Pandit S. A., H. L. Scott. 2009. *Biochim. Biophys. Acta.*–Biomembranes. 1788:136–148.

[24] Longo, G. S., M. Schick, and I. Szleifer. 2009. *Biophys. J*. 96 (10): 3977–3986.

[25] Greenwood, A. I., S. Tristram-Nagle, and J. F. Nagle. 2006. *Chem. Phys. Lipids.* 143:1–10.

[26] Radhakrishnan, A., and H. M. McConnell. 1999. *Biophys. J*. 77 (3):1507–1517.

[27] Radhakrishnan, A. 2010. Phase Separation in Binary and Ternary Cholesterol-Phospholipid Mixtures. Biophys. J. 98:L41–L43.

[28] Goñi, F. M., A. Alonso, L. A. Bagatolli, R. E. Brown, D. Marsh, M. Prieto, and J. L. Thewalt. 2008. *Biochim. Biophys. Acta.* 1781:665–684.

[29] Bunge, A., P. Müller, M. Stöckl, A. Herrmann, and D. Huster. 2008. *Biophys. J*. 94:2680–2690.

[30] Filippov, A., G. Orädd, G. Lindblom. 2003. *Biophys. J*. 84:3079–3086.

[31] Maulik, P. R., and G. G. Shipley. 1996. N-palmitoyl sphingomyelin bilayers: Structure and interactions with cholesterol and dipalmitoylphosphatidylcholine. *Biochemistry (N.Y.)*, 35:8025–8034.

[32] Estep, T. N., D. B. Mountcastle, Y. Barenholz, R. L. Biltonen, and T. E. Thompson. 1979. *Biochemistry.* 18 (10):2112–2117.

[33] Seelig, J. 1977. Deuterium magnetic-resonance – theory and application to lipid-membranes. *Q. Rev. Biophys*. 10:353–418.

[34] Davis, J. H. 1983. The description of membrane lipid conformation, order and dynamics by ^{2}H-NMR. *Biochim. Biophys. Acta.* 737:117–171.

[35] Bloom, M., F. Linseisen, J. Lloyd-Smith, and M. Crawford. 1998. Insights from NMR on the functional role of polyunsaturated lipids in the brain. In: Bruno Maraviglia, editor, *Magnetic Resonance and Brain Function*, Fermi international school of Physics, Varenna, Italy. Italian Physical Society.

[36] Abragam, A. 1961. The principles of Nuclear Magnetism. Oxford University Press, Oxford.

[37] Lloyld-Smith, J. 1996. Broadline ^{1}H and ^{2}H nuclear magnetic resonance studies of binary lipid mixtures containing docosahexaenoic acid. *M.Sc. thesis*. University of British Columbia.

[38] Veatch, S. L., S. S. W. Leung, R. E. W. Hancock, and J. L. Thewalt. 2007. Fluorescent probes alter miscibility phase boundaries in ternary vesicles. *J. Phys. Chem. B.* 111:502–504.

[39] Rose, M. E. 1957. *Elementary Theory of Angular Momentum*. Wiley and Sons Inc., New York.

[40] Brown, M. F., A. A. Ribeiro, and G. D. Williams. 1983. New view of lipid bilayer dynamics from 2H and C13-NMR relaxation time measurements. *Proceedings of the National Academy of Science of the United States of America*. 80:4325–4329.

[41] Pauls, K. P., A. L. MacKay, O. Soederman, Myer Bloom, A. K. Tanjea, and R. S. Hodges. 1985. Dynamic properties of the backbone of an integral membrane polypeptide measured by ^{2}H-NMR. *European Biophysical Journal*. 12:1–11.

[42] Bloom, M., and E. sternin. 1987. Transverse nuclear spin relaxation in phospholipid bilayer membranes. *Biochemistry*. 26:2101–2105.

[43] Morrison, C., and M. Bloom. 1994. Orientation dependence of ^{2}H nuclear magnetic resonance spin-lattice relaxation in phospholipid and phospholipid:cholesterol systems. *J. Chem. Phys*. 101:749–763.

[44] Bloom, M., C. Morrison, E. Sternin, and J. L. Thewalt. Spin schoes and the dynamic properties of membranes. In: D. M. S. Bagguley, editor, *Pulsed Magnetic Resonance: NMR, ESR and Optics*, pages 274-316. Clarendon Press, Oxford, 1992.

[45] Nevzorov, A. A., and M. F. Brown. 1997. Dynamics of lipid bilayers from comparative analysis of ^{2}H and ^{13}C nuclear magnetic resonance relaxation data as a function of frequency and temperature. *J. Chem. Phys*. 107:10288–10310.

[46] Monck, M. A. 1993. Studies of the Orientational Order and Bilayer Thickness in Biological Model Membranes. Ph. D. University of British Columbia.

[47] Bloom, M., and T. Bayerl. 1995. Membranes studied using neutron scattering and NMR. Can. J. Phys. 73:687–696.

[48] Rommel, E., F. Noack, P. Meier, and G. Kothe. 1988. *J. Phys. Chem*. 92:2981–2987.

[49] Bloom, M., and E. Evans. 1991. Observations of surface undulations on the mesoscopic length scale by NMR. In: Biologically Inspired Physics, pp 137–147 (ed. L. Peliti) Plenum Press, New York.

[50] Lipowsky, R. 1991. The conformation of membranes. *Nature.* 349:475–481.

[51] Needham, D., and E. Evans. 1988. *Biochemistry*. 27:8261–8269.

[52] Muhr, P., W. Likussar, and M. Schubert-Zsilavecz. 1996. Structure investigation and proton and carbon-13 assignments of digitonin and cholesterol using multidimensional NMR techniques. *Magn. Reson. Chem.* 34:137–142.

[53] Peng, X., A. Jonas, and J. Jonas. 1995. One and two dimensional ^{1}H-NMR studies of pressure and tetracaine effects on sonicated phospholipid vesicles. *Chem. Phys. Lip.* 75:59–69.

[54] Holopainen, J. M., J. Lemmich, F. Richter, O. G. Mouritsen, G. Rapp, and P. K. Kinnunen. 2000. Dimyristoylphosphatidylcholine/C16:0-ceramide binary liposomes studied by differential scanning calorimetry and wide- and small-angle X-ray scattering. *Biophys. J.* 78:2459–2469.

[55] Davis, J. H., K. R. Jeffrey, M. Bloom, M. I. Valic, and T. P. Higgs. 1976. Quadrupolar echo deuteron magnetic resonance spectroscopy in ordered hydrocarbon chains. *Chem. Phys. Lett.* 42:390–394.

[56] Solomon, I. 1958. Multiple echoes in solids. *Phys. Rev.* 110:61–65.

[57] Hoult, D. I., and R. E. Richards. 1975. *Proc. R. Soc. Lond. A.* 344:311–340.

[58] Schindler, H. G., and J. Seelig. 1975. Deuterium order parameters in relation to thermodynamic properties of a phospholipid bilayer. A statistical mechanical interpretation. *Biochemistry*. 14:2283–2287.

[59] Davis, J. H., and K. R. Jeffrey. 1977. The temperature dependence of chain disorder in potassium palmitate-water. A deuterium NMR study. *Chem. Phys. Lipids*. 20:87–104.

[60] Lafleur, M., B. Fine, E. Sternin, P.R. Cullis, and M. Bloom. 1989. Smoothed orientational order profile of lipid bilayers by ^{2}H-nuclear magnetic resonance. *Biophys. J.* 56:1037–1041.

[61] Boom, M., J. H. Davis, and A. L. Mackay. 1981. *Chem. Phys. Lett*. 80**:**198.

[62] Sternin, E., M. Bloom, and A. L. MacKay. 1983. De-Pake-ing of NMR spectra. *J. Magn. Reson.* 55:274–282.

[63] Bayerl, T. M., and M. Bloom. 1990. Physical properties of single phospholipid bilayers adsorbed to micro glass beads. A new vesicular model system studied by 2H-nuclear magnetic resonance. *Biophys. J.* 58:357–362.

[64] Schäfer, H., B. Mädler, and E. Sternin. 1998. Determination of Orientational Order Parameters from 2H NMR Spectra of Magnetically Partially Oriented Lipid Bilayers. *Biophys. J.* 74:1007–1014.

[65] Sternin, E., H. Schäfer, I. V. Polozov, and K. Gawrisch. 2001. Simultaneous Determination of Orientational and Order Parameter Distributions from NMR Spectra of Partially Oriented Model Membranes. *J. Magn. Reson.* 149:1–4.

[66] Tikhonov A. N., and V. Y. Arsenin. 1977. Solutions of Ill-Posed Problems. Wiley, New York.

[67] Bertero, M., C. D. Mol, and G. A. Viano. 1980. The stability of inverse problems. *In* Inverse Scattering Problems in Optics. H. P. Baltes, editor. Springer, New York. 161.

[68] Whittall, K., E. Sternin, M. Bloom, and A. MacKay. 1989. Time- and frequency-domain “dePakeing” using inverse theory. *J. Magn. Reson.* 84:64–71.

[69] Lawson C. L., and R. J. Hanson. 1974. Solving Least Squares Problems. Prentice–Hall, Englewood Cliffs, New Jersey, P. 160.

[70] Golub G. H., and C. Reinsch. 1970. *Numer. Math.* 14**:**403.

[71] Kölbel W., and H. Schäfer. 1992. *J. Magn. Reson.* 100:598.

[72] Groetsch, C. W. 1984. The Theory of Tikhonov Regularization for Fredholm Equations of the First Kind. Pitman, London.

[73] Schäfer, H., B. Mädler, and F. Volke. 1995. De-pake-ing of NMR powder spectra by non-negative least squares analysis with Tikhonov regularization. *J. Magn. Reson. A.* 116:145–149.

[74] Honerkamp, J., and J. Weese. 1990. Tikhonov’s regularization method for ill-posed problems. A comparison of different methods for the determination of the regularization parameter. *Contin. Mech. Thermodyn.* 2:17–30.

[75] Weese, J. 1992. A reliable and fast method for the solution of Fredholm integral equations of the first kind based on Tikhonov regularization. *Comp. Phys. Commun.* 69:99 –111.

[76] Schäfer, H., and H. Bauch. 1995. Determination of the local polarization distribution from ^{1}H ENDOR line shape analysis. *Phys. Lett. A.* 199:93.

[77] Schäfer, H., and R. Stannarius. 1995. Calculation of orientational distributions of partially ordered samples from NMR spectra. *J. Magn. Reson. B.* 106:14 –23.

[78] Brumm, T., A. Mops, C. Dolainsky, S. Bruckner, and T. M. Bayerl. 1992. Macroscopic orientation effects in broadline NMR-spectra of model membranes at high magnetic field strength, a method preventing such effects. *Biophys. J.* 61:1018–1024.

[79] Reinl, H., T. Brumm and T. M. Bayerl. 1992. Changes of the physical properties of the liquid-ordered phase with temperature in binary mixtures of DPPC with cholesterol, a ^{2}H-NMR, FT-IR, DSC, and neutron scattering study. *Biophys. J.* 61:1025–1035.

[80] Pott, T., and E. J. Dufourc. 1995. Action of Melittin on the DPPC-Cholesterol Liquid-Ordered Phase: A Solid State ^{2}H- and ^{31}P-NMR Study. *Biophys. J.* 68:965–977.

[81] Morrow, M. R., R. Srinivasan, and N. Grandal. 1991. The phase diagram of dimyristoyl phosphatidylcholine and chain-perdeuterated distearoyl phosphatidylcholine: A deuterium NMR spectral difference study. *Chemistry and Physics of Lipids*. 58:63-72.

[82] Lange, A., D. Marsh, K. H. Wassmer, P. Meier, and G. Kothe. 1985. Electron spin resonance study of phospholipid membranes employing a comprehensive line-shape model. *Biochemistry*. 24:4383–4392.

[83] Prosser, R. S., J. H. Davis, C. Mayer, K. Weisz, and G. Kothe. 1992. Deuterium NMR relaxation studies of peptide-lipid interactions. *Biochemistry.* 31:9355–9363.

[84] Filippov, A., G. Oradd, and G. Lindblom. 2003. The effect of cholesterol on the lateral diffusion of phospholipids in oriented bilayers. *Biophys. J*. 84:3079–3086.

[85] Weisz, K., G. Grobner, C. Mayer, J. Stohrer, and G. Kothe. 1992. Deuteron nuclear magnetic resonance study of the dynamic organization of phospholipid/cholesterol bilayer membranes: molecular properties and viscoelastic behavior. *Biochemistry*. 31:1100–1112.

[86] Trouard, T. P., A. A. Nevzorov, T. M. Alam, C. Job, J. Zajicek, et al. 1999. Influence of cholesterol on dynamics of dimyristoylphosphatidylcholine bilayers as studied by deuterium NMR relaxation. *J. Chem. Phys*. 110:8802–8818.

[87] Davis, J. H. 1986. NMR studies of cholesterol orientational order and dynamics, and the phase equilibria of cholesterol/phospholipid mixtures. *In* Physics of NMR Spectroscopy in Biology and Medicine. B. Maraviglia, editor. North Holland, Amsterdam, pp. 302–312.

[88] Davis, J. H. 1979. Deuterium magnetic resonance study of the gel and liquid crystalline phases of dipalmitoyl phosphatidylcholine. *Biophys. J*. 27:339–358.

[89] Huschilt, J. C., Hodges, R. S., & Davis, J. H. 1985. Phase Equilibria in an Amphiphilic Peptide-Phospholipid Model Membrane by Deuterium Nuclear Magnetic Resonance Difference Spectroscopy. *Biochemistry*. 24: 1377–1386.

[90] Bunge, A., P. Muller, M. Stockl, A. Herrmann, and D. Huster. 2008. Characterization of the Ternary Mixture of Sphingomyelin, POPC, and Cholesterol: Support for an Inhomogeneous Lipid Distribution at High Temperatures. *Biophys. J*. 94:2680–2690.

[91] Niemela, P., M. T. Hyvonen, and I. Vattulainen. 2004. Structure and Dynamics of Sphingomyelin Bilayer: Insight Gained through Systematic Comparison to Phosphatidylcholine. *Biophys. J*. 87:2976–2989.

[92] Varma, R., and S. Mayor. 1998. GPI-anchored proteins are organized in submicron domains at the cell surface. *Nature*. 394:798–801.

[93] Veatch, S. L., and S. L. Keller. 2003. Separation of liquid phases in giant vesicles of ternary mixtures of phospholipids and cholesterol. *Biophys. J.* 85:3074–3083.

[94] Carrington, A., and A. D. McLachlan. 1967. *Introduction to Magnetic Resonance*. Harper & Row, New York, NY.

[95] Scheidt, H. A., D. Huster, and K. Gawrisch. 2005. Diffusion of cholesterol and its precursors in lipid membranes studied by ^{1}H pulsed field gradient magic angle spinning NMR. *Biophys. J.* 89:2504–2512.

[96] Veatch, S. L., I. V. Polozov, K. Gawrisch, and S. L. Keller. 2004. Liquid domains in vesicles investigated by NMR and fluorescence microscopy. *Biophys. J.* 86:2910–2922.

[97] Seelig, J. 1981. Membranes and Intercellular Communication [Balian, R., Chabre, M., & Devaus, P. F., Eds.) pp 18-78, North-Holland, Amsterdam.

[98] Levine, **Y.** K., and M. F. H. Wilkins. 1971. *Nature* (London), *New Biol.* 69:230.

[99] McConnell, H., A. Radhakrishnan. 2005. Theory of the deuterium NMR of sterol-phospholipid membranes. *PNAS.* 103:1184–1189.

[100] Morrow, M., J. H. Davis. Biochemistry. 1988. 27:2024–2032.

[101] Stohrer, J., G. Gröbner, D. Reimer, K. Weisz, C. Mayer, and G. Kothe. 1991. Collective lipid motions in bilayer membranes studied by transverse deuteron spin relaxation. *J. Chem. Phys.* 95:672–678.

[102] Lafleur, M., P. R. Cullis, and M. Bloom. 1990. Modulation of the Orientational Order Profile of the Lipid Acyl Chain in the L-alpha Phase. *European J. Biophysics.* 19:55–62.

[103] Lafleur, M., P. R. Cullis, B. Fine and M. Bloom. 1990. Comparison of the Orientational Order of Lipid Chains in the L-alpha and the H11 Phases. *Biochemistry.* 29:8325–8332.

[104] Bloom, M., and T. M. Bayerl. 1995. Membranes studied using neutron scattering and NMR. *Can. J. Phys*. 73:687–696.

[105] Kusumi, A., I. Koyama-Honda, and K. Suzuki. 2004. Molecular dynamics and interactions for creation of stimulation-induced stabilized rafts from small unstable steady-state rafts. *Traffic*. 5:213–230.